MINISTRY OF EDUCATION, RESEARCH, YOUTH AND SPORT

THE ANNALS OF "DUNAREA DE JOS" UNIVERSITY OF GALATI

Fascicle IX
METALLURGY AND MATERIALS SCIENCE

YEAR XXVIII (XXXIII),
June 2010, no. 2

ISSN 1453-083X

2010
GALATI UNIVERSITY PRESS

THE ANNALS OF "DUNAREA DE JOS" UNIVERSITY OF GALATI.
FASCICLE IX. METALLURGY AND MATERIALS SCIENCE
N^0. 2 – 2010, ISSN 1453 – 083X

Table of Content

THE ANNALS OF "DUNAREA DE JOS" UNIVERSITY OF GALATI.
FASCICLE IX. METALLURGY AND MATERIALS SCIENCE
N^0. 2 – 2010, ISSN 1453 – 083X

RESEARCH ON THE COMPLEX MICROALLOYED ZINC MELTS

Tamara RADU, Lucica BALINT, Maria VLAD
„Dunărea de Jos" University Galaţi
email: tradu@ugal.ro

ABSTRACT

Microalloyed zinc melts are used in hot dip galvanized processes in order to improve products quality. Experiments aimed at obtaining zinc coatings with increased resistance to corrosion, which adhere very well to steel support, which are not conducive Fe-Zn reactions, don't have negative environmental impacts and present uniformly dispersed phase structure in zinc matrix. To achieve these targets were chosen microalloying elements: nickel, tin, bismuth (compared to lead) and aluminium. There were made various degrees of microalloyed zinc to determine the influence of these factors on the characteristics of the melt and obtained layers. The degree of assimilation of elements in melted zinc was determined by spectrophotometer of samples alloy, taken from melt at different time intervals. There was also presented evidence of elements influence on alloy microstructure.

KEYWORDS: zinc melts, coatings, microalloyed process, microstructure.

1. Introduction

Improvement of characteristics for the use of hot-dip galvanised products is a primary objective of the producers.

To increase the resistance to corrosion, adherence, limiting pollution and zinc-iron reaction, are used more and more microalloyed zinc melts with various elements: aluminium, nickel, titanium, copper, tin, bismuth, etc. Microalloyed zinc melts in galvanising are important in the case of Sandelin steel zincking. It is characterized by the formation of thick layers and which can be hot - dip galvanised only in microalloyed zinc melts. There is a great interest in carrying out research which explores the influence of the alloying elements in zinc melts on coating layers characteristics and the characteristics of the melts [1, 2, 3, and 4]. The paper aims at analysis the effect of small quantities of nickel, tin, bismuth and aluminium on the zinc melts.

High purity SHG zinc it was microalloyed and the level of impurities is shown in Table 1.

Table 1. *The chemical composition of zinc used in experiments, in %*

Zn	Pb	Cu	Fe	Sn	Al	Cd
99.996	0.0014	0.0004	0.0005	0.0005	0.0005	0.0004

2. Experimental researches

In the framework of the research were analysed four different zinc melts microalloyed with nickel, tin, bismuth, lead and aluminium whose chemical composition is presented in Table 2.

Table 2. *The chemical composition of microalloyed Zn melts, in %*

Alloy	Ni	Bi	Sn	Pb	Al	Zn
Zn-Ni-Bi-Sn	0.16	0.71	2.95	0	0	96.18
Zn-Ni-Pb-Sn	0.16	0	2.88	0.72	0	96.24
Zn-Ni-Pb-Bi-Sn	0.16	0.41	3.49	0.43	0	95.51
Zn-Sn-Bi-Al	0	0.44	0.86	0	0.33	98.37

2.1. Microalloying with nickel

According to Zn - Ni phase diagram, nickel and zinc form intermetalic compounds and solid solutions - based compounds. Nickel is insoluble in zinc and at 418^{o}C and 94.8%Zn forms the (σ + Zn) eutectic. Alloying with Ni was made directly through the use of finely crushed Ni, (fine pieces < 1mm) and mechanical stirring. Microalloyed process is longer, lasting for at least one hour at the temperature of 700^{0}C. Assimilation efficiency is low because nickel was lost in slag and dross. Assimilation efficiency of the direct alloying experiments was found in 77%, measured three hours after the introduction of nickel (to calculate a concentration of 0.21%Ni and 0.16%Ni was obtained). In the literature, it is recommended both direct alloying with metallic nickel and the use of alloys with a maximum of 5% nickel.

2.2. Microalloying with bismuth

In the equilibrium diagrams of Zn-Bi, there is an insolubility of the two metals which form a eutectic at 97.3% Bi and 254.5 ^{0}C. Given the low melting temperature of bismuth (271^{0}C) microalloying was made with metallic bismuth, grinding and mixing in the melt by mechanical stirring.

Assimilation process of bismuth in the melt was stable, maximum efficiency is obtained. Bismuth is a micro alloying element used to replace lead, the same effect of melt fluidity and reduction of surface tension without being toxic.

Microalloying the melt with 0.1%Bi, influences surface tension and fluidity similarly using a Pb content of ~ 1% [2]. Although bismuth is more expensive, the quantity needed for alloying bath is much lower, costs are compensated. Bismuth is also very stable in the melt and requires replenishment of the proportional added zinc.

2.3. Microalloying with lead

Lead is the main impurity in zinc. The diagram of equilibrium Pb – Zn shows that these two elements are insoluble in liquid and solid state.

Present in zinc, lead influence on the characteristics is shown in Figures 1 and 2, lead decreases surface tension and increases the zinc melts fluidity.

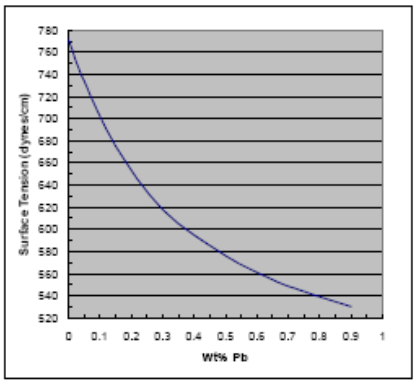

Fig.1. *The effect of lead on surface tension of zinc melts, [3]*

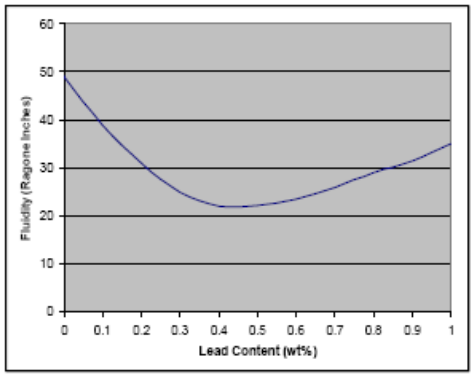

Fig. 2*. The effect of lead on fluidity of zinc melts, [3]*

2.4. Microalloying with tin

In the experiments, microalloying with tin was made with metallic tin. Sn-Zn equilibrium diagram shows a total insolubility of this element in zinc with the formation of a eutectic at 198.5^{0}C and 91.2% Sn. Tin, like most analyzed elements, forms intermetallic compounds with nickel.

2.5. Microalloying with cadmium

Cadmium is often present in zinc and can be considered an impurity. He is among the few elements which are soluble in zinc at room temperature and 0.1%Cd. Under 0.6%Cd does not affect coating structure being present in the dissolved layer foil which gives it greater resistance to corrosion. Microalloying with cadmium was made with metallic cadmium. Assimilation efficiency was achieved by 96% (addition of alloying was calculated for a concentration of 3% and 0.26% was obtained.

2.6. Microalloying with aluminium

In galvanizing melts aluminium has a major influence on slag formation, in decreasing its quantity, favouring a clean and shiny surface. Zinc melts density decreases by adding aluminium (aluminium has a density of approximately 2.5 times lower than zinc), Fig.3.

By increasing aluminium content in the melt, surface tension increases (Fig. 4).

Fig. 3. *The effect of aluminium on the density of zinc melts.*

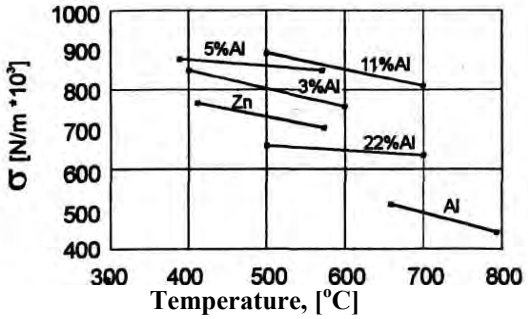

Fig. 4. *The effect of aluminium on surface tension of zinc melts.*

Given the differences in specific gravity between the two metals and the high reactivity of aluminium, microalloying with this item is recommended to be made with Zn-Al alloy. In the experiment was used commercial alloy (Zn + 4% Al). Equilibrium diagram Zn – Al shows an insolubility of Al in zinc at room temperature and solubility of 0.1% Zn in aluminium.

Zinc solubility in aluminium increases significantly with temperature. At 227 °C and 77.7% formed the eutectic (α + Zn).

3. Microstructure analysis of microalloyed zinc melts

At microalloying zinc with nickel, composite structure is obtained, consisting of intermetallic compounds (Zn-Ni, Zn-Ni-Sn, Ni-Sn) finely dispersed in zinc matrix (Fig. 5, Fig. 6).

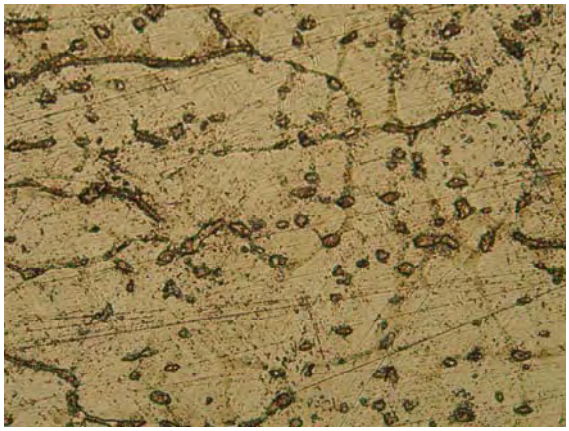

Fig. 5. *Microstructure of zinc microalloyed with Ni-Sn- Bi, X400.*

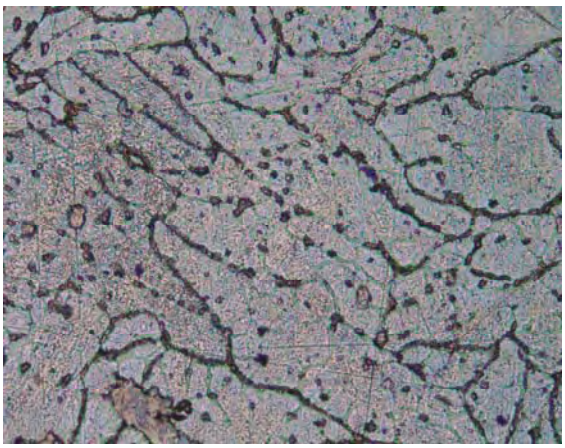

Fig. 6. *Microstructure of zinc microalloyed with Ni-Sn- Pb, X400*

Simultaneous use of lead and bismuth, and increasing the amount of tin finish striking structure, with the growing amount of intermetallic compounds. (Fig. 7)

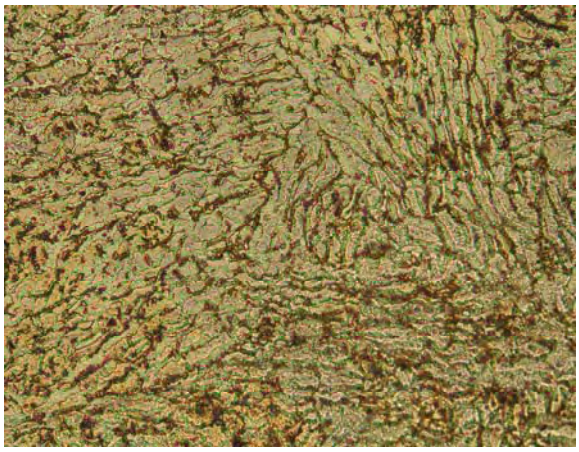

Fig. 7. *Microstructure of zinc microalloyed with Ni-Sn- Pb-Bi, X400.*

Metallographic analysis of microalloyed zinc with tin, bismuth and aluminium also reveals changes in microstructure, appearance of zinc-tin eutectic and bismuth crystals insertion (insoluble zinc) in the interdendritical space, as shown in Fig. 8.

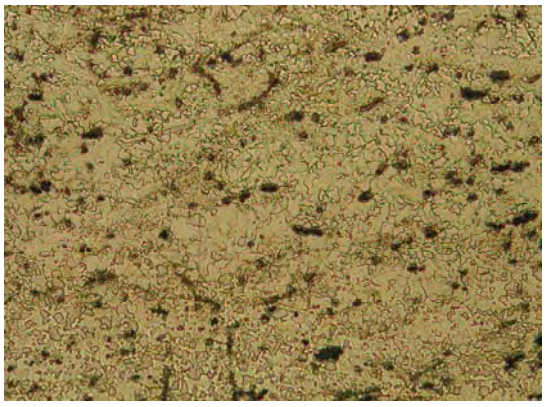

Fig. 8. *Microstructure of zinc microalloyed with Sn-Bi-Al, X400.*

4. Conclusions

1. Microalloying was made directly, using metallic elements, finely crushed, followed by mechanical mixing. At microalloyingwith nickel, was applied a maintenance at 700^{0}C.

2. All equilibrium diagrams of microalloying element and zinc have insolubility in the solid state, with formation of eutectic. Nickel forms intermetallic compounds with zinc and other studied elements.

3. The degree of assimilation of microalloyed element in the melt (calculated as the difference between the introduced metal content in the melt and the chemical composition analysis results) was different, depending on the element:

- Bismuth is assimilated 100% and it is stable in the melt, replenishment is required only when is made addition of zinc;
- Nickel is assimilated in proportion of 77%, it is lost in dross and slag;
- Tin and cadmium are assimilated at a rate of about 96% and are stable in the melts;
- Aluminium is well assimilated only using zinc-aluminium alloy, because it is lighter than zinc and has high affinity for oxygen. Aluminium is very reactive, it is consumed quickly and must be periodically added to zinc melts.

4. Bismuth is a novelty element for microalloying zinc melts, used to replace lead, having the same effect on melt fluidity and reduction of surface tension without being toxic.

5. At microalloying zinc melt with nickel composite structure is obtained consisting of intermetallic compounds (Zn, Ni, Zn-Ni-Sn, Ni-Sn) finely dispersed in the matrix of zinc.

6. Metallographic analysis of microalloyed zinc with tin, bismuth and aluminium also reveals changes in microstructure, appearance of zinc-tin eutectic and bismuth crystals insertion in the interdendritical space.

References

[1]. Bo Zhang, *Development of Corrosion Resistant Galvanising Alloys*, Metallurgy and Materials School of Engineering, The University of Birmingham, July 2005;

[2]. *Galvanizing Reactive Steels, a guide for galvanizers and specifies*," International Lead Zinc Research Organization, Research Triangle Park, NC;

[3]. Krepski, R.P., *The Influence of Lead in After-Fabrication Hot Dip Galvanizing*, 14th
International Galvanizing Conference (Intergalva'85), Munich;

[4]. John Zervoudis and **Graeme Anderson**, p. 4, *A Review of Bath Alloy Additives and their Impact on the Quality of the Galvanized Coating*, Teck Cominco Metals Ltd. 120 est, Suite 1500 Toronto, Ontario, Canada;

[5]. Metals Handbook, Tenth Edition, Volume 1, "*Properties and Selection: Irons, Steels and High Performance Alloys*," ASM International, Metals Park OH.

THE ANNALS OF "DUNAREA DE JOS" UNIVERSITY OF GALATI.
FASCICLE IX. METALLURGY AND MATERIALS SCIENCE
N^0. 2 – 2010, ISSN 1453 – 083X

SANITARY SILICONE USED TO MAKE SMALL ART CAST PARTS

Tibor BEDŐ, Viorel ENE, Ioan CIOBANU
Transilvania University of Brasov, Faculty of Materials Science and Engineering
email: bedo.tibor@unitbv.ro

ABSTRACT

Also known as investment or precision casting process, the "lost wax process" was used in ancient times from China to Egypt to cast exquisite objects which are now displayed as artifacts in museums. The process is called "lost wax" because the wax is lost or burned off in the process. The process starts with the making of a rubber mould of an original piece. The rubber mould is then used to create wax duplicates of the original piece. The mould making process is an art in itself and requires a skilled craftsman to create a good long lasting mould. The paper presents the use of "sanitary silicone" to make "rubber mould".

KEYWORDS: lost wax process, sanitary silicone, plaster mould

1. Introduction

Metal casting is an ancient technique that has a variety of applications and purposes. Civilizations from the dawn of time to present day have used metal working as a way of creating artistic, religious, and practical items.

The process of metal casting involves melting metals at high temperatures and using molds to then shape the metal into new items. Metal casting is just one form of metal working that has seen a recent surge in popularity as resources are becoming more affordable and communities are springing up to share information, ideas, and projects [1].

While metal casting is used on an industrial level as the process cuts cost and proves to be highly efficient, many individuals participate in metal casting as a hobby and in artistic endeavors.

Many people are drawn to metal casting for one reason or another, although there seems to be two main motivations that stand out.

The first motivation that brings hobbyists to practice metal casting is need; people may need to create items or parts for other ventures. Metal casting is a great way to build hard to find pieces for models, restoration projects, and even just small replacement parts needed for common household items. The second motivation for using metal casting is using it as a way to create sculptures or other artistic endeavors. Metal casting is only limited by the individual's desire, so for those with the time and the need, virtually anything is possible.

There are many types and kinds of art casting: wax art casting, sand art casting, lost wax casting and many more.

The Lost Wax Casting process is the preferred method used when art casting. This process was used in ancient times to create bronze items. Small foundries like the type found in backyards, personnel workshops, and garages are able to use the "lost wax casting" process with a certain amount of professionalism.

2. The "rubber mould" made by sanitary silicone

Most of the art casting of lost wax is processed by use of lost wax ceramic method of casting. This can make it a possibility of reproduction of maximum detail from original concept. Smaller works like the abstract works, animal Figures and many more are designed on such department.

The lost wax casting process is rather simple when compared to other casting methods but it can be time consuming and attention to detail is important. The artists will start with an original piece sculpted from wax, clay or even metal. The original will be used to make the mould. If the piece to be cast is large, multiple moulds will be needed. A mould is made from the pattern using flexible gel or similar rubber-like materials stabilized by a plaster jacket of several pieces.

To achieve mould from the pattern we have used sanitary silicon which adheres well to most building

materials such as ceramics, glass, wood, aluminium, etc. (so, even materials that can be executed models).

Next are the technical features of sanitary silicone used in the experiments (given by manufacturer [2]):

-skin-forming time at 23 °C 25 min
-extrusion rate 800 g/min
-density at 23 °C 0,98 g/cm^3
-tensile strength 0,6 N/mm^2
-ultimate elongation 200 %
-hardness, Shore A 18
-tear strength 4,0 N/mm
-movement capability 20 %
-temperature resistance (cured product)
-40 °C . . . +100 °C

Because the mould making process is an art in itself, was chosen as a model a conical wheel made of steel (Figure 1).

Fig. 1. *The conical wheel used in the experiment.*

The conical wheel metal model was coated with a layer of 4-5 mm sanitary silicone and, after that, was left to dry for 24 hours. After drying the silicone layer was sectioned and the model was removed from inside.

The result was a mould of sanitary silicon, as shown in Figure 2. Once the mould was finished, molten wax was poured into it to fill the entire mould. The molten wax was left to cool until it solidified completely.

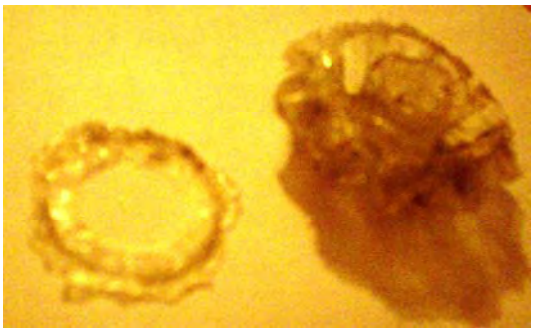

Fig. 2. *The sanitary silicone mould.*

This wax copy of the original model was removed from the mould and became the casting pattern itself (Figure 3).

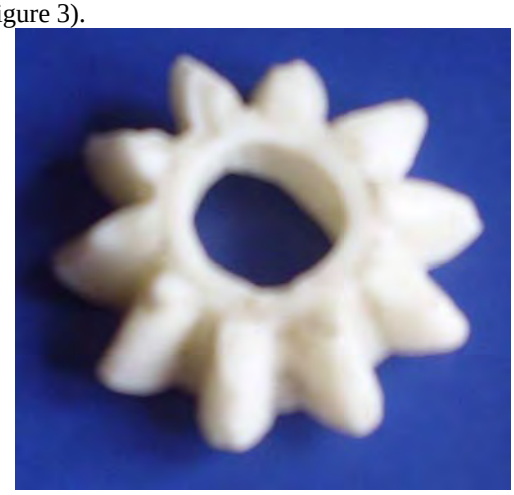

Fig. 3. *The wax copy of the model.*

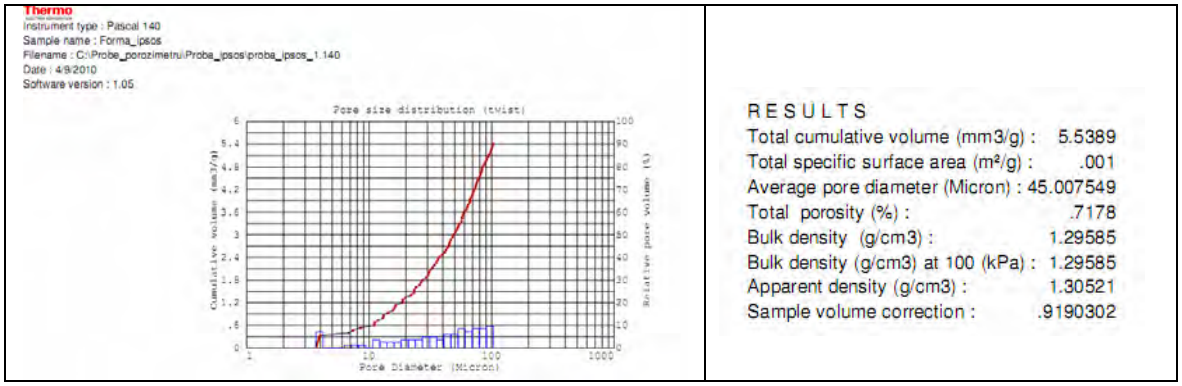

Fig. 4. *The porosity of the plaster mould.*

On the wax copy of the model were glued the casting gate pattern and the vent tube pattern.

Concerning the vent tube some clarifications should be made. The mould will be made of plaster. The mould porosity determination was made with a THERMO PASCAL 140 porosimeter resulting in a porosity of about 0.7% (Figure 4). Given the low value of porosity the discharge of gas from the mould is difficult. For this reason, and in order to completely remove the wax pattern from the plaster mould, was taken into consideration a bigger vent tube section (Figure 5).

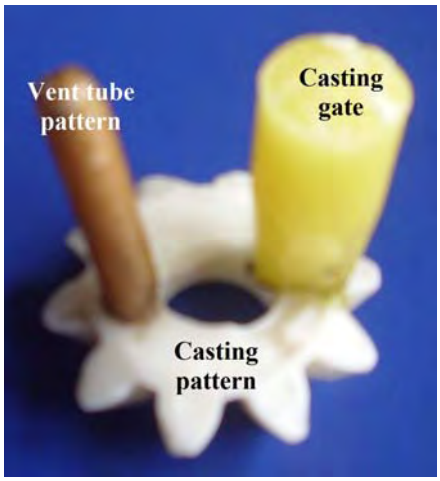

Fig. 5. *The wax casting pattern.*

Fig. 6. *The mould box.*

The wax casting pattern was placed into a mould box and plaster was cast around it (Figure 6). The plaster mould was left to harden for 48 hours.

The hardened plaster mould was placed cup-down in a laboratory furnace, at 250^{o}C, whose heat hardened the plaster, and the wax melted and ran out. Now all that remained of the original work is the negative space, formerly occupied by the wax, inside the hardened plaster mould. In the plaster mould were made sections and its structure has been examined under a microscope (Figures 7 and 8).

Fig. 7. *Section in the mould ready for casting.*

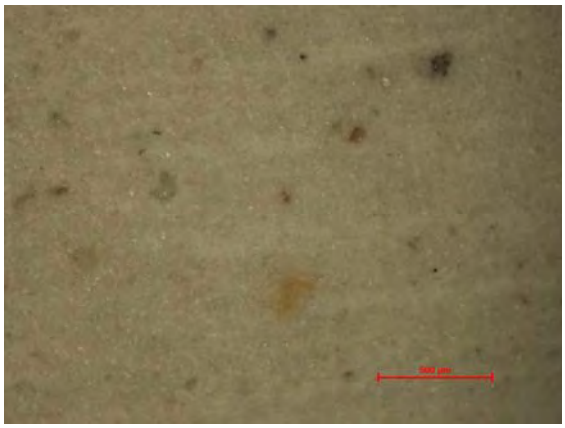

Fig. 8. *Plaster mould structure (10x).*

The plaster mould is reheated in the kiln to harden the patches and remove all traces of moisture, then placed cup-upwards into a box filled with sand, and molten metal is poured through the ducts, filling the space left by the wax [3]. When cooled, the outer plaster is removed, and the metal may receive finishing touches.

3. Conclusions

Based on these experiments we can tell:

- to cast small parts of category parts with average geometrical configuration, small pieces of art, we can use plaster casting moulds;
- lost-wax process is best used for the pieces in this category;
- to achieve the mould where will be poured the wax (to be a faithful copy of the original model) the sanitary silicone can be used, with good results;
- to obtain a good silicone mould, the silicone thickness must not exceed 8 – 10 mm;

- the optimum silicone mould release is performed between 24 and 30 hours of coverage model with the silicone layer.

We can say that inner moulds are usually made of latex, polyurethane rubber or silicone, which is supported by the outer mould.

References

[1]. http://www.metalcastingzone.com
[2].http://www.penosil.com/en/Products/silicone-and-acrylic-sealants/penosil-standard-sanitary-silicone
[**3].** http://en.wikipedia.org/wiki/Lost_wax_casting

THE ANNALS OF "DUNAREA DE JOS" UNIVERSITY OF GALATI.
FASCICLE IX. METALLURGY AND MATERIALS SCIENCE
N^0. 2 – 2010, ISSN 1453 – 083X

KINETICS AND THERMODYNAMIC TRANSFORMATION OF A SPECIAL S.G. CAST IRON

Ioan MILOSAN
Faculty of Materials Science and Engineering
Transilvania University of Braşov
email: milosan@unitbv.ro

ABSTRACT

The paper contains a study about the kinetics and thermodynamics transformation of a S.G. Cast Iron during the isothermal heat treatment. With the help of Johnson-Mehl and Arrhenius equations, there were described the activation energy "Q", rate coefficients dependent on temperature "k", exponent of reaction "n" and a constant dependent on frequency "A".

KEYWORDS: bainitic s.g. cast iron, heat treatment, phase transformation

1. Introduction

Austempered ductile iron (ADI) with a bainitic matrix, obtained by heat treatment and isothermal hardening is the material which combines a lot of superior attributes of the classical ductile iron or forged iron [1-4]. The paper presents an application for calculating the kinetics and thermodynamics parameters in the case of a phase transformation in solid state in A.D.I. S.G. grade. It is pointed out the influence of some factors (the temperature and the maintained time at the isothermal level) on the phase transformation and properties in the studied cast iron. The kinetics of austenitization of S.G. Cast Iron, was described by the Johnson-Mehl-Avrami equation. For the determination of the activation energy "Q", it was used the Arrhenius equation.

2. Materials

The studied cast iron has the following chemical composition (% in weight): 3.63%C; 2.88%Si; 0.45 %Mn; 0.012%P; 0.006%S; 0.05%Mg; 0.40% Ni, 0.42%Cu. This cast iron was made in an induction furnace.

3. Heat treating

The parameters of the heat treatment performed were the following: the austenizing temperature, T_A = 900[°C]; the maintained time at austenizing temperature, τ_A = 30[min]; the temperature at isothermal level, t_{iz} = 350 and 400[°C]; the maintained time at the isothermal level, T_{iz} = 1; 2; 5; 10; 15; 20; 25; 30; 35; 40; 45 and 50 [min].

All these 2 experimental lots A (T_{iz} = 350°C) and B (T_{iz} = 400°C) were performed at isothermal maintenance in salt-bath. The cooling after the isothermal maintenance was done in air.

4. Experimental procedure

From this material, 19 typical HB test specimens were done (ϕ 20 x 50 mm) and after the heat treating, it was determined the results of HB. The aim of the experiments is to determine the hardness (HB) at the isothermal temperature.

5. Experimental results and discussion

The experimental values of the hardness are presented in Table 1 (where: H_0 – initial hardness, corresponding to τ_{iz} = 1 min; H_t – hardness obtained after a maintaining time (t) at the isothermal level, [%]; H_f – final hardness, corresponding to the maintaining time at the isothermal level, which is considered as a final time for the first stage of transformation of the bainitic reaction).

Table 1. *Experimental values of hardness, for various T_{iz} and τ_{iz}.*

No.	Temperature at isothermal level	Maintained time at the isothermal level	Initial hardness	Final hardness	Hardness after a maintaining time
Symbol	T_{iz}	τ_{iz}	H_0	H_f	$H_{(t)}$
u.m.	[°C]	[min]	[HB]		
1	350	1	485	365	485
2		2			471
3		5			451
4		10			438
5		20			426
6		30			415
7		35			408
8		40			393
9		45			390
10		50			379
11		55			365
12	400	1	426	325	426
13		2			398
14		5			390
15		10			375
16		20			363
17		30			344
18		35			333
19		40			325

For the study of the phase transformation kinetics, it was used the first stage of the bainitic reaction [2, 4]:

$$\gamma \rightarrow (\alpha) + (\gamma) \quad (1)$$

where:
γ - metastable austenite;
(α) - bainitic ferrite;
(γ) - austenite enriched in carbon

In this research work, it was used the method of the variation hardness analysis function of the time at the isothermal level

(τ_{iz}), considering that these values depend on the proportion of the transformed fraction "$X_{(t)}$". It was utilised the expression:

$$X_{(t)} = \frac{H_0 - H_{(t)}}{H_0 - H_f}, [\%] \quad (2)$$

where:
$X_{(t)}$ – the transformed fraction;
H_0 – initial hardness, corresponding to
τ_{iz} = 1 min;
H_t – hardness obtained after a maintaining time (t) at the isothermal level, [%];
H_f – final hardness, corresponding to the maintaining time at the isothermal level, which is considered as a final time for the first stage of the transformation of the bainitic reaction.

In Figure 1 are represented the sigmoidal solid curves of the austenitic transformation during the bainite reaction.

As the transformation fraction curves have sigmoidal shape, it was used the "Johnson-Mehl-Avrami" equation:

$$X(t) = 1 - \exp(-k\,t^n) \quad (3)$$

where:
X(t) - the transformed fraction;
k - rate constant dependent on temperature;
n - exponent of the reaction.

In order to determine "k" and "n", the natural logarithmic expression was used:

$$\log[-\log(1-X)] = (n\log k + \log\log e) + n\log t \quad (4)$$

The plot of "log [-log (1-X)]"against "log t" in the isothermal temperature range of 350-400°C [2, 4], for the isothermal level maintaining time range of 1 – 55 minutes, is shown in Figures 2 and 3.

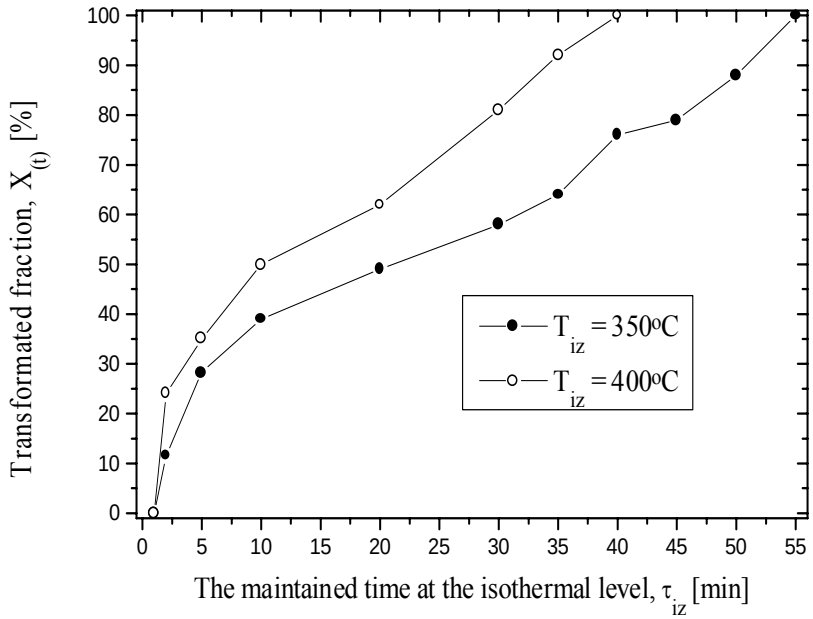

Fig. 1. *Transformed fraction curves at T_{iz} = 350 and 400 °C, for different maintaining time τ_{iz}, at the isothermal level.*

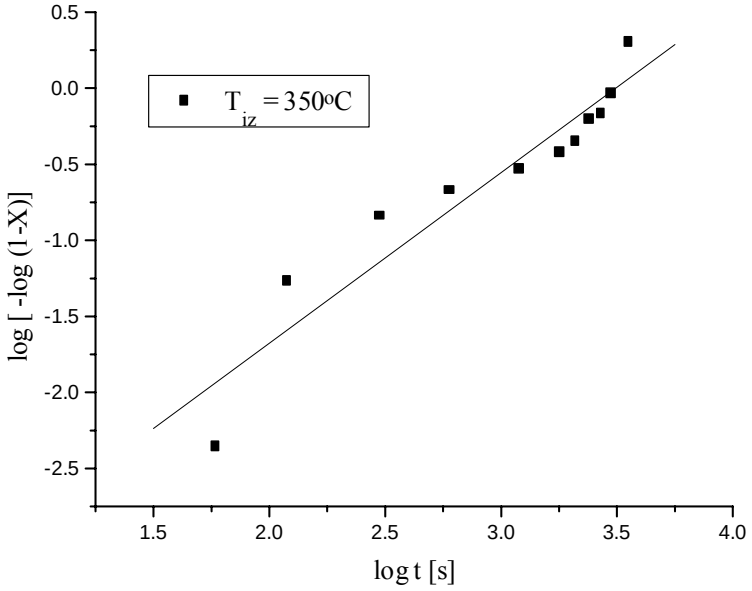

Fig. 2. *Plot of "log[-log(1-X)] against "log t" in the isothermal temperature 350 °C.*

The obtained equations from the linear regression adjustment are:

$$Y_{350} = - 3.92023 + 1.1218*X \quad (5)$$

For this equation, the coefficients of determination $R^2 = 0.95$.

$$Y_{400} = - 4.05426 + 1.25209*X, \quad (6)$$

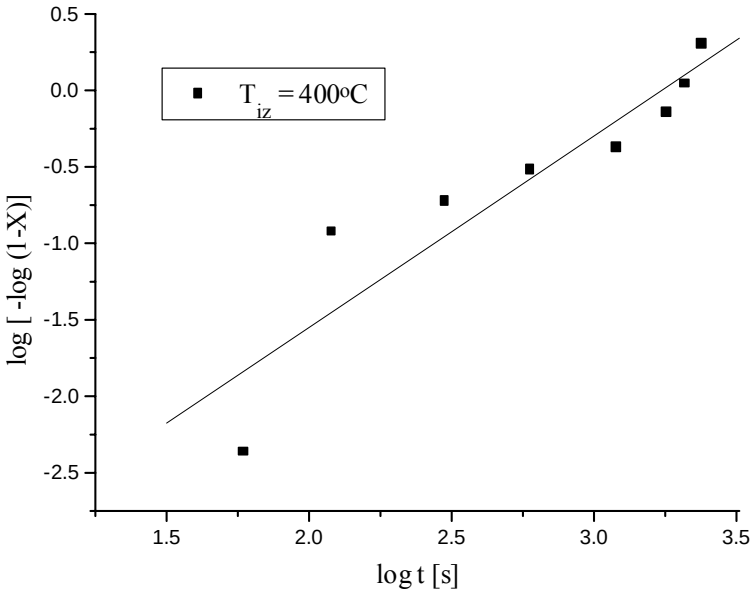

Fig. 3. *Plot of "log[-log(1-X)] against "log t" in the isothermal temperature 400℃.*

For this equation, the coefficients of determination, R^2 = 0.95. Values of "n" and "k" determined from the slopes and intercepts of the linear regression lines are listed in Table 2.

Table 2. *Values of the reaction exponent "n" and the bainitic reaction rate "k" for the formation of bainite*

Lot	**Temperature at isothermal level**	**Reaction exponent**	**Bainitic reaction rate**
Symbol	T_{iz}	n	k
u.m.	[°C]		[1/s]
A	350	1.12	6.66 x 10^{-4}
B	400	1.25	11.26 x 10^{-4}

According to Liu [2], if the "n" exponent is between 1 and 2.3, the transformation is interface controlled.

At the same maintaining time in the isothermal level, the transformation process is different in each of the maintaining isothermal temperatures. The bainitic reaction rate "k" increases when the isothermal temperature increases from 380 to 400° C.

For the determination of the activation energy "Q", it was used the Arrhenius equation:

$$k = A\, e^{-Q/RT};\ [1/min] \quad (7)$$

where:

k-constant rate dependent on temperature [1/s];

Q-activation energy, [J /mol];

T-temperature, [K]

R-gas constant 8.31, [J/mol.K]

A-constant dependent on frequency [1/s].

In order to determine "Q" and "A", the natural logarithmic expression of eqn. (7) was used:

$$\log k = -\log e \frac{Q}{R}\frac{1}{T} + \log A \quad (8)$$

The plot of "log k" against "1/T" in the isothermal temperature range of 350 - 400°C, for the isothermal maintaining time, in the range of 1 – 55 minutes, is shown in Figure 4.

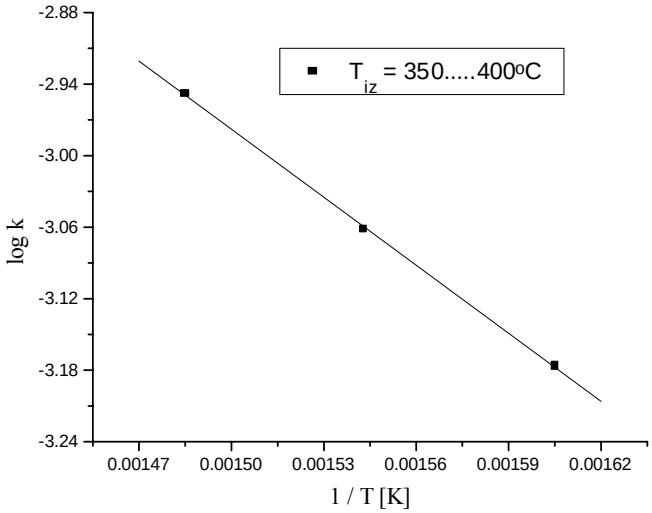

Fig. 4. *Linear transform of the Arrhenius equation for the studied S.G. cast iron, T_{iz} =350...400 ℃.*

The equation of the linear regression is:

$Y_{380 - 400}$ =-0.1245–1902.18772*X, (9)

For this equation, the coefficients of determination, $R^2 = 0.99$.

Values of "Q" and "A" determined from the slope and intercept of the linear regression line are: Q = 37036 [J/mol] and A = 0.75 [1/s]

The activation energy of isothermal transformation is the same numerical order like the values obtained in the technical specialized literature [2, 4].

From the linear regression, it was observed that the value of activation energy increases with the increasing of the maintaining temperature, from 350 to 400°C.

6. Conclusions

The isothermal bainitic transformation in a Ni-Cu S.G. cast iron was studied in the temperature range of 350-400° C and with a maintaining time between 1-55 minutes.

The main results are summarized as follows:

(a) The kinetics of austenitization of S.G. cast iron can be described by the Johnson-Mehl-Avrami equation.

(b) The reaction exponent "n"= 1.12–1.25 and the transformation is interface controlled.

(c) The bainitic reaction rate "k" increases with increasing isothermal temperature from 350 to 400°C.

(d) The activation energy of isothermal transformation was 37036 [J/mol]

(e) The constant dependent on frequency was 0.75 [1/s].

References

[1]. Simon, **D.,** *ADI- a new material for the automotive engineer*, Foundry Trade J., 2, p. 66, 1996.

[2]. Liu, Y.C., Schissler, J.M., Chabout, J.P., Vetters, H., *Study of The Structural Evolution of Austempered Ductile Iron (ADI) during Tempering at 360℃"*, Metallurgical Science & Tech. 13, p. 12, 1995.

[3]. Pérez, M. J., Cisneros, M. M., Valdés, E,, Mancha, H., Calderón, H. A. and Campos, R. E., *Experimental Study of the Thermal stability of Austempered DuctileIrons,* Journal of Materials Engineering and Performance, Volume11 (5), October, p. 519, 2002.

[4]. Milosan, I. - *The Kinetics and Thermodynamic Transformation of a Cr-Ni-Cu Low-Alloy S.G. Cast Iron,* Metalurgia International, 10, p. 70, 2009.

THE ANNALS OF "DUNAREA DE JOS" UNIVERSITY OF GALATI.
FASCICLE IX. METALLURGY AND MATERIALS SCIENCE
N^0. 2 – 2010, ISSN 1453 – 083X

GLASS- CARBON BIOACTIVE COATINGS ON A TiO_2- Nb_2O_5 SUBSTRATE

Dimitar TEODOSIEV[1], Lubomir ANESTIEV[2], Jordan GEORGIEV[2], Nartzislav PETROV[3], Petar TZVETKOV[4] and Hristiana NIKOLOVA[5]

[1]Space Research Institute, Bulgarian Academy of Sciences, Sofia, Bulgaria
[2]Institute of Metal Science, Bulgarian Academy of Sciences, Sofia, Bulgaria
[3]Institute of Organic Chemistry, Bulgarian Academy of Sciences, Sofia, Bulgaria
[4]Institute of General and Inorganic Chemistry, Bulgarian Academy of Sciences, Sofia, Bulgaria
[5]Technical University of Sofia, Bulgaria
email: dteod@space.bas.bg

ABSTRACT

The research carried out studies the processes of coating and impregnation of non-active glass carbon coatings on TiO_2-Nb_2O_5 substrates, intended for surgery implants for hip joint prostheses. It was found that the coating procedure implemented and the subsequent impregnation, lead to filling of the substrate' pores with glass carbon, thus resulting in a substantial decrease of the substrate's roughness. It was found that preliminary treatment of the substrate aiming at a formation of TiC on its surface is important for the subsequent buildup of a stable glass-carbon coating. The tribological measurements carried out show substantial decrease of the friction coefficient of vitreous carbon (VC) – hip joint, which is the prerequisite for using these coatings as surgery implants for hip joint prostheses.

KEYWORDS: Titanium ceramics, bioactive coating

1. Introduction

The usage of ceramics for biomedical technical applications has gained considerable momentum since the end for 1960. The bioceramic materials were used initially as alternative of the metal implant materials, aiming at the improvement of the biological compatibility implant- human tissue. Since then they have developed in an independent class of biomaterials widely used nowadays at their own right as tissue - bone, implants.

Some inert bioceramics of the Al_2O_3, ZrO_2 type, showed excellent tribological properties and stability towards skin-deep traumas, when used as endoprostheses, mainly in the production of heads for pelvic thigh anchylosises.

The alumina ceramics Al_2O_3 have been used in the world orthopedic practice, as well in Bulgaria, for more than 30 years.

The clinical results from this period demonstrated that the wearing out between the head from alumina ceramics and the cup from polyethylene [1-8] is negligible making it an excellent material for bone implants. However, the usage of ceramics as implants is not without problems.

Due to their insufficient mechanical strength, risks of a sudden breakage could not be eliminated.

Another, still unsolved problem, concerning the materials used for heads of pelvic thigh anchylosis, is their limited life span, which is an issue of crucial importance, especially when these are implanted in young patients. Therefore, a sharp increase of their service life say up to 20 years is highly desirable.

To address the challenges above, in the BAS, a new inert bioceramic material, based on the oxide ceramics TiO_2 (Rutile) - Nb_2O_5, was developed and since then intensively investigated [9-13].

The concept behind the development of the new biocompatible composite ceramic material, based on TiO_2 (Rutile) and Nb_2O_5 with additions of nano-carbon ingredients, is that the vitreous carbon covers the ceramic substrate surface more effectively. Thus, a target surface roughness of the coated substrate down to 3 microns could be reached.

Moreover, a coating consisting entirely of carbon will not be rejected from the organism of the patient.

The method developed for synthesis of this new ceramic material is based on the assumption that during the thermal treatment, the titanium dioxide ceramic and the deposited carbon glass coating will

react and form a thin layer of titanium carbide in the ceramic-coating interface.

It is assumed, that part of the carbon will be consumed for reduction of the titanium dioxide lying near the interface, and that another part will participate in building of transitional carbide layers filling the pores of the ceramic body. The transitional carbide layer would also serve as anchor of the glass-carbon layer, thus reducing risk of breakage between the ceramics and the coating. It is expected that a coating of carbon glass produced by thermal deposition, would have very high rank of roughness, thus eliminating the necessity of end polishing of the friction surfaces.

The aim of the present paper is a study of newly developed biocompatible composite ceramic material, based on TiO_2 (Rutile) - Nb_2O_5 ceramic with additions of nano-carbon ingredients, intended for production of endoprotheses.

2. Experimental procedure

2.1. Synthesis of the ceramic substrate TiO_2 - Nb_2O_5

The ceramic substrate specimens studied were prepared by mixing TiO_2 and Nb_2O_5 powders in proportions ensuring concentration of 8 wt.%. Nb_2O_5 in the final product. The choice of Rutile as base powder of the mixture is due to its structure. The Ti atoms in the Rutile (TiO_2) occupy the centre of a slightly deformed octahedron formed by the Oxygen atoms. This positioning of the Rutile's atoms determines its great capacity to incorporate in its lattice donor elements, or donor ions.

Because the Nb^{5+} ion radius of the Nb_2O_5 substance is commeasurable with the Ti^{4+} radius (RTi^{4+} = 0,69 A, RNb^{5+} = 0,70 A) it is easily embedded into the Rutile cell's voids, resulting in negligible change of the Rutile lattice parameters. Thus, when Nb_2O_5 is added in small quantities it would not deform the Rutile lattice and the mechanical properties of TiO_2 ceramic would be preserved [14-15].

The concrete ceramic synthesis procedure used, is as follows: firstly, the mixture is granulated and then under isostatic pressure it is formed into the desired form of the substrate.

The substrate specimens prepared for this study were with diameter of 35-36 mm and 10mm thick. The as prepared substrate specimens were sintered at temperature of 1450ºC according to a predetermined temperature regime.

The next step of the production of the coated ceramics is the generation of carbides on the substrates' surface. For this purpose the ceramic substrate, in our case the prepared TiO_2 - Nb_2O_5 sinter, is covered with polymer organic material, with complex structure of the type (CnHm). During the heating the polymer decomposes to: carbon, which subsequently forms the desired carbide structure; H_2 and organic radicals (CxHy).

The presence of H_2 in the furnace atmosphere favours the reduction of the oxides at the ceramic's surface, by extracting and chemically bonding the labile Oxygen O^{2+} ions. The freed chemical bonds are later saturated by the carbon atoms obtained by the decomposition, thus, forming the desirable carbide layer on the substrate surface.

Obviously, the temperature regime of heating and the thickness of the polymer coating are crucial for obtaining a quality carbide layer. For this purpose the "heat-hold-cool" regime was selected after modeling and numerous trial-error experiments. It was found that most favorable for the formation of the desirable structure of the substrate is heating with 10K/min up to 1450^{o}C in inert gas atmosphere with subsequent cooling with approximately the same cooling rate.

The processes, taking place during the carbide layer production, were constantly monitored using sophisticated thermal analysis apparatus, Setaram **DTA-TG-MS LABSYS-evo**. Powder X-ray diffraction (XRD) patterns for characterization of the samples were collected at room temperature on a **Bruker D8 Advance** diffractometer using CuKα radiation and Sol-X detector.

The measurement range was from 10^o to 80^o 2θ with a step of 0.04^o 2θ and 1 s/step counting time. Phase analysis of the powder patterns was done using EVA v.12 program and ICDD PDF-2 database, 2006-release.

2.2. Coating of the substrate specimens

This is the last stage of production of glass carbon coated bioceramics.

As mentioned, it is done to improve the mechanical and the tribological quality of the final product, TiO_2-Nb_2O_5, and as well for the ceramic's compatibility with the human tissue.

The procedure itself is as follows: firstly, the specimens are saturated in organic solution of polymer hydrocarbons with controlled concentration.

The process of preparation and degradation of the polymer used are described in details in the ***Appendix***; secondly the specimens are dried in vacuum at 150^{o}C; lastly the specimens are heat treated at 1000-1100°C in inert gas atmosphere using an empirically selected temperature regime, which is: heating of 15 to 20 °C/min.; holding at 1000-1100°C for 30-50 min. and cooling to room temperature.

This procedure is repeated several times until the desirable roughness grade and layer thickness is reached.

3. Results and discussion

3.1 X-ray phase analysis and SEM results

Before coating, the structure of the as sintered specimens, has been studied with X-ray and SEM analyses. The results obtained are shown in Figs.1 and 2. The X-ray analysis showed, as expected, that the crystal reflection planes after combined sintering of the TiO_2 and Nb_2O_5 powders are changed, which is evinced by a shift of the reflects observed, to a smaller reflecting angles. As known, this is a result of the distance increase between the crystal reflection planes due to the formation of a compound formed by the interaction between TiO_2 and Nb_2O_5 powders.

It our particular case, the compound formed has a crystal lattice, of the type $\mathbf{(Ti^{4+}_{1-2x}\ Nb^{5+}_{x}\ Ti^{3+}_{x})O_{2-x}}$.

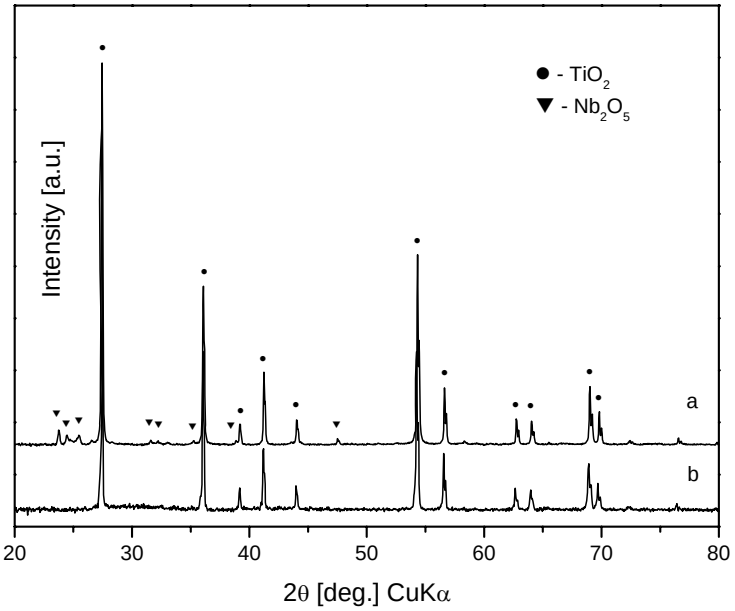

Fig. 1. *X-ray phase analysis of Rutile $TiO_2 – Nb_2O_5$ ceramics.*

The formation of this compound results from the charge conservation law, where one of Ti^{3+} for every Nb^{5+} is reduced, thus keeping the mean charge of 4^+ for every Ti atom preserved. The microstructure of the sintered substrates was studied by SEM.

The micrographs obtained are shown in Fig.2.

As seen, the structure of the ceramic substrate is characterized by oval voids measuring 3-4 μm and isometric grains measuring up to 20 μm.

This type of microstructure with strongly developed surface was intendedly pursued and is very favorable for obtaining strong bonds between the VC coating and the carbide layers of the ceramic matrix. The experiments carried out, showed that part of the Nb_2O_5 reduces to NbO_2, during the sintering, which gives a characteristic bluish black colour of the sinter. It should be noted, that this transformation does not affect the mechanical or chemical properties of the substrate.

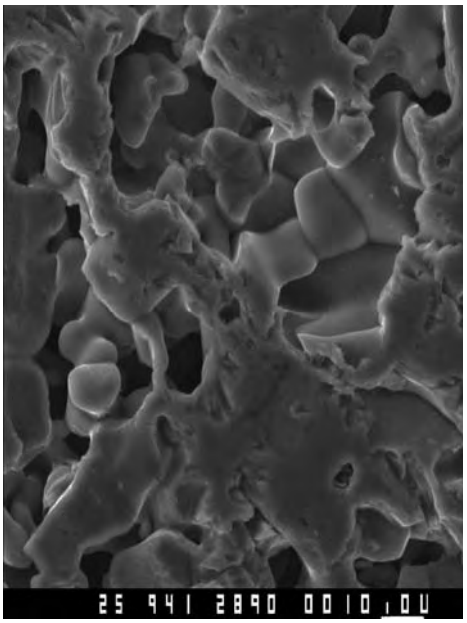

Fig. 2. *SEM image of TiO_2-Nb_2O_5, specimen. x940*

3.2 Thermo-gravimetric experiments

Fig. 3 shows the results obtained by the thermo -gravimetric analysis of the specimens prepared from granulated TiO_2-Nb_2O_5.

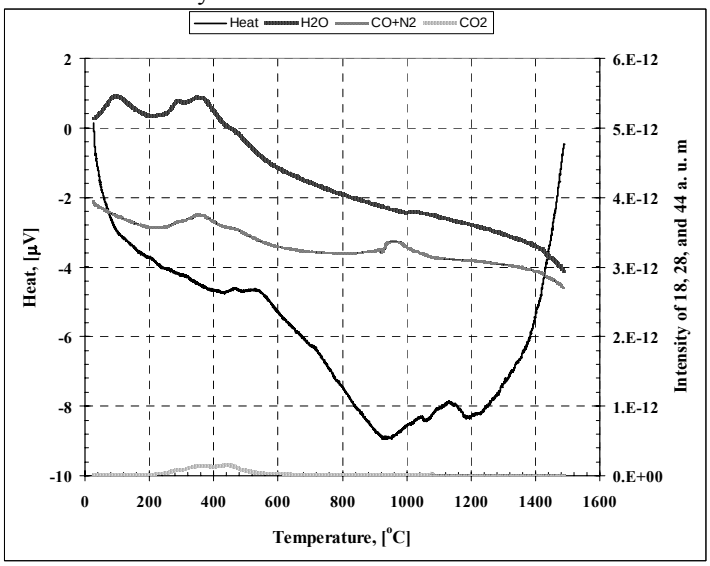

a)

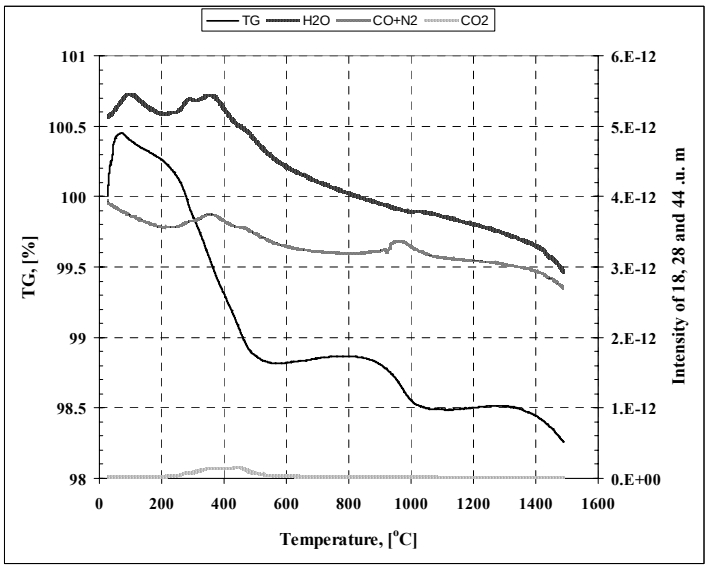

b)

***Fig.3a** and **3b**. DTA and gravimetric curves obtained during the precursory treatment of the ceramic substrate surface with carbon aiming at the development of TiC on the substrate surface.*

The gravimetric results show that the first stage at the sintering of the specimens is the evaporation of the residual moisture followed by degradation of the PVC used. This process continues up to 600ºC and is characterized by a considerable weight decrease of the specimen. The sintering itself takes place in the temperature interval 850-1200ºC. At this stage the weight still decreases but it is not so intensive compared to the first stage. It was concluded that this is due to the reduction of the oxides forming the substrate. At the end of this stage two characteristic endothermic peaks are observed on the DTA curve, due to the formation of carbides on the substrates' surface. It should be reminded, that the formation of carbides is of crucial importance for the mechanical strength of the final VC coating. The DTA-gravimetric experiments carried out, were crucial for the determination of the optimal temperature regime of sintering. Analyzing the results obtained at different temperature regimes, the following optimal regime of sintering was selected: heating rate of 5ºC/min. from room temperature to 600ºC; heating rate of 10ºC/min. from 600ºC to 1450ºC and holding at temperature of 1450ºC for 45 to 60 min. The lower heating rates at the beginning are to avoid the distortion and the subsequent crumbling of the specimen, due to intensive separation of moisture and hydrocarbon radicals.

3.3. Tribological experiments. The friction coefficient

The coefficient of friction (CoF), symbolized below by the Greek letter μ, is a dimensionless scalar value which describes the ratio of the force of friction *F* between two bodies and the force pressing them together *N* (the normal force): $\mu = F/N$. It should be noted that the friction coefficient is velocity sensitive, i.e. its value depends on the velocity between the friction surfaces.

The results reported here are obtained from measurements of the friction coefficient between coated with vitreous carbon (VC) and not coated ceramic specimens of TiO_2-Nb_2O_5 with substrate of low molecular polyamide, used for production of acetabular capsules at endoprosthesing.

Table 1

№	Nomenclature	Without coating		After coating with VC	
		Initial friction coefficient, μ_0	Dynamic friction coefficient, μ	Initial friction coefficient, μ_0	Dynamic friction coefficient, μ
1.	П	0.14	0.11	-	-
2.	600/07.10.2009	0.22	0.12	-	-
3.	2.15-400	0.25	0.16	0.14	0.09
4.	2.16-400-1	0.22	0.16	-	-
5.	2.17-220	0.26	0.14	-	-
6.	3.15	0.22	0.15	-	-
7.	3.16	0.40	0.28	0.24	0.17
8.	3.19	0.38	0.32	-	-
9.	4.15-400	0.20	0.14	-	-
10.	4.16-П	0.12	0.08	-	-
11.	4.17-200	0.24	0.14	-	-
12.	4.18-400-1	0.21	0.12	-	-
13.	4.19-600	0.16	0.11	-	-

The experiments were carried on cylindrical specimens at N=50 –150 N and velocities of 10 – 300 mm/s.

Two values of CoF were measured: the Initial friction coefficient, μ_0, where the specimens are stationary in respect to the substrate and dynamic friction coefficient, μ, for moving specimens.

The results obtained are summarized in Table 1.

The results presented show that the specimens coated with VC have smaller static and dynamic CoF compared to the not coated ones. It is worth noting, that the higher values of μ_0 compared to μ, are due to several factors, such as the material's nature, the material's physical condition and its roughness.

3.4 Microstructure-roughness measurements

As part of the material characterization, the roughnesses of the specimens before and after coating with VC were also measured, using profile meter **Rugosurf 10G**.

The results obtained are summarized in Table 2.

The measurements were carried out at a base length of 0.25 mm and averaging of 5 base lengths. The mean deviation of the profile from the mean line R_a and the roughness height R_z obtained as a mean of the highest and lowest points within the base length were determined.

The results of the measurements microstructure roughness for the specimens studied are summarized in Table 2.

The results obtained show that the mean deviation of the profile R_a of the studied specimens varies within the 0.47 – 1.00 μm range, the R_z is within the limits of 3.00 – 6.00 μm, except for the specimens #4 and #8. It is obvious that VC reduces the roughness of the ceramics' surfaces, which is a prerequisite for using coated ceramics for surgery implants at hip joint prosthesing.

Table 2

№	Nomenclature	Without coating		After coating with VC	
		R_a, μm	R_z, μm	R_a, μm	R_z, μm
	П	0.685	4.574	-	-
	600/07.10.2009	0.630	3.911	-	-
	2.15-400	0.959	4.910	0.612	3.98
	2.16-400-1	1.454	8.430	-	-
	2.17-220	1.020	5.742	-	-
	3.15	0.471	3.432	-	-
	3.16	0.485	3.053	0.363	2.646
	3.19	2.914	14.344	-	-
	4.15-400	0.834	5.086	-	-
	4.16-П	0.605	3.907	-	-
	4.17-200	0.884	5.156	-	-
	4.18-400-1	0.734	4.860	-	-
	4.19-600	0.709	4.082	-	-

4. Conclusion

The processes of coating and impregnation of non-active glass carbon coatings on TiO_2-Nb_2O_5 substrates, produced by sintering and intended for surgery implants for hip joint prostheses, were studied. It was found that a precursory development of TiC on the substrate surface, facilitates the subsequent buildup of a stable glass-carbon coating. A temperature regime for the coating procedure using modeling and trial-error experiments was determined and implemented.

The tribological measurements carried on ceramic specimens, coated with the method described, show substantial decrease of the friction coefficient glass carbon – hip joint, which is the prerequisite for using these coatings as surgery implants for hip joint prostheses.

Appendix

The PVC degradation

The precursor for glassy carbon coating was produced by thermal decomposition of PVC. The PVC used shows two stages of degradation. During the first stage, which is between 200 and 360°C, mainly HCl, benzene, and very little alkyl aromatic or condensed ring aromatic hydrocarbons are formed. About 15% of the polyene generates benzene, the main part accumulating in the polymer and being active in intermolecular and intramolecular condensation reactions, by which cyclohexene and cyclohexadiene rings embedded in an aliphatic matrix are formed.

Alkyl aromatic and condensed ring aromatic hydrocarbons are formed in the second stage of degradation, between 360 and 500°C, when very little HCl and benzene are formed. In this stage the polymeric network formed by polyene condensation breaks down in the process of aromatization of the above C rings.

In the specific research the PVC degradation was carried out at 380^{o}C, temperature with a heating rate of 5^{o}C/min and soak time at the final temperature for one hour. This allows completely eliminate the Cl as HCl and is obtained a final product with appropriate composition for formation of stable coating of classy carbon on the TiO_2-Nb_2O_5 substrate surface.

Acknowledgements

The financial support of this research from the Bulgarian Research Fund Grant DO 02-234/2008 is highly appreciated.

References

[1]. Disegi J. and L. Eschbach, *Stainless steel in bone surgery, Injury*, Int. J. Care Injured, vol. 31 (2000), S-D2-6.
[2]. Pohler E. M., *Unalloyed titanium for implants in bone surgery,* Injury, Int. J. Care Injured, vol. 31 (2000), S-D7-13.
[3]. Marty A., *Cobalt-base alloys used in bone surgery,* Injury, Int. J. Care Injurd, vol. 31 (2000), S-D18-21.
[4]. Eschbach L., *Nonresorbable polymers in bone surgery,* Injury, Int. J. Care Injured, vol. 31 (2000), S-D22-27.
[5]. Marti A., *Inert bioceramics (Al_2O_3, ZrO_2) for medical application,* Injury, Int. J. Care Injured, vol. 31 (2000), S-D33-36.
[6]. T. V. Tamaraiselvi and S. Rajeswari, *Biological Evaluation of Bioceramic Materials – A Rewiev,* Trends Biomater. Artif. Organs, vol. 18 (10, PP. 9-17 (2004)

[7]. P. N. De Aza, A. H. De Aza, S. De Aza, *Crystalline Bioceramic Materials*, Bol. Soc. Esp. Ceram. V., 44 [3] 135-145 (2005)
[8]. Sunho Oh, Namsik Oh, Mark Appleford, Joo L. Ong, *Bioceramics for Tissue Engineering Applications – A Review***,** American Journal of Biochemistry and Biotechnology 2 (2): 49-56, 2006, ISSN 1553-346
[9]. Bulgarian Patent, № 36107.
[10]. Bulgarian Patent, № 16834.
[11]. Bulgarian Patent, № 30527.
[12]. Bulgarian Patent, № 24996.
[13]. Bulgarian Patent, № 31847.
[14]. Jordanova M., D. Teodosiev, J. Georgiev, *Composite ceramic materials based on vitreous carbon as transplantation materials in the human organism – Obtaining and structure,* Acta morphologica et antropologica, vol. 6, 2001, pp. 64-69.
[15]. Jordanova M., D. Teodosiev, J. Georgiev, *Composite ceramic materials based on vitreous carbon as transplantation materials in the human organism – Basic structural and functional tests*, Acta morphologica et antropologica, vol. 6, 2001, pp. 70-75.

THE ANNALS OF "DUNAREA DE JOS" UNIVERSITY OF GALATI.
FASCICLE IX. METALLURGY AND MATERIALS SCIENCE
N^0. 2 – 2010, ISSN 1453 – 083X

MAKING ART REPLICAS MODELS USING 3D SCAN AND ELECTRODEPOSITING

Aurelia STANESCU, Alexandru STANESCU, Bogdan FLOREA
MApN, AMCSIT, Politehnica University of Bucharest
email: florea_b2004@yahoo.com

ABSTRACT

This paper presents a modern fast and efficient way, of faithfully reproduction works of art by implementing modern technology of 3D scanning and printing processes combined harmoniously with metallic coating made by electro deposition.

KEYWORDS: electrodepositing, reproduction, 3D scanning

1. Introduction

A replica is a copy, which is intended to be a faithful reproduction of the original and the reproduction is defined as a copy of an original artwork (drawing, painting, sculpture etc.).

Reproductions used for historical purposes, by their exposure into museums, do not contribute only to increase of artistic and historical knowledge of a large segment of the contemporary civilized world.

Making replicas of art objects without moving them or coming in direct contact with them, especially for those whose integrity may suffer, is a real advantage.

The proposed method allows the production of replicas of art objects at different scales, depending on needs, which are made without direct physical contact between an original object and the various stages of making his reply.

Not always it is necessary for life-size reproduction of an art objects made by means of a mould directly executed on the object. Sometimes it is preferred a perfect copy, but on a smaller scale, this way a museum is able to have in a relatively small space a large number of artefacts (replicas) of art objects.

2. The principle of the method

Modern technique allows today implementation in practice the ideas above presented. With a high-resolution 3D scanner, we get high fidelity reproduction of the details.

Backing besides can be made at any distance towards the original location. In this way any museum in the world can have any replica of an art object, regardless of its original size and location.

As a principle, the procedure of making replicas of art models by 3D scan and electrodepositing is the following:

1. 3D scanning of art objects.
2. Software processing of obtained information.
3. Streaming of information in electronic form to the new location (museums, exhibitions, art galleries etc.).
4. 3D printing on a scale which can be different from 1:1.
5. Preparing model by painting with electro-conductive solutions.
6. Electrodepositing metallic material on art objects reply (gives increasing strength and appearance as close to reality - see bronze, copper).
7. Any subsequent processing (touches, coating decorative organic layer).

This film is presented in the scheme from Figure 1.

If reading the data requires a portable 3D scanner and a laptop, for practical realization of replicas, the entire installation (computer, 3D printer, painting and drying installations, electrodepositing installations with all annexes) can be embedded in a mobile container.

That container will be connected to water and electricity.

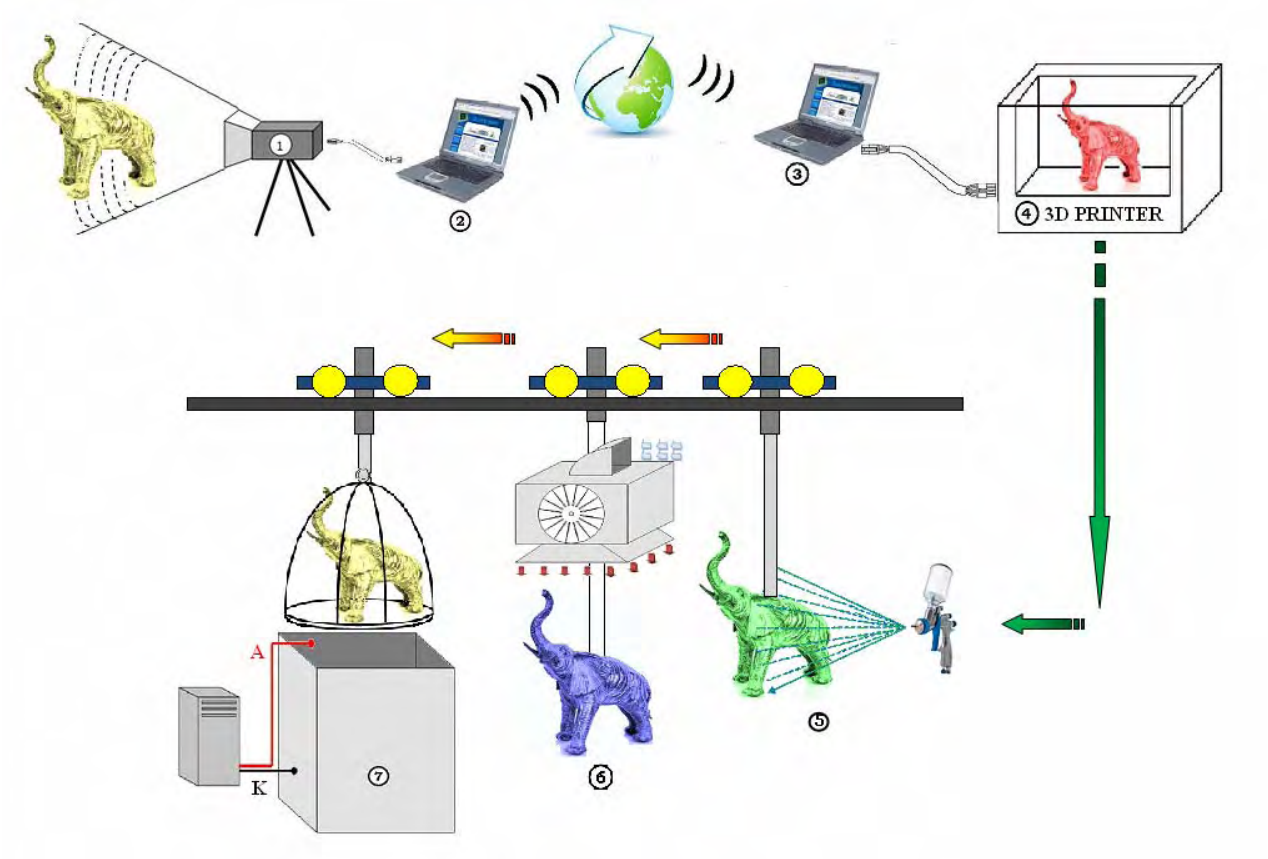

Fig.1. *Progress operations for the realisation replicas of models art by 3D scan and printing and electrodepositing: 1 – 3D scanner (portable); 2 – processing and information storage unit (laptop); 3 – laptop whit corresponding software; 4 – 3D printer; 5 – painting installation; 6 – drying installation; 7 – electrodepositing vat.*

3. The procedure of art models replicas made by 3D scanning patterns and electrodepositing

Large field work of current 3D scanner allows that a scanned object can have dimension size of a few centimetres (the different religious items, ornaments, jewellery, amulets, statues) to tens of meters (historic buildings, architectural complex etc.). The information obtained can be sent further as such or processed.

For large models a trick can be used. Based on calculations of resistance, it can drop some volume of material from the inner mass of the art object, without affecting the structure of resistance and without having repercussions on the details, however small these may be.

We get such a monolithic piece, but with an inner cavity like a scab. Once completed this stage, digital saved information will be electronically transmitted to the new location where, through a 3D printer, a copy of the real object will be made.

The process makes us think of teleportation.

In case it wants to get a reply whose size can' not be made from a single printing, pieces will be executed which will be assembled finally like a puzzle. As noted above, the development of cavities leads to reduced materials consumption, reduced energy consumption and of course achieving a reply with a lightweight (a major advantage in case it needs repositioning or movement to a new location).

After any possible finishing and the critical visual inspection of the model obtained, this will be covered with a fine film of electrical conductive paint. Thus prepared, the obtained replica fixed to a metal carriage is placed in a vat of electrodepositing to be covered with a metallic layer so that it will provide the necessary hardness and look as close to as possible real.

The control of the electrodepositing process was realized based on WinCC software version 6.2., a program called "control program of electrodepositing process", (PCPE); with it we can view, modify and control the process parameters.

It enables communication with field elements of input/output type from PLC that manages the process. In addition to input signals corresponding to values of external variables, it also allowed the definition and use of internal tags running but only on local computer. In accord with current regulations about the noxious, the operator will be completely isolated from the area where the electrodepositing process develops.

He will introduce the process parameter values based on synopsis, displayed on the monitor, according to the data set for a given technological flux.

On this synopsis are marked positions parts during the process and state level solutions in vats.

When launched in execution, the PCPE will appear synoptic from Figure 2 with fields **Timp** (Time) and **Temp** (temperature) set to zero. Having prepared these fields, the operator will enter data starting from the right side, which corresponds to the area **SETARE PARAMETRI.**

In the **ELECTRODEPUNERE** field will enter the type of metallic material to be electrodeposited, the values of the surface to be covered in [mm^2] and the value which must thickness have, in [μm]. In the program, the name at the metallic material is associated with the values for density, valence and atomic mass. In that way it will reduce the time to introduce the initial data and eliminate the error of human factor.

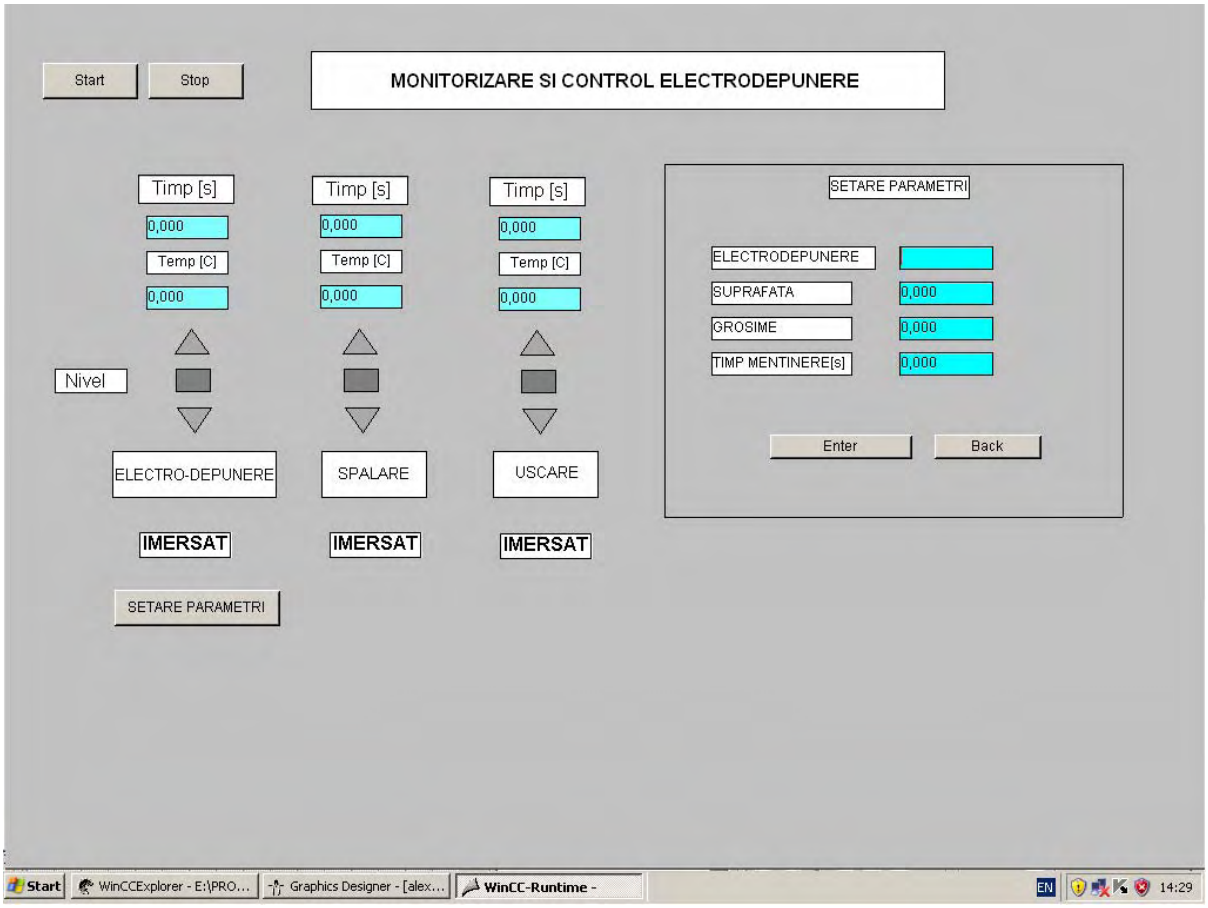

Fig. 2. *Synoptic 1 – Monitoring and control electrodepositing.*

Once these data entered, the **Enter** key will be press and in the field corresponding to maintenance time its value will be shown in seconds, calculated using the program, based on mathematical relations, according to the formula:

$$t = \frac{S \cdot \delta \cdot \rho \cdot z \cdot F \cdot \eta}{A \cdot I} \text{ [s]} \qquad (1)$$

The same value will appear in the field corresponding to electrodepositing time.

The program operates with material constants for chromium, nickel, copper, zinc, gold and silver. It can be used for other metallic materials by adding their specific constants. Values for current intensity and efficiency will be updated for each process and are specific to each installation.

Having calculated the value for maintaining time in electrodepositing vat we will go back in the left field **Monitorizare şi control electrodepunere** (**Back** key)**,** but which has now set all values for time and temperature. At this stage, a synopsis that monitors the whole process must have all the fields values completed.

With all these parameters set, it will start the process by enabling key ***START.*** Above each cell, it is shown the maintenance set time properly calculated and the temperature of vats solution. Pieces position in the area of certain tanks will be indicated by changes of colour field of corresponding vat in green, by correspondence with the associated tags and that the pieces are immersed in the solution will be flagged by the green colour field with inscription IMERSAT.

Indication of these positions is made on the received PLC signal from optical position sensors. PLC sends digital signal to the computer which through software will change the colour of the respective field.

Still with the help of synopsis is made indication of the level solutions in vats.

Based on the digital signal received from the sensors, the level will light one of those three indicators.

Normal is when the rectangle becomes green. Activating one of the two red triangles means exceeding or declining to maximum or minimum the rates required. Level adjustment is made by PLC which transmits simultaneously signal to the pump and solenoid (digital outputs).

The operator is able to manually break operation process by activating the ***STOP*** key**.**

This is necessary when damage occurs in the process or when process parameters need modification in order to obtain different thickness of coating.

4. Conclusions

The method enables the realization of replicas of art objects without direct physical contact made between an original object and the various stages of making its reply. The fact that reproduction is not accomplished through a matrix directly executed on the object allows the obtaining of replicas at different scales of art objects, depending on the needs. Also is not affected the integrity of the original. A museum can condense into a relatively small space a large number of artefacts (replicas) of art objects, made from a small-scale. On this way we have a very good control of the electrodepositing process for obtaining the best quality of the metallic material deposited layer. It also minimizes the negative impact of the noxious wastes that they may have on the environment.

References

[1]. Alexandru Stănescu - *Conducerea complexă a proceselor de protecţie anticorozivă prin depuneri metalice*, Teză de doctorat, Bucureşti, 2009;
[2]. B. Florea, P. Volintiru, Al. Stănescu, P. Vasilescu - *Program de simulare a conducerii proceselor metalurgice*, Ed. Fundaţiei Universitare Dunărea de Jos, Galaţi, Conferinţa Ştiinţifică *UgalMat*, 2005;
[3]. Al. Stănescu, B. Florea, A. Stănescu - *Stadiul actual şi necesitatea conducerii complexe a proceselor de acoperiri metalice prin electrodepunere,* Rev. METALURGIA, România, nr.1, 2009;
[4]. I. D. Gamburg - *Materialov i tehnologhi – Galvaniceschie pocrîtia*, Moscova, Ed. Tehnosfera, 2006;
[5]. Gh. Hagymaş, C. Firoiu, O. Radovici - *Coroziunea şi Protecţia Metalelor*, Bucureşti, Ed. Tehnică, 1963;
[6]. Ernest Grunwald - *Tratat de galvanotehnică*, Cluj-Napoca, 2005;
[7]. http://en.wikipedia.org/wiki/Electroplating
[8]. www.festo.com – documentatie tehnica Festo
[9]. www.**scan**ner3d.ro/
[10]. www.**printare3d**.ro/.../utilajul-de-**printare-3d**.html
[11]. www.bluenote.ro/index.php
[12]. www.visualart.ro › ... › 3D Graphics.

THE ANNALS OF "DUNAREA DE JOS" UNIVERSITY OF GALATI.
FASCICLE IX. METALLURGY AND MATERIALS SCIENCE
N^0. 2 – 2010, ISSN 1453 – 083X

ELECTROCHEMICAL CORROSION BEHAVIOR OF 7075 ALUMINUM ALLOY AFTER AGEING TREATMENT

Roxana ŞTEFĂNICĂ, Carmen NEJNERU, Vasile MANOLE, Ramona CIMPOEŞU HANU
Technical University "Gheorghe Asachi" of Iaşi,
email: r_carabet@yahoo.com

ABSTRACT

The electrochemical corrosion behavior of 7075 aluminum alloy subjected to different artificial ageing treatments maintaining times was examined. This aluminum alloy is typically used in aerospace structural components such as the wing spars of aircrafts and maritime industry as different mechanic parts. Heat treatments applied on this kind of alloys influence considerably the material properties like corrosion resistance.

The specimens from the electrochemical corrosion point of view were investigated in aerated and recirculated seawater solution – source Mediterranean Sea. Using a scanning electron microscope the material surface was analyzed before and after electro-tests following the microstructure, modifications, pitting holes appearance and the effects of corrosion tracked through EDAX and VoltaMaster results analysis.

KEYWORDS: electrochemical corrosion, aluminum alloy, artificial ageing.

1. Introduction

The corrosion behavior of metallic materials is determined not only by their chemical compositions but also by their microstructures [1].

Aluminum, a very reactive metal, forms a thin solid protecting film of oxide, which prevents the further corrosion of the material. However, in contact with solutions containing complex agents (i.e. halides), aluminum undergoes localized corrosion. Due to lightweight and high strength properties, the aluminum alloys find application in aerospace industries. Over the years, various protection methods have been developed to prevent the degradation processes of the aluminum and its alloys. Application of organic coating is a good way of taking advantage of the mechanical property of the metal while protecting it from corrosion. Adhesion of these organic coatings on aluminum is very poor and needs some pretreatment like chromating.

The chromate coatings are formed by immersion of clean substrate in an acid or alkaline solution containing hexavalent chromium Cr (VI), which provides corrosion protection [2]. The carcinogenic nature of chromate conversion coatings forces an alternative method and there is a high demand for a friendly environmental surface treatment. Localized corrosion (pitting, exfoliation, and intergranular attack) degrades fatigue performance of high strength of aluminum alloys [3–6].

The expense of replacing aircraft components as well as the intrinsic human variability and qualitative basis associated with corrosion grind-out techniques suggest the benefit of the next generation of damage tolerant prediction of the effect of existing corrosion on subsequent fatigue.

Introduced in 1943, alloy 7075 has been the standard workhorse 7XXX series alloy within the aerospace industry ever since. It was the first successful Al-Zn-Mg-Cu high strength alloy using the beneficial effects of the alloying addition of chromium to develop good stress-corrosion cracking resistance in sheet products. Although other 7XXX alloys have since been developed with improved specific properties, alloy 7075 remains the baseline with a good balance of properties required for aerospace applications.

This heat treatable alloy is considered high in strength. Corrosion resistance and workability is appreciated as fair, rated low on workability and welded only by the resistance process. Alloy 7075 is available in bare and alclad sheet and plate product forms in the annealed state as well as several tempers of the T6, T73 and T76 types.

Alloy 7075, a cold finished aluminum wrought product, has the highest strength of all aluminum screw machine alloys. The -T6 and -T651 tempers have a typical tensile strength of 83 ksi, which is higher than many mild steels. Due to its very high strength, alloy 7075 is used for highly stressed structural parts. Applications include aircraft fittings, gears and shafts, fuse parts, meter shafts and gears, missile parts, regulating valve parts, worm gears, keys, and various other commercial aircraft, aerospace and defense equipment. Rod and bar product forms can machine on multi-spindle and CNC machining equipment. Alloy 7075 has moderate corrosion resistance.

The overaged -T73 and -T7351 tempers offer good stress-corrosion cracking resistance as compared to the -T6 and -T651 tempers. (Caution: direct contact with dissimilar metals can cause galvanic corrosion.)

It is well known that aluminum and its alloys have excellent resistance to general corrosion except in solutions of low or high pH. The purpose of the present investigation was to study the corrosion and protection of aluminum alloy Al 7075 (UNS A97075) (1) in sea water [7].

In this study electrochemical corrosion behavior of this material in different heat treatment states, like artificial ageing or extra-ageing is analyzed and compared with cycling thermal heating at the same temperature, reduces the maintaining period from 5 to 7 cycles.

2. Experimental details

For these studies, a "7075" trademark aluminum alloy was used. This is an aluminum alloy with many applications, mentioned earlier in the introduction as having the composition:

Zn = 6.088%, Fe = 0.4980%, Mn = 0.31%, Si = 0.412%, Cu = 1.987%, Mg = 2.873%, Cr = 0.895%, Ti=0.21% and the rest is aluminum.

The manufacturer indicates that the 7075 base alloy is suitable for producing corrosion resistant long life metal frameworks and plate casting, easy to process and polish providing an aesthetic outlook. The material meets AMS 4154 (Extruded Shapes), AMS 4323 (Forging - Open Die) and ASTM B209 Directive prescriptions.

From this commercial material by hardening heat treatments, with different maintaining temperatures and cyclic treatments with a different cycle number samples were obtained and researched from the electrochemical corrosion behavior point of view.

Corrosion behavior was realized by rapid electrochemical tests, particularly by dynamic potentiometry.

The measurements of open potential circuit and potentiodynamic polarizations were performed on a VoltaLab 21 Electrochemical System (PGP201 - Radiometer Copenhagen) equipped with the acquisition and processing data software VoltaMaster 4. A three-electrode electrochemical cell was used [8]. From the prepared samples, the working electrodes performed in cylindrical form and mounted in a Teflon support to enable the connection to rotating port-electrode of the electrochemical cell. The free area was precisely measured before embedding in the Teflon support. A saturated calomel electrode (SCE) was used as a reference and platinum as auxiliary electrode.

Each specimen was polished with SiC paper, gradually, down up to 4000 grit specification, degreased with acetone and washed in distilled water.

As corrosion medium an aerated solution of Mediterranean sea-water was used, having the composition**:** Cl^- - 8.26: HCO^-_3 – 0.183; CO^{2-}_3 – 0.022; SO^{2-}_4 – 1.137; Na^+ - 4.47; K^+ - 0.158; Ca^{2+} - 0.203; Mg^{2+} - 0.557 and for this chemical composition the solution has a salinity of 15.0 g L^{-1}. Linear polarization measurements were performed, in aerated solution, at potentials near the E_{corr}, in the potential range ± 150 mV against the open circuit potential and a potential scan rate of 0.5 mV/s. The polarization resistance (R_p) was calculated as tangent slope at the electrode potential vs. current density curve in the E_{corr} point.

The cathodic Tafel slope (b_c) was calculated as the potential change over one decade (one order of magnitude) decrease in the current density at potentials near the E_{corr}. The anodic Tafel slope (b_a) was determined in a similar way.

Linear polarization method is used to determine when a test electrode is at its steady state. Polarization resistance is used to estimate the general corrosion rate of the metal.

Based on these data, the corrosion current density (J_{corr}) - which is a measure of the corrosion rate, was calculated with the Stern-Geary equation:

$$J_{corr} = \frac{b_a b_c}{2.3 R_p (b_a + b_c)} \qquad (1)$$

The corrosion rate, expressed as penetration rate - the layer thickness of the metal removed from the alloy surface in the time unity, was evaluated with the relation:

$$v_p = 3.27.\overline{\left(\frac{A}{z}\right)}.\frac{J_{cor}}{\rho} \quad , \mu m/year \qquad (2)$$

where: A – is the atomic mass of the corrodible metal (g/mol), z – number of electrons changed in the corrosion process, ρ - density of the removed component (g/cm^3) and J_{corr} – instantaneous current density (μA/cm^2). After the electrochemical treatments, a study of the modifications of the alloys surface was performed on a VEGA-TESCAN

Scanning Electron Microscope equipped with QUANTAX Bruker AXS Microanalysis system.

3. Experimental results

Investigations of material 7075 in equilibrium state, using an AES equipment reveal compounds like MgZn and $Al_{4.2}Cu_{3.2}Zn_{0.7}$, but other energies equivalent to compounds like Mg_2Si, Al_3Mg_2, $AlCr_2$, AlCu, Al_2Fe, Al_5Fe_2, Al_6Cu_2Fe, Al_2CuMg, Al_6CuMg_4, $Al_{23}CuFe_4$ [9-11] were observed on energy spectrum but with difficulties of being separated from all the spectrum energies. Scanning electron microscopies of the material, helping to determine the alloy compounds by their crystallization system, are presented, in fracture, in Figure 1 at 100 a) and 5000 b) orders of magnitude.

Surfaces examination of the specimens showed that microstructure is compact with different compounds formed on the surface of the specimen and with appearance of the pits. Other studies have found that pits were the initiators of cracks as well [12–17]. Multiple pit sites could be found on coupons in all the highest stress levels (i.e., DS = 700 MPa and DSsc = 350 MPa), and in most cases cracks would be initiated from several sites where pits could be found on the surface of the specimen. It is believed that these pits formed at the site of inclusions (such as particles of $Al_{23}CuFe_4$, and Al_2CuMg.) These inclusions are typical in heterogeneous alloys such as 7075-T651 [14, 16].

Anodic slip dissolution appears to be in the dominant mechanism for many cases of crack propagation in high stress regions, while pitting was the cause of crack propagation in specimens subjected to lower cyclic stress levels [18].

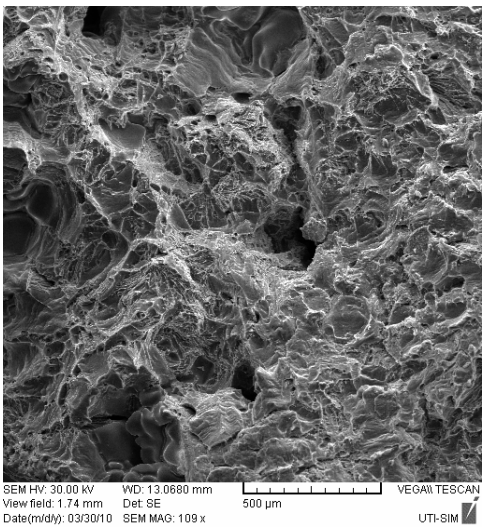

a)

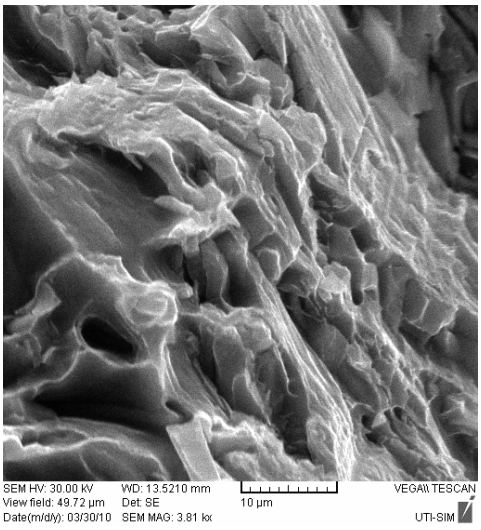

b)

Fig. 1. *Magnification of fracture surfaces by SEM microscopies of aluminum based alloy equilibrium state a) 100 and b) 5000 x order of magnitude*

The electrochemical corrosion tests were carried out on samples heat treated by going to 120°C temperature and maintaining them at different time periods like 8, 10 or 14 hours.

In the first two cases the alloy is reaching a classical artificial ageing time that in 14 hours maintaining case the material, under precipitates increasing and connecting, reach an extra-ageing.

Having the intension of studying the effects of cyclic treatments applied on this aluminum type of alloys three different numbers of cycles like 3, 5 or 7 with temperature increasing at 120 °C as well and maintaining for them 20 minutes, in order to analyze and compare the material behavior, for all six cases, at electrochemical corrosion.

In Figure 2 are presented SEM microscopies, at 1000-x order of magnitude, for all treatments applied. The images were realized with a secondary detector using a 10 mm working distance and a 7 scanning rate.

All microstructure surfaces look affected by electrochemical corrosion test; the material under cyclic treatments seems to be cleaner. The worst behavior, as it was expected from scientific literature [19], was the extra-agenized material with 14 hours maintaining that presents a pitting affected surface, similar with the other samples, but also many chemical new compounds on the area different from the base material.

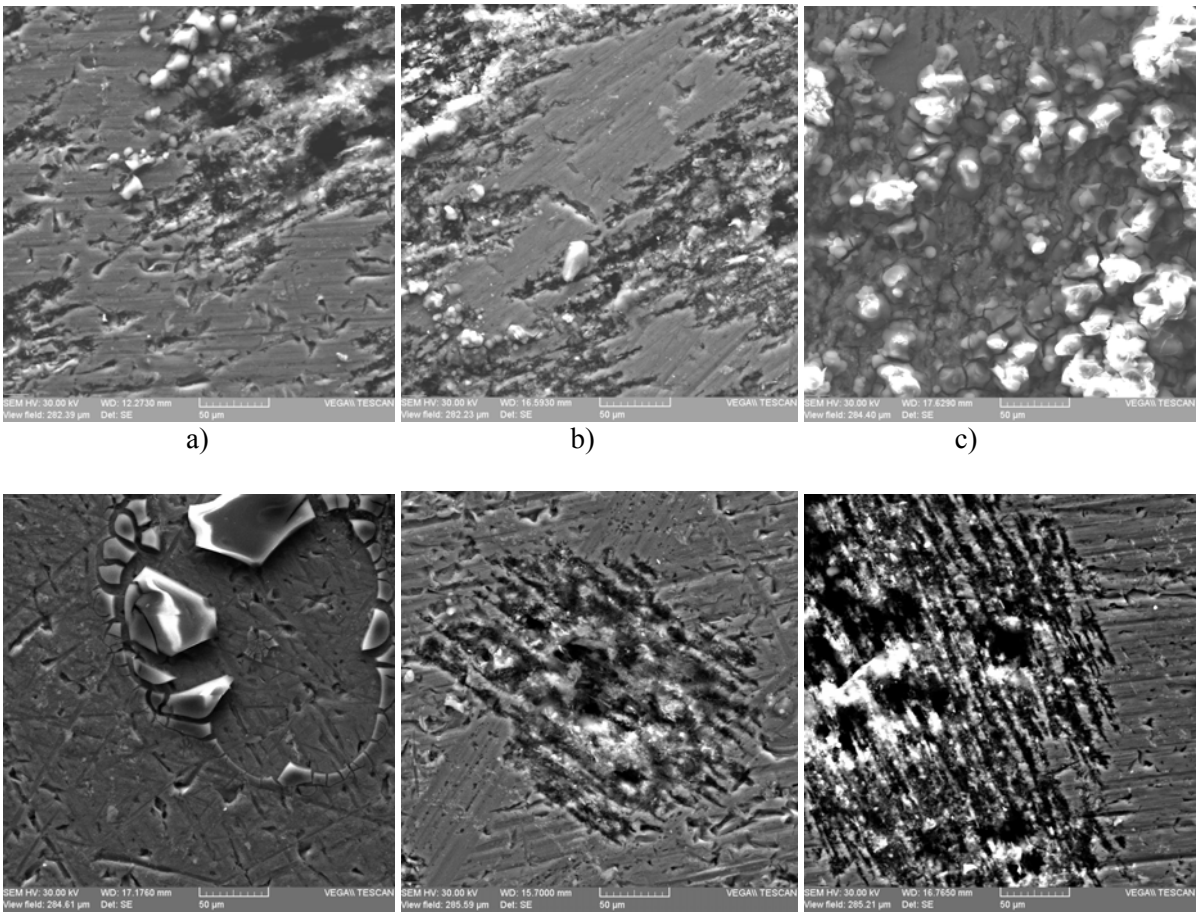

a) b) c)

d) e) f)

Fig. 2. *Surface of 7075 alloy after different treatments applied like artificial aging for a) 8 hours b) 10 hours c) 14 hours or cyclic treatment of d) 3 cycles e) 5 cycles and f) 7 cycles*

Realizing the chemical compositions, with the EDAX equipment, after electrochemical corrosion test on a 285 μm (1000x amplifying power) after 10 areas average for each sample, the normal wt. % percentage of the elements are presented in Table 1.

In Table 1 are analyzed the elements of the 7075 material and the sea water corrosion solution as well looking for modifications on percentages to conclude which state is better from this point of view. At a first look, the aluminum behaves better in all cyclic treated samples having bigger percentage of this chemical element with a very big difference compared to the sample over maintained.

The presence of oxygen and the oxides appearance produce a passivation process of the material increasing the corrosion resistance but an increase percentage value represents the formation of many types of oxides.

Table 1. *Chemical compositions of the investigated material in different states*

Chemical element [wt %]/ Alloy state	**Al**	**Fe**	**O**	**Zn**	**Si**	**Mg**	**Cu**	**Na**	**Cr**	**Mn**	**Ti**
Aged 8 hours	62.122	1.068	16.369	4.321	3.267	1.79	1.71	0.547	0.89	0.503	0.35
Aged 10 hours	69.468	1.097	17.980	4.831	3.064	1.85	0.70	1.01	0.15	0.515	0.28
Aged 14 hours	48.95	0.665	42.089	0.191	1.26	1.29	1.04	1.55	0.19	0.26	0.91
Cycled 4 times	71.09	1.489	19.012	5.373	1.67	1.24	0.54	0.12	0.62	0.66	0.75
Cycled 6 times	78.022	0.203	12.942	4.842	1.31	2.09	0.58	0.11	0.56	0.68	0.735
Cycled 7 times	73.67	0.228	14.654	5.431	1.45	1.68	0.62	0.35	0.52	0.55	0.59

Losing percentages of materials like aluminum or copper automatically increases the other amounts like iron, silicon or manganese [8]. The element with a weak behavior, obvious in the sample aged for 14 hours, is zinc that in extra-ageing case, probably based on what compounds are formed decreases substantially from 6,088 to 0,191 percentages. The potassium percentage indicates the salts compounds formed on the surface and affects the corrosion resistance playing a pitting starting point roll, small amounts of this element being found in every corroded hole. The corrosion potential in quasi equilibrium conditions (obtained at lower potential scan rate), $E_{0,}$ is more negative for the agenized samples than for the cyclically treated samples. Accordingly, the instantaneous current density and corrosion rate are lower in the case of the second treatments applied on the alloy.

However, the differences regarding the corrosion behavior of the samples in sea water solution are relevant by comparing those two applied treatments and by selfless comparison between them.

More over, the values of the corrosion rates are very high in some cases, indicating a reduce corrosion resistance of this alloy excepting the 3 cycles applied sample.

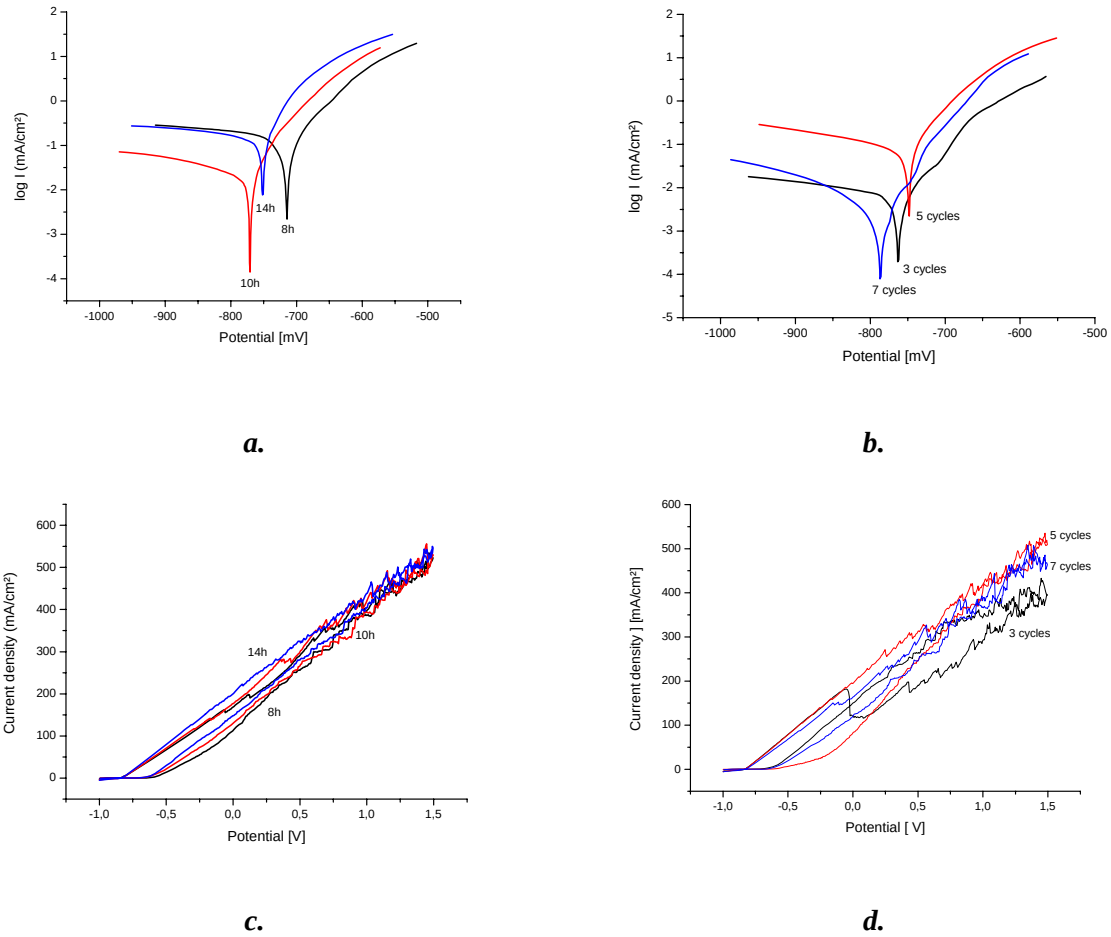

Fig. 3. *Linear potentiodynamic polarization curve a) 8, 10 and 14 hours aged samples, b) 3, 5 and 7 cycles and single cyclic polarization curve c) 8, 10 and 14 hours aged samples and d) 3, 5 and 7 cycles.*

Linear potentio-dynamic polarization curves and single cyclic polarization curves are presented in Figure 3 expressing a higher corrosion character in aged samples, facts observed in Table 2 as well in all characteristics especially the informative corrosion rate per year (Vcor) with approximate values.

All the cyclic diagrams, Figure 3c) and d), represent the pitting character of the corrosion with smaller values in cyclically treated sample case. The cyclic voltammograms of all six samples show a very close similarity (Fig. 3 (c and d)); excepting the 5

cycles heat-treated sample the other curves practically overlap.

The recorded curves revealed the passive region over a large domain of potential, from a negative value to the breakdown potential situated at 557 and 523 mV (SCE) respectively.

At over-potentials higher than the breakdown potential, the corrosion currents increase appreciably and vary linearly with electrode over-potential, indicating a direct dependence between corrosion current and over-potential.

Table 2. *Corrosion parameters evaluated from linear and cyclic polarization curves*

Sample	Linear polarization					
	E_0	b_a	b_c	R_p	J_{cor}	v_{cor}
u.m.	[mV]			[kΩ.cm^2]	[μA/cm^2]	
8 hours	713.5	91.3	2638.5	180.65	0.2432	≈ **2904**
10 hours	770.2	72.9	2834.3	773.22	0.0634	≈ **741.6**
14 hours	751.7	50.8	1068.8	108.6	0.1814	≈ **2121**
3 cycles	762.6	60.1	710	2.92	0.0095	≈ **111.22**
5 cycles	749.4	54.2	363.3	208.5	0.0842	≈ **917.42**
7 cycles	785.8	66.7	703.4	7.94	0.0250	≈ **293.34**

The anodic and cathodic branches of the polarization curve in this domain practically overlap, except for the potential range between E_{BD} and E_{RP}, where a small hysteresis loop appears. The voltammogram shapes indicate rather a pitting corrosion in spite a general corrosion. Scanning Electron Microscope (SEM) studies presented in Figure 2 confirm this assertion.

The most representative parameter, the corrosion rate per year, reveals a very good resistance of sample cycled for these times, around 111.22 μm, but all the others are quite big, 741-2990 μm, for a material used in practical applications in contact with other metallic materials working in an electrolytic solution like a marine medium.

4. Conclusions

– A material with many practical applications and superior mechanical properties was analyzed from the electrochemical corrosion point of view in a sea water solution.

– Trying to improve this important property, six different heat treatments based on ageing and cyclic treatment were applied studying the obtaining costs, properties modification and corrosion behavior.

– Appreciating the amount of material loss in electrochemical corrosion process for ageing treated samples can be considered dangerous for any applications in a seawater environment.

– The cyclic treated samples present, in all cases, a better behavior at electrochemical corrosion having the advantages of a lower cost production as well.

References

[1]. K.M. Gruenberg, B.A. Craig, B.M. Hillberry, R.J. Bucci, A.J. Hinkle - *Predicting fatigue life of pre-corroded 2024-T3 aluminum,* Intl. J. Fatigue 26 (2004) 629– 640.

[2]. S. Kim, J.T. Burns, R.P. Gangloff - *Fatigue crack formation and growth from localized corrosion in Al–Zn–Mg–Cu*, Eng. Fract. Mech. 76 (2009) 651–667.

[3]. K. Sharp, T. Mills, S. Russo, G. Clark, Q. Liu - *Effects of exfoliation corrosion on the fatigue life of two high-strength aluminum alloys,* Aging Aircraft 2000, FAA/DoD/NASA, 2001.

[4]. B.R. Crawford, C. Loader, A.R. Ward, C. Urbani, M.R. Bache, S.H. Spence, D.G. Hay, W.J. Evans, G. Clark, A.J. Stonham - *The EIFS distribution for anodized and pre-corroded 7010-T7651 under constant amplitude loading,* Fatigue Fract. Eng. Mater. Struct. 28 (2005) 795–808.

[5]. R.P. Gangloff, J.T. Burns, S. Kim - *Laboratory characterization and fracture mechanics modeling of corrosion–fatigue interaction for aluminum alloy substitution,* Final Report, Contract F09650-03-D-0001, WPAFB, OH, 2005.

[6]. D.L. DuQuesnay, P.R. Underhill, H.J. Britt - *Fatigue crack growth from corrosion damage in 7075-T6511 aluminium alloy under aircraft loading,* Intl. J. Fatigue 25 (2003) 371–377.

[7]. E. McCafferty and P. Trzaskoma-Paulette - *Dissolution and Protection of Aluminum Alloy 7075 in Hydroxide Solutions,* Journal Corrosion Volume 53, Number 03, 1997, NACE International, Paper Number 97030179.

[8]. Carmen Nejneru, Nicanor Cimpoeşu, Sergiu Stanciu, Petrică Vizureanu, Andrei Victor Sandu - *Sea water corrosion of a shape memory alloy type cuznal,* Metalurgia Internaţional Editura Ştiinţifică F.M.R. vol. XIV, special issue nr. 7, 2009 pg. 95-105

[9]. Masatsugu Kamiya and Takao Yakou, *Role of second-phase particles in chip breakability in aluminum alloys International Journal of Machine Tools and Manufacture,* Volume 48, Issue 6, May 2008, Pages 688-697.

[10]. Ming Gao, C.R. Feng and Robert P. Wei - *An analytical electron microscopy study of constituent particles in commercial,* Metallurgical and Materials Transactions A, Springer Boston Issue Volume 29, Number 4 / April, 1998, Pages 1145-1151, DOI 10.1007/s11661-998-0240-9.

[11]. Jacob L. Cartner, Warren O. Haggard, Joo L. Ong, Joel D. - *Bumgardner Stress corrosion cracking of an aluminum alloy*

used in external fixation devices, Journal of Biomedical Materials Research Part B: Applied biomaterials, volume 86B, Issue 2**,** Pages 430-437, Published Online.

[12]. Shi P, Mahadevan S. *Damage tolerance approach for probabilistic pitting corrosion fatigue life prediction*. Eng Fract Mech 2001;68:1493–507.

[13]. Rokhlin SI, Kim J-Y, Nagy H, Zoofan B. *Effect of pitting corrosion on fatigue crack initiation and fatigue life.* Eng Fract Mech 1999;62:425–44.

[14]. Duquette DJ, Corsetti LV. *The effect of mean stress and environment on corrosion fatigue behaviour of 7075-T6 aluminum.* Metall Trans 1974;5(May):1087–93.

[15]. Wan K-C, Chen GS, Gao M, Wei RP. *Interactions between mechanical and environmental variables for short fatigue cracks in a 2024-T3 aluminum alloy in 0.5M NaCl solutions.* Metall Mater Trans A 2000;31A(March):1025–34.

[16]. Jabubowski M. *Fatigue, Crack propagation in austenitic stainless steel under low frequency loading and salt water conditions.* Fatigue Fract Eng Mater Struct 1998;21:937–46.

[17]. Hasse I, Nocke K, Worche H, Zouhar G, Tempus G., *An investigation of the fatigue behaviour of aluminum alloy AA 6013 T6 in a corrosive medium.* Prakt Metallogr 2001;36(3).

[18]. R.M. Chlistovsky, P.J. Heffernan, D.L. DuQuesnay, *Corrosion-fatigue behaviour of 7075-T651 aluminum alloy subjected to periodic overloads* International Journal of Fatigue 29 (2007) 1941–1949

[19]. Lin C-K, Yang S-T. *Corrosion fatigue behaviour of 7050 aluminum alloys in different tempers.* Eng Fract Mech 1998;59(6):779–95.

THE ANNALS OF "DUNAREA DE JOS" UNIVERSITY OF GALATI.
FASCICLE IX. METALLURGY AND MATERIALS SCIENCE
N^0. 2 – 2010, ISSN 1453 – 083X

CHARACTERISATION OF NIOBIUM CARBIDE COATING OBTAINED BY CHEMICAL VAPOUR DEPOSITION

Stela CONSTANTINESCU
"Dunarea de Jos" University of Galati
email: stela.constantinescu@email.ro

ABSTRACT

The experiments conducted to obtain thin layer of carbide by the vapour chemical deposition method have followed an original path to make NbC directly in the working room thus avoiding the import of these hazardous substances. The $NbCl_4$ vapoursare obtained in a heat treatment chamber by adding chloride acid vapours passed over the incandescent ferro-niobium.

Characterisation of coating deposed by CVD method was done using scanning electron microscopy (SEM), X-ray diffraction (XRD) and microhardness measurements. The thickness of the NbC layer was determined using an optical microscope and the Kalotest device. The thickness of the CVD deposit layer increases with the time of exposure to the working temperature. The values of the NbC thin layers measured by the Kalotest device are in good agreement with the values measured by microscopic analysis but slightly lower. SEM measurements were used to investigate the coating morphology and interface structure. X-ray mapping was also performed to identify the chemical elements in a semi-quantitative analysis. Dron X-ray diffractometer with Mo K_α radiation operating was used for phase(s) identification.

KEYWORDS: thickness, NPCVD, widia, layers, interface, microhardness, pressure.

1. Introduction

The vapour chemical deposition is a widely spread method of making thin layers. It has been gaining ground lately as opposed to the conventional vapour, chemical and special deposition procedures.

Compared with the other methods, the vapour chemical deposition features the following advantages: highly pure thin layers obtained by a suitable choice of the initial materials and reactions; perfectly crystalline layers due to growth under appropriate equilibrium conditions, relatively high temperatures possibility to cover the samples with thin layers of complex shape, the process is and can be automated and adapted to full scale processing of a large number of sub-layers. [1]

If the vapour chemical deposition takes place within a tubular continuous reactor, a gas carrying the reacting species is passed over the sub-layer.

At the sub-layer surface, the reacting elements undergo a number of chemical reactions leading to product formation. Part of the products are deposited on the sub-layer and part of it goes back to the gas stream.

Before examining the vapour chemical deposition reactions it must be determined if the reaction is thermodynamically possible. The reaction will be thermodynamically possible if the calculated concentrations (partial pressures) of the reactants, under equilibrium conditions, are less than their original concentrations. The calculation of the equilibrium concentrations from the equilibrium constant involves a good choice of the number of gas spaces which can be higher than two and the number of independent relations. A relation implies the equilibrium expression depending on the free standard reaction energy and temperature. The other relation consists in that the system pressure is the sum of the partial pressures. If some reactants possess more than one valence state, the reaction should contain the reactant under its most stable valence state. [2]. Hard alloys made out of metallic carbides manufactured to an industrial scale for cutting processing can be divided in two categories, according to their use. The second category of industrial products comprises the alloys out of many carbides used in cutting process of materials with long and continuous chips (all sorts of steel).

2. Methods

2.1. Materials

S.N.U.N. 15.04.08 type NbC coated and uncoated samples have been investigated. Active and constructive dimensions of samples S.N.U.N. 15.04.08. used were: α= 8, γ=4, χ =40, λ= 0.

For this purpose for samples preparation the maximum limit of the cutting speed was taken higher than the usual speeds to obtain plate durability under the most difficult operation condition which should not excessively increase the time of the experiments and the material consumption. [3].

2.2. Deposition Method

The experiments conducted to obtain a thin layer of carbide by the vapor chemical deposition method have followed an original path to make $NbCl_4$ directly in the working room thus avoiding the import of these hazardous substances. The $NbCl_4$ is obtained in the heat treatment chamber by adding chloride acid vapors passed over the incandescent pure titanium. Lab-scale systems have been designed with the possibility of use at industry scale for small production. The support temperature was established at about 1130^{o}C so that the NbC can provide a suitable deposition of the thin NbC layer. The thickness of the deposit layer increases with the time of exposure to the working temperature. The NbC coated plates feature higher endurance capabilities than those uncoated for the same cutting speed both for steel and white cast iron.

2.3. Characterization

The characterisation of the coating deposed by CVD method was done using scanning electron microscope (SEM), X-ray diffractometer (XRD) and microhardness measurements. The thickness of the NbC layer was determined by the microscope and the Kalotest device. [4].

The parameters of the cutting conditions were chosen in the range of the values used on the working machines at the Arcelor Mittal Steel Galaţi.

The advance(s), is 0,096 mm/rot and deep cut (t) is 0,5 mm, respectively for all the samples.

Table 1. *Domains of the parameters values of the cutting conditions*

Rot. speed, n, [rot/min]	450	500	530	570	610	630
Speed cutting, v, [mm/min]	110	123	130	140	150	154

In Table 1 the values of the parameters of the cutting conditions for S.N.U.N. 15.04.08.are shown.

The operation of the latter is based on a housing which cuts the deposited NbC layer. The values of the thin NbC layers as measured by the Kalotest device are in good agreement with the values measured by microscopic analysis but slightly lower. Samples for metallography were prepared by polishing, this prevented damage to the dissimilar interface (strate – substrate) during polishing. SEM was used to investigate the coating morphology and interface structure. X-ray mapping were also performed to characterise the elements in a semi-quantitative analysis. Dron X-ray diffractometer with Mo K_α radiation operating was used for phase(s) identification. Microhardness was determined by Neophot Micromet micro-hardness tester at a load of 100 gf. [5].

3. Results and discussion

Mention must be made that the optimum layers in the cutting process are the NbC layers having thickness within 4 - 10μm above these values, the layers lose tenacity and become fragile. As result of the thermal treatment which means heating up to 1130^{0}C degrees for various exposure times, layer thickness within 2,5 - 15μm was achieved .[6,7]. The plates were covered with an adherent coat of NbC of yellow color.

The thickness of the thin layers increases with the time of exposure to the working temperature as illustrated in Fig.1.

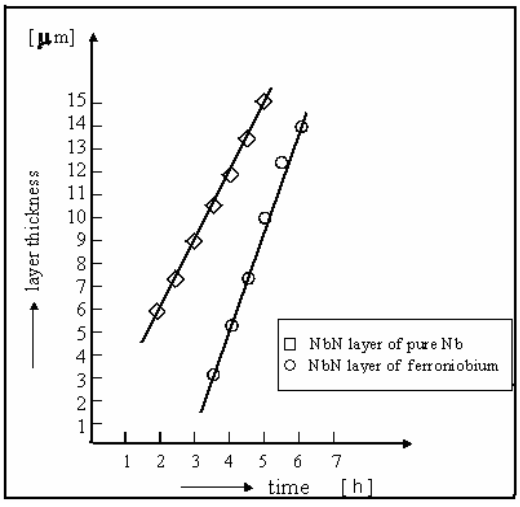

Fig.1. *The thickness of the thin NbC layers increases with time.*

Micro-hardness of WC-NbC-Co alloys is affected by a large number of elements connected to the raw material, purity and component dispersion in the alloy and the solid solution quality and grain size of components. In the factory process, these elements are

playing an ultimate role in the effective micro-hardness measurement of the material with a given chemical composition (Fig.2).

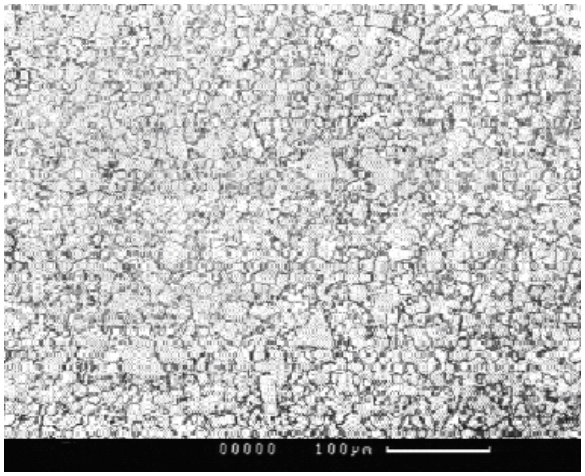

Fig.2. *Metallographic appearance of alloy with 80%WC, 18%NbC, 6%Co.*

Micro-hardness is not a constant like Vickers hardness, in spite of the geometrical similarity, but decreases with higher testing charges depending on the size of the print.

The micro hardness tests show that we have NbC, value $HV_{0,05}$ = 29500 MPa is in good agreement with the data from the literature.

Measurements were made on NbC covered thin plates which thickness range between 6, 8 and 10µm. [8]. Micrography, Fig. 3, 4, 5, shows an adherent layer which is uniform and homogenous over the entire depth.

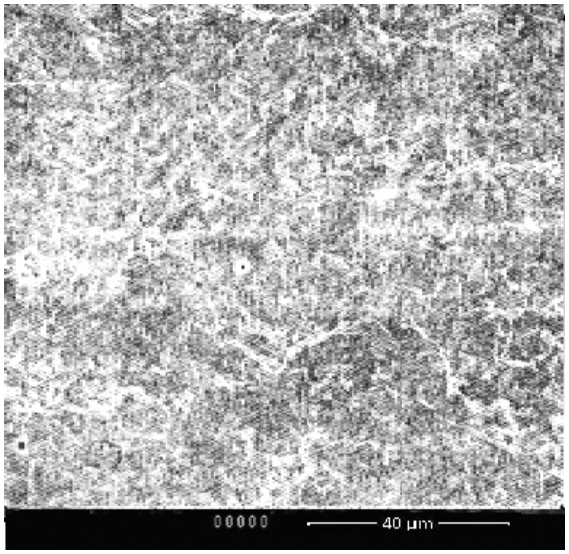

Fig.3. *SEM image (micrograph) of an uncoated plate surface.*

Figures 3 and 4 show superficial aspects of the layers deposited by CVD compared to the monolayer NbC uncovered a plate appearance, classic, studied by electron microscopy. It is clear difference in size of crystals of layer size and size uniformity and surface roughness [9].

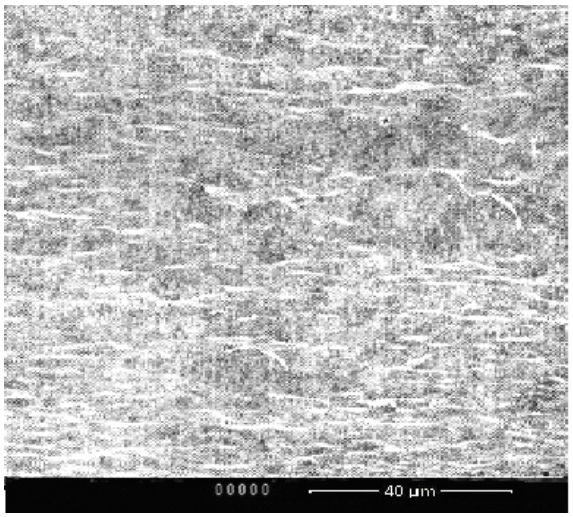

Fig. 4. *SEM image of the monolayer covered surface of NbC.*

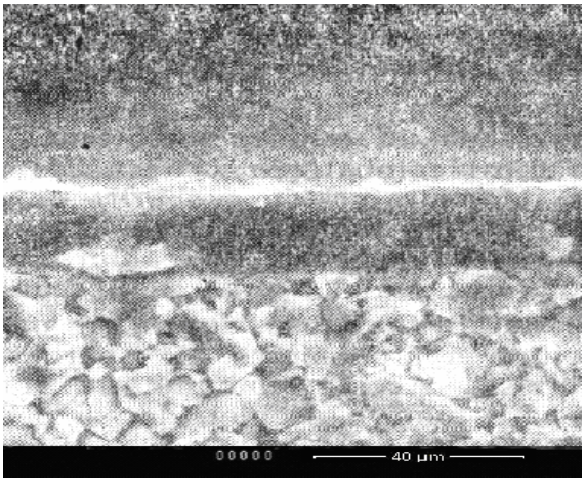

Fig.5. *SEM cross section of NbC sample covered with a 6µm NbC.*

In Figure 5, the metallographic appearance is set for good quality coated plates. NbC coating is composed of uniform thickness and the grain, have crystal columnar layer. Almost uniform grain isomorphic layer and its purity ensure proper behavior at cutting premises [10].

As regards the requirements imposed on the substrate, they have the maximum compressive strength combined with good impact resistance, good tensile strength at bending, and a high temperature and good resistance to thermal shocks.

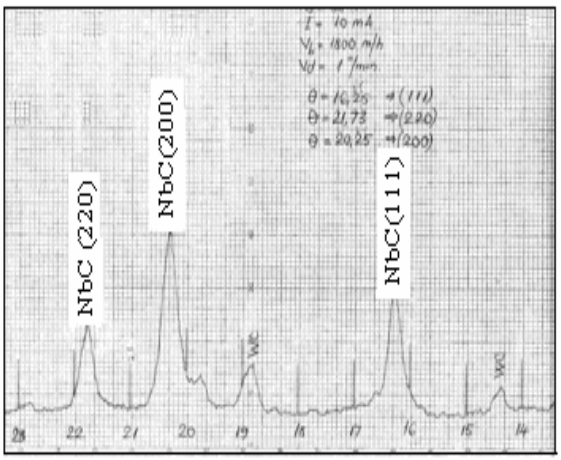

Fig.6. *X- ray diffraction spectrum of NbC coating.*

The best results are obtained for layer depth of 8 μm, with homogeneous and even structure, a feature that can be emphasized by means of diffraction pattern analysis, Fig. 6. The values of the thin NbC layers as measured by the Kalotest (Fig.7) device are in good agreement with the values measured by microscopic analysis but slightly lower.

The thickness of the layer deposited increases with the time of exposure at the working temperature.

The steel ball diameter is 12 mm. Since the shell diameter is much less than the one of the ball, the layer thickness can be calculated by the values x and y from the relation below:

$$S = \frac{x \cdot y}{R}$$

Where: R= the steel ball rase.

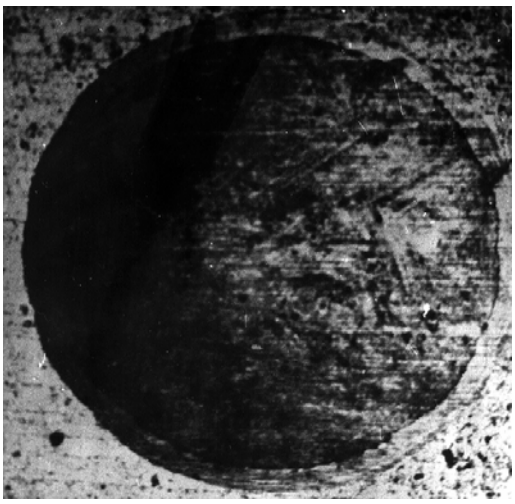

Fig.7. *The sphere shell of NbC by the Kalotest.*

As seen in Figures 8, 9, 10, uncoated surface NbC samples have surface oxides by 70% if the samples coated with the thickness of 6μm NbC have slight traces of surface oxides on 5% non-stick surface and covered with NBN samples with thickness of 8μm surface shows no oxides. It is noted that in corrosion test in water, samples covered with NbC channel are stronger compared to uncoated NbC samples.

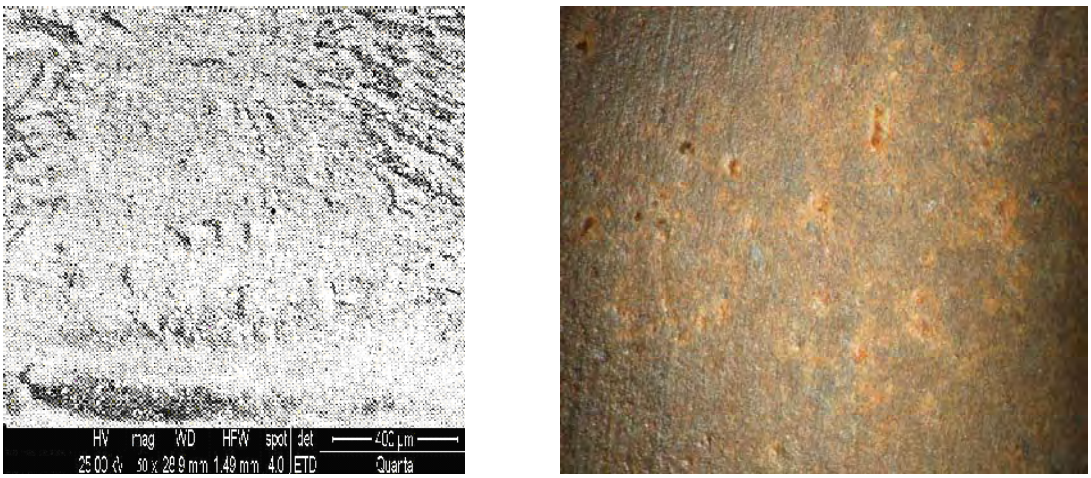

a) *b)*

Fig. 8. *Surface of uncoated NbC samples: a) before corrosion, b) after corrosion.*

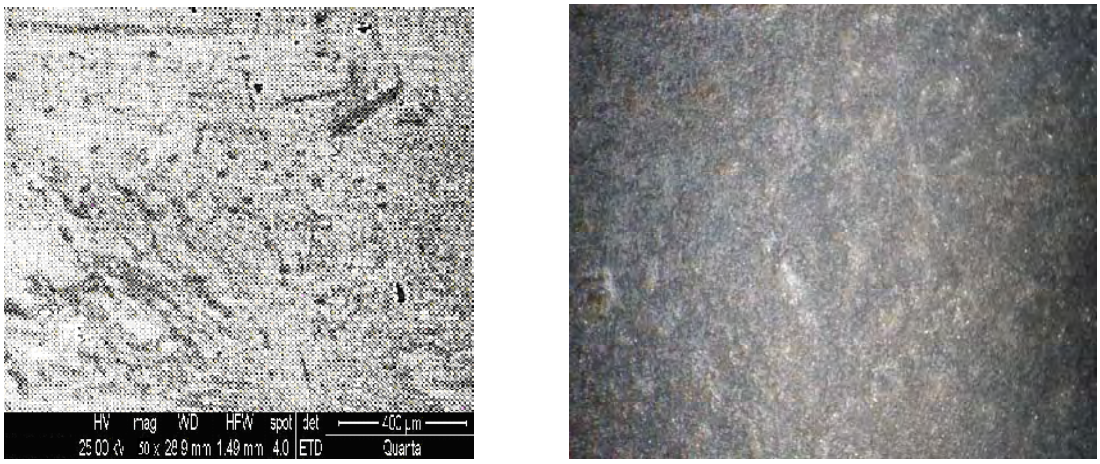

a) *b)*

Fig. 9. *Surface of covered NbC samples 6 µm: a) before corrosion, b) after corrosion.*

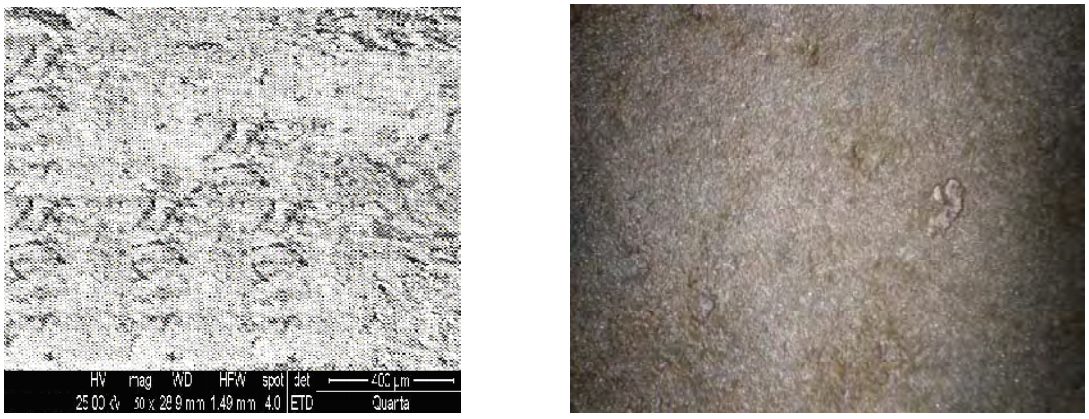

a) *b)*

Fig. 10. *Surface of covered NbC samples 8µm: a) before corrosion, b) after corrosion.*

4. Conclusions

The obtained coatings have good wear resistance, abrasion resistance, corrosion resistance and a strong layer -sub layer interface. This leads to formation of thick and rough coating. The coating is finely grained, adherent, dense and fee from cracks. However, some porosity is observed in the coating layer. The widia plates coated with NbC thin layers entirely suppress the inconveniences of a relatively rough topography of the common sinterized carbides while preserving the adequate material mechanical strength. The thickness of the NbC thin layers increases with the time of coating. The layer begins loosing its tenacity if its thickness increases considerably exceeding the thickness of 10µm mainly due to the lower strength characteristics. This together with the increase in the inner tensions results in cracks and breakings in the layers. This has been attributed to poor wetting characteristics. Corrosion test in water of the samples covered with NbC show better corrosion behavior with respect to the uncovered ones.

References

[1]. S. Constantinescu - *Metals properties and physical control methods*, Didact. and Pedag. Publishing House, ISBN 973 – 30 – 1709 - 4 Bucharest, Romania, 2004
[2]. S. Constantinescu, L. Orac - *Materials properties and control methods*, Ed. Europlus, ISBN 978-973-1950-01-3, Galati, 2007
[3]. S. Constantinescu, T. Radu - *Advanced methods of obtaining thin coats,* Ed.Ştiinţifică F.M.R. ISBN 973-8151-25-2 Bucureşti, 2003
[4]. A.Y. Cho, J.R. Arthur -*Progress in Solid State Chemistry*, Ed. Pergamon Presa, New York vol. 10, 1995, p. 157- 164
[5]. C. Ciocardia et all - *Hard alloys sintered from metallic carbides*., Bucharest, Technical House, 1984, p.103-112
[6]. S. Constantinescu - *Studies on Thin Carbide and Nitride Layers Deposition on Metal Basis, Based on Chemical Reaction at High Temperatures*, Academic Thesis, Galati, 1998.
[7]. ******** *Bimetallic corrosion*, Guides to good practice in corrosion control, www.npl.co.uk
[8]. A. Tomescu, M. Constantinescu - *Chemistry and corrosion*, Didact. and Pedag. Publishing House Bucharest, Romania, 1985
[9]. C.E. Morosanu, V Solluz - Thin Solid Films 52, 1978, p.181-190
[10]. T. O. Sedgwick, H. Lydtin - *Eds, CVD*, Seventh International Conference, The Electrochem. Soc., Inc., Princeton, New York.

THE ANNALS OF "DUNAREA DE JOS" UNIVERSITY OF GALATI.
FASCICLE IX. METALLURGY AND MATERIALS SCIENCE
N^0. 2 – 2010, ISSN 1453 – 083X

THE INFLUENCE OF THE HEAT TREATMENT UPON THE RESISTANCE TO CORROSION OF THE COMPOSITE OBTAINED USING THE ELECTRODEPOSITING OF TiO_2 IN A NICKEL MATRIX

Raul NOVAC, Olga MITOSERIU
"Dunarea de Jos" University of Galati

ABSTRACT

The resistance to corrosion of a composite material obtained using the electro-depositing of TiO_2 in a nickel matrix subjected to heat treatment was studied using the galvanostatic method; the samples were obtained by the electrodepositing of TiO_2 (60%) in a nickel matrix on a copper basis. A Watts electrolyte was used for the electrodepositing. The resistance to corrosion of a sample without composite layer was compared with the resistance to corrosion of a sample with a composite layer subjected to heat treatment.

KEYWORDS: composite coatings, nickel matrix, electrochemical depositing, TiO_2 particles.

1. Introduction

One of the methods by which we can obtain a composite material is electrodepositing.

The process of electrodepositing of the composite layers consists of including solid particles in a suspended state into a bath of electrolyte in the metal that electro-crystallizes and which constitutes the metallic matrix. These particles are considered insoluble. The electrochemical joint depositing cannot be regarded as an electrochemical process separated from the electrodepositing of the metal itself.

Generally speaking, the electrodepositing of a metal on a base material can have as goal the increase of the resistance to corrosion and the wear of the respective part or the improvement of the aspect of the part using decorative depositing.

2. Experiment

The electrodepositing of the composite layer was obtained using continuous current with the help of a potentiostat, measuring instruments and electrolytic cell.

The samples with a surface of 12 cm^2 were made from copper. For the electrodepositing a Watts electrolyte was used having the following composition:

- $NiSO_4 \cdot 7H_2O$.....250g/l
- $NiCl_4 \cdot 6H_2O$.....50g/l
- H_3BO_3 .....40g/l

The temperature of the electrolyte was 50±2ºC, pH 3, bustling 750 rot/min, the time for the electrodepositing being 120 minutes, the percentage of powder in the electrolyte is between 20-80%.

After the electrodepositing process the samples were dried and afterwards heat treated in a protected atmosphere with the following parameters:

- The temperatures used: 500ºC and 700ºC
- Time 60 minutes
- Furnace cooling

After the heat treatment the micro-strength of the deposited layer was measured and the resistance to corrosion using the Taffel curves was calculated.

3. Results and discussions

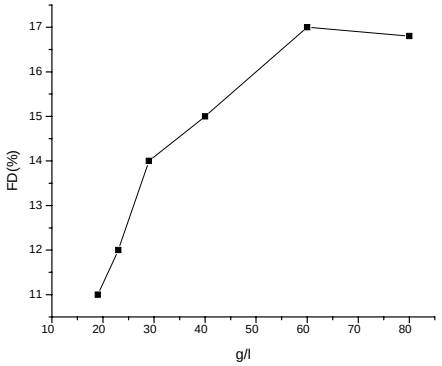

Fig. 1. *The variation of the dispersed phase in the composite layer depending upon its concentration in the electrolyte.*

By modifying the parameters of the electrodepositing there are obtained needle like shapes in which the percentage of the dispersed phase may vary according to Fig.1

3.1 The micro-strength

By using the above mentioned parameters of the electrodepositing it is obtained a composite layer of TiO_2 (17%) in the nickel matrix.
The heat treatment influences the deposited layer strength. The results are shown in the Table 1.

Table 1. *The variation of the micro-strength depending on the temperature of the heat treatment*

Sample	Micro-strength [HV_{50}]
Sample without composite covering	180-200
Untreated sample	400-420
Heat treatment at 500ºC	750-770
Heat treatment at 700ºC	530-550

It can be noticed an increase i the micro-strength in the case of the samples with electrochemical covering compared to those without covering and an increase of the micro-strength of the samples treated at 500ºC compared to the untreated samples; this increase is due to the difference between the expansion coefficient between the layer and the sub-layer which leads to the appearance of certain tensions in the deposited layer. The increase in temperature of the heat treatment at 700ºC leads to a decrease of the micro-strength of the samples.

3.2. Resistance to corrosion

The copper samples were covered using electrodepositing, subjected to heat treatment and afterwards it was checked the resistance to corrosion using electrochemical tests in a solution of NaCl 15%.

There were calculated for each sample the corrosion index and the penetration index; the results are presented in the table 2.

Table 2. *The parameters of the corrosion*

Sample	I_{cor}[mA]	I_p[mm/year]
Sample without compound layer	270	0.06856
Untreated sample	50	0.01325
Sample treated at 500ºC	125	0.04533
Sample treated at 700ºC	45	0.01279

It can be noticed that the maximum corrosion speed appears in the case of the samples without the compound layer. The sample treated at 700ºC has a better resistance to corrosion than the samples with treatment at 500ºC.

The corrosion behaviour of the two samples with heat treatment can be explained using:

- the presence of the heat tensions within the deposited layer
- it is well known the fact that the nickel has an inter-crystalline corrosion phenomenon in the interval 300ºC-500ºC[1].

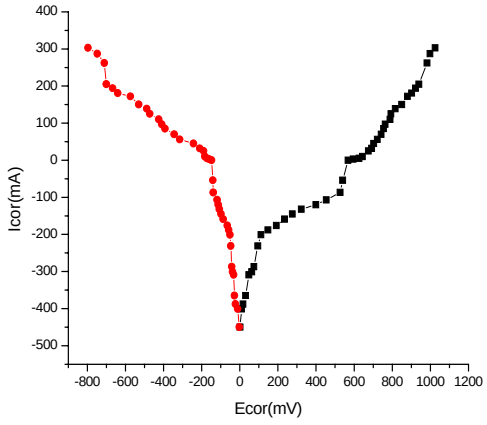

Fig. 2. *Taffel curves for the sample without heat treatment.*

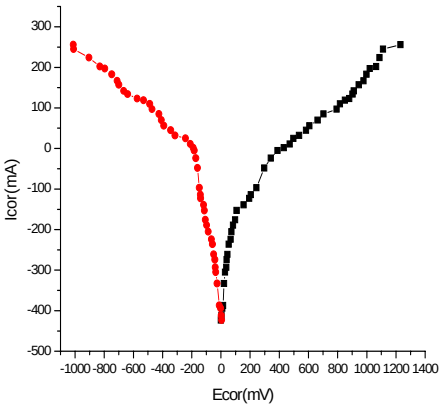

Fig. 3. *Taffel curves for the sample with heat treatment at 500ºC.*

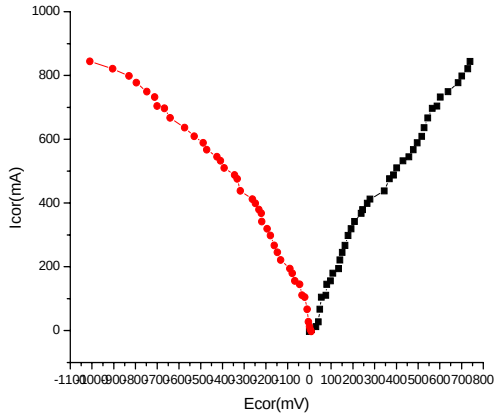

Fig. 4. *Taffel curves for the sample with heat treatment at 700ºC.*

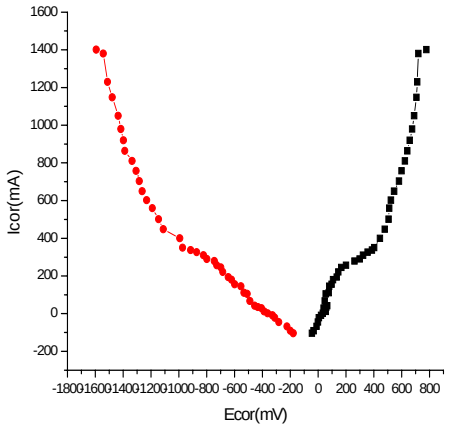

Fig. 5. *Taffel curves for the sample without composite layer.*

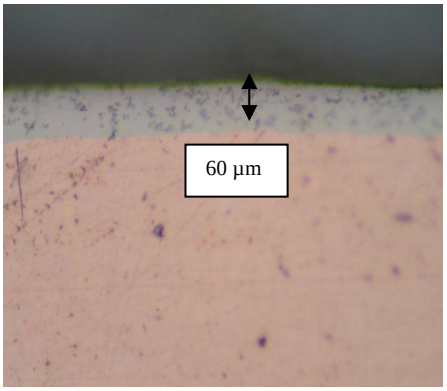

Fig.6. *The microstructure of the sample with composite layer (T=500ºC).*

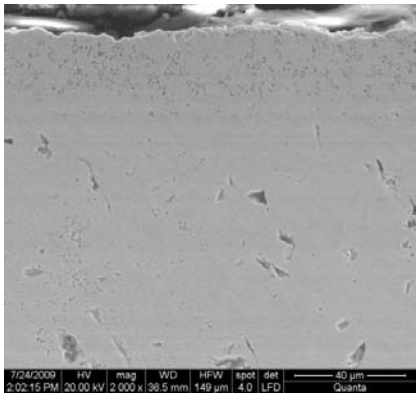

Fig.7. *SEM made for the sample with composite layer (T=500ºC).*

4. Conclusions

The heat treatment at temperatures of 500ºC determines an increase i the micro-strength of the deposited layer, but the composite has a corrosion resistance inferior to the samples treated at 700ºC.

The composite samples have a resistance to corrosion superior to the samples without composite layer.

References

[1]. R.W Cahn, P. Haasen, E.J. Kramer - *Materials Science and Technology*, volume 15
[2]. K. Parker, *Plating and Surface Finishing*, 68(12), 1981
[3]. N. Guglielmi, J. Elecrochem. - Soc.8, 119 (1972) 1009-1012
[4]. J .Fransaer, J. P. Celis and J.R. Roos - *Electrochem. Soc*
[5]. J.P.Celis and J.R. Roos - *Electrochem.* Soc 139, 413-425 (1992).
[6]. O. Mitoseriu, E. Drugescu, F. Potecasu, L. Benea, G. Carac - *Composite Coatings Obtained by Sedimentation Codeposition During Copper, Cobalt* and Iron Electroplating, International Journal MATERIALS AND MANUFACTURING PROCESSES (USA), VOL XI, pag.417-422. 1998,
[7]. S.R. Saifulin - 1992, *Physical Chemistry of Inorganic Polymeric and Composite Materials*, Ellis Horwood Ltd. London, New York.

THE ANNALS OF "DUNAREA DE JOS" UNIVERSITY OF GALATI.
FASCICLE IX. METALLURGY AND MATERIALS SCIENCE
N^0. 2 – 2010, ISSN 1453 – 083X

BIOLOGICAL BEHAVIOR AND CORROSION OF PROSTHETIC AND ORTHODONTIC TITANIUM IMPLANTS

Elisabeta VASILESCU
„Dunarea de Jos" University of Galati
email: elisabeta.vasilescu@yahoo.com

ABSTRACT

Titanium and its alloys are used in dentistry for implants because of their unique combination of chemical, physical, and biological properties. For dental implants, biocompatibility depends on mechanical and corrosion/degradation properties of the material, tissue, and host factors. Corrosion can severely limit the fatigue life and ultimate strength of the material leading to mechanical failure of the dental materials. Titanium and its alloys provide strength, rigidity, and ductility similar to those of other dental alloys. Whereas, pure titanium castings have mechanical properties similar to Type III and Type IV gold alloys, some titanium alloy castings, such as Ti-6Al-4V and Ti-15V have properties closer to Ni-Cr and Co-Cr castings with the exception of lower modulus.

This article presents a few considerations and results of studies regarding the biological behavior and corrosion resistance of the commercially pure titanium (CP Ti), titanium alloys (e.g. Ti6Al4V) by comparation with other alloys (stainless steel orthodontic mini implants for example, fig.) used in prosthetic or orthodontic implant technology. The goal of the study is to determinate the main parameters (factors) and the way they affect (integrity, stability) the utilisation performance of the stainless steel orthodontic mini implants.

KEYWORDS: miniimplant, orthodontic anchorage, biocompatible metallic material, titanium, stainless steel

1. Introduction

Biocompatibility would be perfect without any biomaterial- tissue interactions and could be ensured by a completely inert biomaterial, which does not exist at this time.

Human body's internal environment is aqueos with a pH of 7,4 and a temperature of 37^{0}C; the aggresive saline content is an excellent electrolyte to facilitate hydrolysis and electrochemical reactions of corrosion and the existance of cell capacity which will certains be catalyzed by chemical reactions and will destroy the various species identified by the body as foreign. Biomaterials degradation occurs by corrosion (conventional) passive and active corrosive in particular, by the presence of cellular and molecular species.

For this reason, the precious metallic biomaterials and their alloys are used (less often because they are expensive) but also the common metals and metal alloys such as: Ti, Ti–Al–V, Ti–Ni, Ti–Al, Fe, Ti–Al–Nb, Co–Cr–Mo, Co–Ni–Cr–Mo, Co–Cr–W–Ni, stainless steel with 18%Cr and 8%Ni.

Table 1. *Chemical composition of unalloyed titanium as biomaterial*

Element	Compositional limit, [%]			
	Grade1 max	Grade 2 max	Grade 3 max	Grade 4 max
Nitrogen	0.03	0.03	0.05	0.05
Carbon	0.1	0.1	0.1	0.1
Hydrogen	0.0125	0.0125	9.0125	0.0125
Iron	0.15	0.2	0.25	0.3
Oxygen	0.18	0.25	0.35	0.45
Titanium	Balance	Balance	Balance	Balance

Titanium is an inert material which has the objective to be a medium in contact with tissue and is inactivated rapidly by forming a thin layer of tough and protective oxide. Surface oxide consists of TiO, TiO_3, Ti_2O_3, Ti_3O_4, and it retains and binds biomolecules. Contaminated surface changes the composition of oxide, favoring inflammation which is followed by formation of granulation tissue.

Table 2. *Mechanical properties of unalloyed titanium as biomaterial*

Grade	Conditions	Tensile strength min, MPa	Yielding strength min, MPa	Elongation min, %	Reduction of area min. %
1	annealed	240	170	24	30
2	annealed	345	230	20	30
3	annealed	450	300	18	30
4A	annealed	550	440	15	25
4B	cold worked	680	520	10	18

Titanium implants are often covered throught the TPFS (Flame Titanium Plasma Spray), by hydroxyapatite or zirconia layers which give them a better osteointegration.

Table 3. *Chemical composition of titanium based alloys as implants for surgery*

Element	Ti6Al4V Wrought	Ti5Al2,5V Wrought	Ti6Al7Nb Wrought
Aluminium	5.5-6.75	4.5-5.5	5.5-6.5
Vanadium	3.5-4.5	-	max.0.5 tantalum
Iron	max.0.3	2-3	max.0.25
Niobium	-	-	6.5-7.5
Oxygen	max.0.2	max.0.2	max.0.2
Carbon	max.0.08	max.0.08	max.0.8
Nitrogen	max.0.05	max.0.05	max.0.05
Hydrogen	max.0.015	max.0.015	max.0.009
Titanium	balance	balance	balance

Table 4. *Mechanical properties of titanium based alloys as implants for surgery*

Alloys	Tensile Strength min, MPa	Yielding Strength min, MPa	Elongation min,%
Ti-6Al-4V wrought	860	780	8
Ti-5Al-2.5V wrought	900	800	8
Ti-6Al-7Nb wrought	900	800	10

Advantages of titanium are shown not only in implants made of it, cones, hand tools and compmnents (which are obtained by cold deformation), but also in different pluridentare fixed partial denture made by casting. Another thing that has been specially designed consist of titanium ceramic bodies. Areas of use of titanium in dentistry and oro- maxilofacial surgery are constantly expanding.

Microstructural aspects of Ti alloys

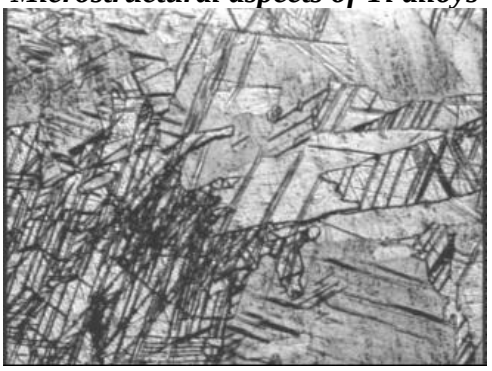

X 100

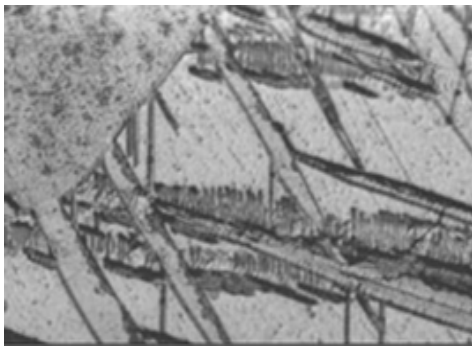

X500

Table 5. *Comparison of metallic biomaterials [21]*

Alloy properties	AISI 316L	CoCr cast	CoNiCr wrought	Ti-6Al-4V	Cp Ti
Corrosion	-	-	+	+	+
Biocompatibility	-	-	-	+	+
Bioadhesion	-	-	-	+	+
Biofunctionality	1.2	1.5	2.3	5.2	1.8
Processability	C D W P	C W P	C D W P	C D W P	C D W P
Casts (DM/Kg) Semifinished product	-60	-60	-70	-75	-70

C-casting; D-deformation; W-Welding; P-powder metallurgy

2. Studies and research on corrosion resistance of metallic biomaterials

Long-term studies on electrochemical behavior of some alloys based on Co-Cr, Ni-Cr, Pd şi Ti in artificial saliva show that titanium has the lowest rate of release of ions followed by alloy Co-Cr, Ni-Cr with more than 20% Cr, Ni-Cr, with less than 20% Cr and Pd alloys. The corrosion resistance of titanium dental purpose is influenced by several factors, which include: type of technolgy used to obtain finished parts, processing handled, finishing and polishing action as well as the action of the cleaning agents and solvents.

Corrosion tests conducted in artificial saliva showed that the penetration potential of titanium is much higher than other dental alloys, thereby justifying its resistance to corrosion (Table 6).

Table 6. *Penetration potential of alloys titanium*

Dentistry alloy/titanium	Penetration potential (mV)
Gaudent S	-100
Au – Ag – Pt	+780
Ni – Cr – Mo	+820
Co – Cr – Mo	+920
Ti unalloyed	> 2000
Dentistry alloy/titanium	Penetration potential (mV)
Gaudent S	-100
Au – Ag – Pt	+780
Ni – Cr – Mo	+820
Co – Cr – Mo	+920
Ti unalloyed	> 2000

Titanium alloys seem to be better tolerated than pure titanium as oxide layer whose form is 10-20 μm. Recent research has shown that the layer of TiO considered so stable regenerates every nanosecond. Traditional corrosion test consists in the measurement of weight change in specimen during exposure to a corrosive environment.

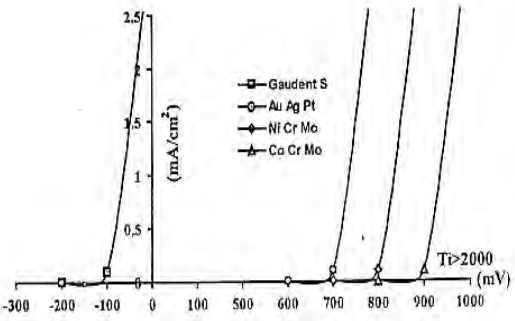

Fig. 1. *Penetration potential values corresponding to some dental alloys and titanium.*

The main disadvantage of weight loss measurement is the inability of the method to predict the corrosion rate if the exposure of the alloy to the corrosive environment is significantly extended more than the experimental exposure. Other testing methods of the implantable metallic materials are based on the use of optical microscopy, X-Ray spectrograph, the spectrochemical analysis and electronic probe microanalysis. While these methods can provide valuable information about the corrosion products, they are tainted by the transport of the products to more dispersed tissues in the body and by the excretion of corrosion products in urine, sweat and faeces. Electrochemical methods have been widely used for estimating corrosion in surgical alloys. The most important methods are electrochemical anodic back EMF, time-potential test, polarization curves and polarization resistance technique.

Considering a specific electrolyte that simulates body fluid, respectively Hank's solution, the current density of different biomaterials as a function of the potential difference between the anodic and cathodic branches of the current potential curves is shown in Figure 2.

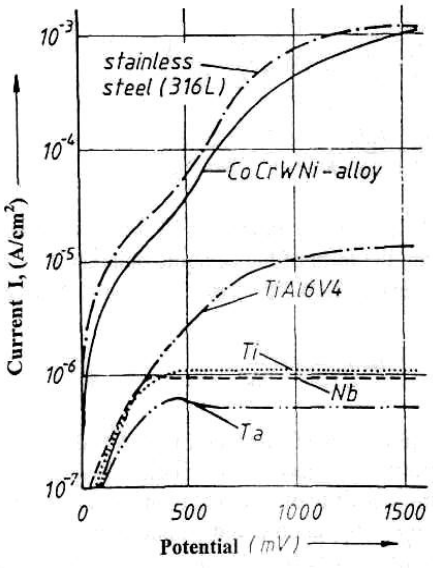

Fig.2. *Current density as a function of the potential difference between the anodic and cathodic branches of the current – potential curves for metals tested in 0.9% NaCl with a stable redox system [Fe $(CN)_6^{4-}$/$F(CN)_6^{3-}$] /21/*

The saline containing this redox system [0,9% NaCl in $Fe(CN)_6^{-4}$/$F(CN)_6^{3-}$] resembled closely in its resting potential that is a tissue culture fluid, which has its redox potential at 400mV. As it can be seen titanium and titanium alloys, tantalum and niobium behave in a more noble way than the stainless steel AISI 316 and a wrought CoNiCr-alloy.

Considering the same Hank's solution (0.17M NaCl; 22^{o}C) the comparative potential/time curve of scratch tests of implant alloy is given in Figure 3.

As it is illustrated in Figure 3 for a metal such as titanium, which is resistant to crevice attack, repassivation occurs within a few seconds.

The potential time transient shows an initial drop in potential at the time of scratch with rapid rise in potential to the prescratch „passive" value.

For alloys, such as 18Cr-10Ni (AISI 316L), an austenitic stainless steel, which requires an oxygen cathode, a different potential curve is recorded.

At the time of the scratch, a potential drops to a value consistent with the active dissolution of the scratch. It never returns to its potential value, since repassivation cannot occur.

Table 7. *Corrosion rates of biomaterials in Hank's solution*

Alloy	**Metal converted into compound,** ng/m^{2}h	**Metal found in tissue**, ng/m^{2}h
Stainless steel – mechanically polished	7.8	0.274
(AISI 316L) – chemically polished	230	-
Vitallium – mechanically polished	150	0.249
(CoCrW-Ni alloy) – chemically polished	20	-
Ti – mechanically polished	4.1	0.430
– chemically polished	3.5	-

Considering another criterion of corrosion resistance, as formation of corrosion products, in Table 7 it is given a comparison of rate of corrosion product formation for biomaterials in Hank's solution during current-time tests with rate of formation of implant corrosion products in rabbits.

So the values in Table 6 represent dissolution rates for titanium alloys several orders of magnitude less rapid than those measured for passive stainless steel alloys.

The same behavior can be observed during the measurements of the polarization resistance of different metallic biomaterials (as given in Table 8).

Breakdown potential measurements of different implant materials in Hank's solution resulted also in a clear order of ranking of the different materials. While commercially pure titanium and TiAl6V4 had high breakdown potentials of 2.4 and 2.0 V respectively or stainless steels and CoCr alloys (cast an wrought) this value amounted only to 0.2 and 0.42V respectively, as given in Table 9.

So, titanium and its alloys, niobium and its alloys and tantalum belong to the group of metals, which in body fluids cannot undergo a breakdown of passivity. In this fluid, a breakdown at a high potential causing a pitting corrosion is impossible because it is more positive than the oxygen reversible reduction and it is less positive than the water or hydrogen- ion reduction.

In all materials the passive layer can be damaged mechanically, e.g. by fretting metal on metal (plate/screw) or by the instruments used during surgery. The time of the repassivation of the material is therefore very important.

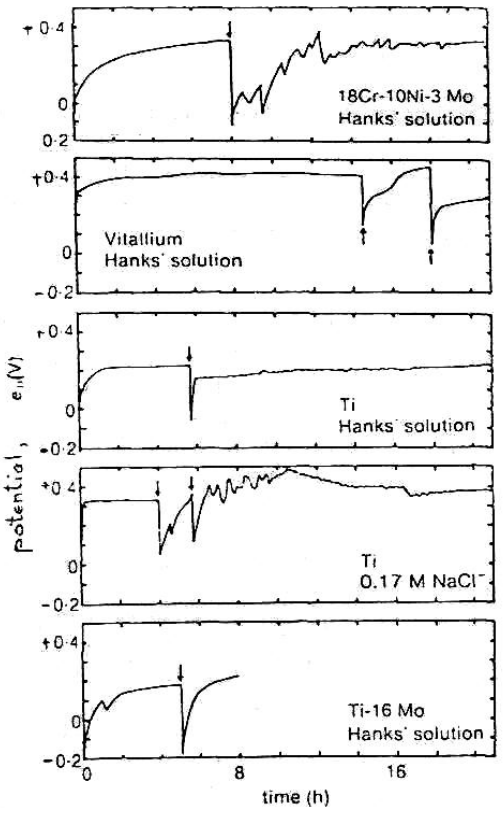

Fig.3. *Schematic diagram to show potential/time curves of scratches test of implant alloys in Hank's solution and 0,17 M NaCl solution at 22°C specimen scratched 22^{o}C ↓ specimen scratched /21/.*

The repassivation behavior of different materials in saline solution was measured using an electrode, which rotates by $10s^{-1}$ in saline solution whereby it is activated by a cutting tool of Al_2O_3. The decrease of the corrosion current is measured in dependence on the time at different potentials. The repassivation is defined to be achieved, if the current density amounts to 1/e (e≈2,718) of the current density in the achieved condition. In addition, the time $t_{0,05}$ of a rest active current density 5% was determined. The values t_e and $t_{0,05}$ of the different measured materials are also given in table 8.

The passive oxygen surface layer (t_e) is reconstructed dependent on the material in some milliseconds. The growth of the surface layer ($t_{0,05}$) of titanium and titanium alloys is accelerated compared to the other materials.

Table 8. *Polarization resistance of metallic biomaterials in 0,9 NaCl with stable redox system [Fe $(CN)_6^{4-}$/$F(CN)_6^{3-}$] /21/*

Metallic biomaterial	**Polarization resistance** [kΩcm^2]
Au	0.28
FeCrNiMo (AISI 316L)	4.38
Co NiCr (wrought)	3.32
Ti	714
TiAl6V4	455
Nb	455
Ta	1430

Table 9. *Breakdown potential in Hank's solution of metallic biomaterials and repassivation time 0,9% NaCl [21]*

Metallic biomaterial	**Breakdown potenţial** (V)	**Repassivation time** (msec)			
		t_c		$t_{0,05}$	
		(s)	(s)	(s)	(s)
AISI 316	+0.2-0.3	>72000	35	>>7200	>6000
CoCr	+0.42	44.4	46	>>6000	>6000
CoCrNi	+0.42	35.5	41	>6000	5300
TiAl6V4	+2.0	37	41	43.3	45.8
Ti	+2.4	43	44.4	47.4	49
Ta	+2.25	-	-	-	-
Nb	-	47.6	43.1	47	85

3. Experimental Conditions

This article draws attention to current concerns of a research team composed of chemists, metallurgists, dentists about stainless steel mini implants for orthodontic anchorage characterization from the chemical and biological point of view compared to the usual metal alloys which are used nowadays in the manufacture. A painstaking ongoing research program aims at the use of advanced investigation methods such as: optical and electronic microscopy, study of corrosion resistance and surface microtopography also keeping the comparison with titanium and its very studied alloys and in many cases with controversial views. Anchorage has long been a challenge since the introduction of fixed appliances in orthodontics [3]. Typically, orthodontic movement of a tooth is anchored by a large group of teeth so as to minimize undesired displacements of anchoring teeth. Adequate anchorage becomes difficult when posterior teeth are missing. Intra- and extra-oral auxiliary devices can be used to assist movement, but the effectiveness of these measures is dependent upon the level of the patient's cooperation [3].

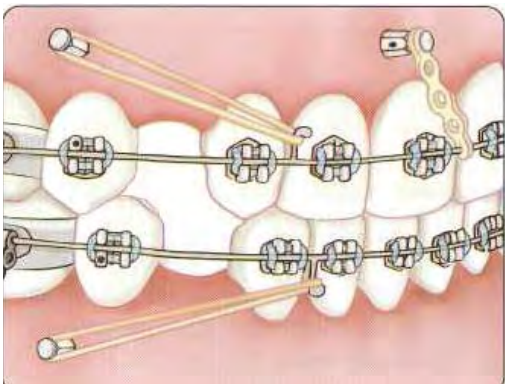

Fig.4. *Insertion procedure of orthodontic mini implants [22].*

Conventional titanium implants have emerged as an excellent alternative to traditional orthodontic anchorage methodologies, mainly when anchorage dental elements are insufficient in quantity or quality. Unfortunately, conventional dental implants can only be placed in limited sites, such as the retromolar and edentulous areas. In addition, conventional dental implants are troublesome for patients because of the

severity of the surgery, the discomfort of the initial healing and the difficulty of maintaining oral hygiene.

Fig. 5. *Stainless steel orthodontic mini implants [22].*

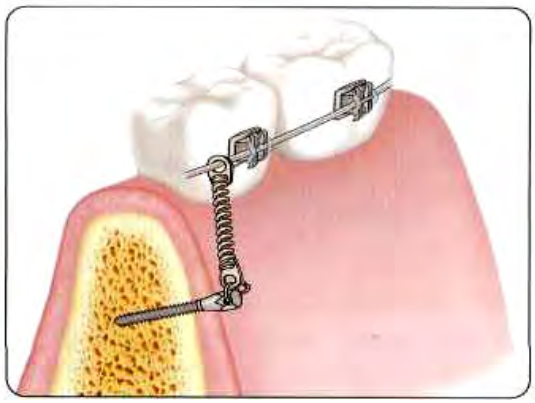

Fig. 6. *Connection of the mini implant to the orthodontic appliances[22].*

Due to these disadvantages, Kanomi proposed titanium mini-implants (1.2 mm in diameter and 6.0 mm in length) for orthodontic anchorage.

They are widely used since they have few implantation site limitations, a simple insertion procedure and easy mechanical force control.

The methodology for implementation of mini-implants has been continuously improved. Some complications persist, and the sources of failure include the inflammation of the soft tissue around the mini-implant and fracture of the mini-implant [3].

A period of healing is usually necessary before applying load to conventional dental implants. This period varies from 4 to 6 months in humans [3]. When the load is placed prematurely, histological analyses have suggested that there is no uniform intimate bone-implant contact due to interplayed fibrous tissue. This phenomenon could be favorable for implants for orthodontic anchorage purposes, since it facilitates the surgical removal of the implant at the end of the orthodontic treatment. On the other hand, the excess of interplayed fibrous tissue could lead to implant failure.

Commercially pure titanium (CP Ti) is widely used as implant material because of its suitable mechanical properties and excellent biocompatibility.

However, CP Ti has lower fatigue strength than titanium alloys. Ti–6Al–4V can be used to overcome this disadvantage [3]. However, the corrosion resistance of the mini-implant decreases when the alloy is used, favoring metal ion release, which has been associated with clinical implant failure, osteolysis, cutaneous allergic reactions, remote site accumulation, kidney lesion, cytotoxicity, hypersensitivity and carci-nogenesis [3].

Fig. 7. *Orthodontic stainless steel mini implants studied.*

Fig.8. *Hexagonally shaped head.*

Orthodontic stainless steel mini implants studied are designed for temporary insertion and can be loaded with tractions (springs, wire, elastics, chains), to get dental movements with the biomechanical advantage of the maximum anchorage and in critical anchorage situations due to the lack of teeth (periodontal involved or edentulous patients).

Following some possible applications are indicated: inter-arch extrusion, intra-arch intrusion on anterior teeth, intra-arch intrusion on posterior teeth, surgical disinclusions (cuspids, etc.), orthodontic

anchorage for distalization, orthodontic anchorage (i.e. after distalisation).

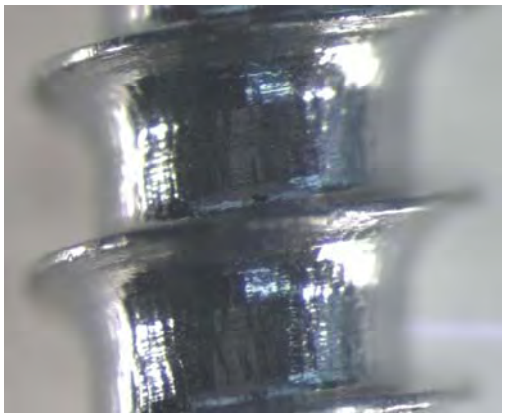

Fig.9. *Cylindrical screw design.*

Fig. 10. *Machined surface.*

Traction devices are tied through the passing hole present on the head of the mini implant or anchorage at the groove featured by some models:

- with low head (transmucosal height of 1.75 mm)
- wich high head (transmucosal height of 3 mm), and two different versions.

The first one with a passing hole on its head, while the second one presents a groove in addition to the hole. The groove- added version has the prominent part similar to an orthodontic button to facilitate the application of chains, elastics or springs.

The application time of the orthodontic traction on the mini implant depends on the clinician's judgement; the mini implant can usually be loaded immediately after insertion or after healing of soft tissues. They can be easily removed after use by simply unscrewing them in the opposite direction.

4. Conclusions

This paper has presented a short summary of the characteristics of metallic biocompatible materials for dental implants, mainly of titanium and titanium alloys, in particular highlighting the corrosion behavior in environments simulating oral environment and by comparison with other alloys, for example stainless steels.

A major research program has begun aiming at the chemical and physico-mechanical characteristics determination but also at characterizing the behavior in oral environment of stainless steel anchorage mini implants. Ongoing investigations are made by modern techniques and equipment performance (SEM, EDX, AFM, after corrosion and tribocorrosion tests etc) samples of materials known but alternative materials.

References

[1]. Nicolas Schi, Brigitte Grosgogeat, Michele Lissac, Francis Dalard, Biomaterials 23 (2002) 1995-2002.
[2]. M.A. Khan, R.L. Williams and D.F. Williams, *Biomaterials* 17 (1996) 2117-2126 © 1996 Elsevier.
[3]. Liliane S. Morais, Glaucio G. Serra, Carlos A. Muller, Leonardo R. Andrade, Elisabete F.A. Palermo, Carlos N. Elias, Marc Meyers, Acta Biomaterialia 3 (2007) 331-339
[4]. H.J. Rack, J.I. Qazi 1, Materials Science and Engineering C 26 (2006) 1269 - 12775.
[5]. M. Karthega, V. Raman, N. Rajendran, Acta Biomaterialia 3 (2007) 1019-1023
[6]. Zhuo Cai, Ty Shafer, Ikuya Watanabe, Martha E. Nunn, Toru, Okabe, Biomaterials 24 (2003) 213-218
[7]. Sergio Luiz de Assis, Stephan Wolynec, Isolda Costa, Electrochimica Acta51 (2006) 1815-1819
[8]. D.D. Deligianni, N Katsala, S. Ladas, D. Sotiropoulos, J. Amedee, Y. F. Missirilis, Biomaterials 22 (2001)1241-1251
[9]. J.Ge and O.B. Isgor, Materials and Corrosion 2007, 58, No. 8, pg. 573, 583, 616
[10]. Hesham E. Khalifa, Kenneth S. Vecchio, Advanced Engineering Materials No. 11/2009
[11]. M.F.Lopez; A. Gutierrez; J.A. Jimenez, Surface Science 482-485
[12]. C. Morant, M.F. Lopez, A. Gutierez, J.A. Jimenez, Applied Surface Science 220 (2003) 79-87
[13]. E. Eisenbarth, D. Velten, M. Muller, R. Thull, J. Breme, Biomaterials 25 (2004) 5705-5713
[14]. Mitsuo Niinomi, Journal of the Mechanical Behavior of Biomedical Materials 1 (2008) 30-42
[15]. S. Sathish, M. Geetha, N.D. Pandey, C. Richard, R. Asokamani, Materials Science and Engineering C 30 (2010) 376-382
[16]. Ramakrishna Venugopalan, Michael A. George, Jeffrey J. Weimer, Linda C. Lucas, Biomaterials 20(1999) 1709-1716
[17]. Yu Zhentao, Zhou Lian, Materials Science and Engineering A 438-440 (2006)391-394
[18]. Robert G. Craig Restorative Dental Materials, 1997 Mosby year Book, Inc.
[19]. William R. Proffit, D. D.S ; PH.D Henry W. Fields, Jr., M.S., M.S.D.; and James L. Ackerman, Peter M. Sinclair, Paul M. Thomas, J.F. Camilla Tulloch, Second Edition Contemporary Orthodontics, Mosby Year Book, 1992
[20]. Kenneth J. Anusavice, D. M. D., Ph. D. Tenth Edition Phillips' Science of Dental Materials, 1996
[21]. B. Ghiban, Metallic Biomaterials, Editura Printech 1999
[22].*** Orthodontic Mini implants, Leone Clinical procedure for positioning.

THE ANNALS OF "DUNAREA DE JOS" UNIVERSITY OF GALATI.
FASCICLE IX. METALLURGY AND MATERIALS SCIENCE
N^0. 2 – 2010, ISSN 1453 – 083X

SOME RESEARCHES CONCERNING THE DEEP DRAWING PROCESS OF THE RECTANGULAR BOX

N. CĂNĂNĂU, Ş. NEGREA, M. ŞEITAN
"Dunărea de Jos" University of Galati
email: ncananau@yahoo.com

ABSTRACT

The deep drawing process of the rectangular boxes is difficult difficulties because of the complexity of the stress and strain states. This paper presents the results of the researches on the variation of the stamping force in function of some deformation factors and the variation of the micro-structure in the maximum deformation zone.

KEYWORDS: sheet, strip, deformation, rectangular box, stress and strain states

1. Introduction

The deep drawing is a deformation process of the sheets and strips for obtaining box type parts (Fig. 1).

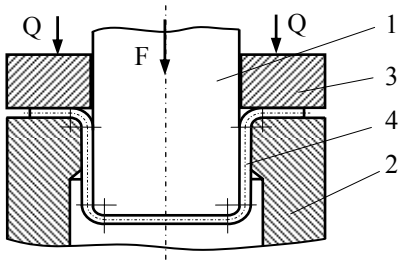

Fig. 1. *Scheme of the stamp process: 1-punch, 2-die, 3-blank hold, 4-stamped part.*

Under the action of the force F on the punch 1, the semi-product 4 flows in the space, between the punch and the die 2. On the blank hold (restraint plate) the force Q is applied and avoids the folds appearance. If the folds appear, the flow of the material is blocked and the semi-product breaks.

The form and dimensions of the plate semi-product are established according to from and dimensions of the final part.

Thus, in case of the revolution parts the plate semi-product has a disc form. The thickness of the disc is equal to the thickness of the sheet or strip and the diameter is established in function of the dimensions of the final part apply the equality of the surface areas.

The surface area of the disc is equal of the surface area of the final part.

In case of the rectangular cup the plate semi-product is composed by two side pairs and four corners in the disc form (Fig. 2).

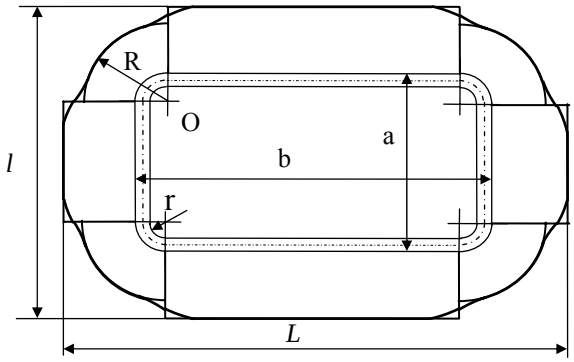

Fig. 2. *The form of the plate semi-product.*

The stresses and strains states, in the zones of the corners are very complex.

During the stamping process the material flows and forms the corner of the part. In the same time, the material of the side, been next by the corner, is drawn in the space of the corner.

Thus, in the corner and in the proximity of the part corner, the important variation of the thickness and of the micro-structure and properties of the material takes place.

In function of the concrete values of the geometrical factor of the stamped part, the deep drawing process is made of one, two or more stamping operations.

For establishing the number of deep drawing operations *n,* are recommended various methods.

One of these is the following:

1. We calculate the value of deep drawing coefficient *m*, defined by the equation below:

$$m = 1.27\frac{a+b}{L+l}$$

2. Using the Table 1 we will establish the number of stamping operations.

Table 1. *Establishing the stamping operations*

n	**Relative thickness**, ($t/(L+l)\times 50$)			
	2÷1.5	1.5÷1.0	1.0÷0.5	0.5÷0.2
2	0.40-0.45	0.43-0.48	0.45-0.50	0.47-0.53
3	0.32-0.39	0.34-0.42	0.36-0.44	0.38-0.46
4	0.25-0.30	0.27-0.32	0.28-0.34	0.30-0.36
5	0.20-0.24	0.22-0.26	0.24-0.27	0.25-0.29

If the calculated coefficient is greater than the maximum value recommended in the Table 1, corresponding to *n=2*, the stamping may be performed by one deep drawing operation. Contrary, the number of stamping operations results from Table 1. The researches systematized in this paper refer to the variation of the stamping force in function of the part height and thickness.

2. Experimental conditions

The experiments were made with a stamping device centered and mounted at the hydraulic press with the maximum force of 120 kN.

The drawing of the stamping device is rendered in Figure 3.

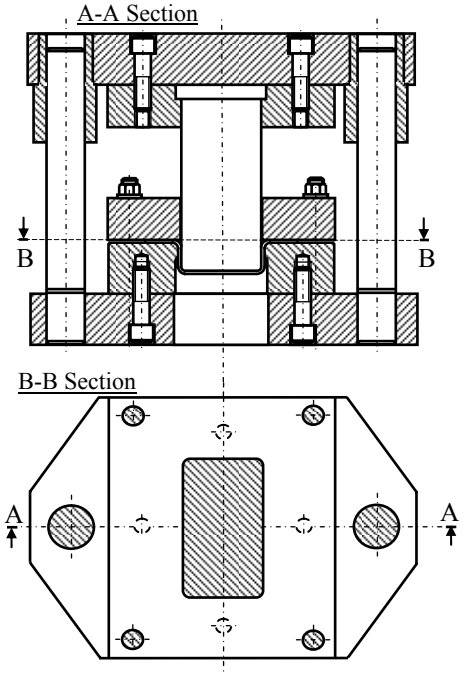

Fig. 3. *Deep drawing device.*

For the experiments we used steel strip for the deep drawing with thickness of 0.3; 0.5 and 0.8 mm.

3. Experimental results and comments

3.1 Variation of the stamping force

The dimensions of the rectangular stamped part are rendered in the Figure 4.

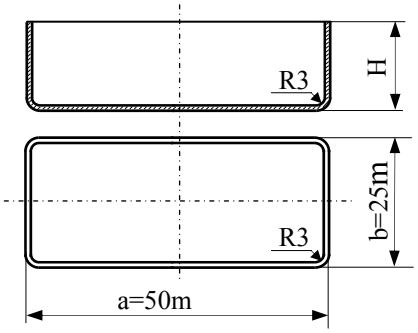

Fig. 4. *Dimensions of the stamped part.*

The height of the stamped parts was of 8.0; 10.0; 12.0; 14; and 16 mm.

The variation of the force in the time of the deep drawing process, for the thickness of the strip of 0.3 mm is rendered in Figure 5.

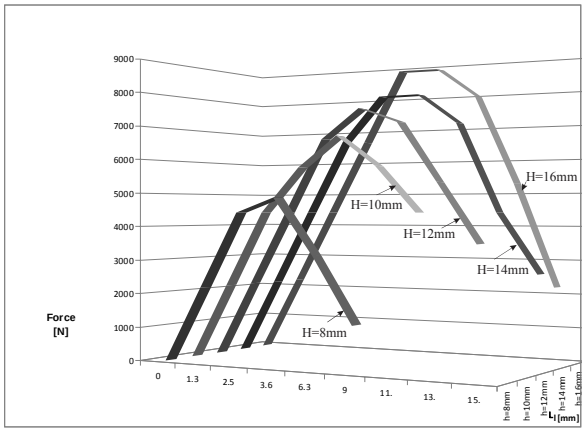

Fig. 5. *Stamping force for thickness of 0.3mm.*

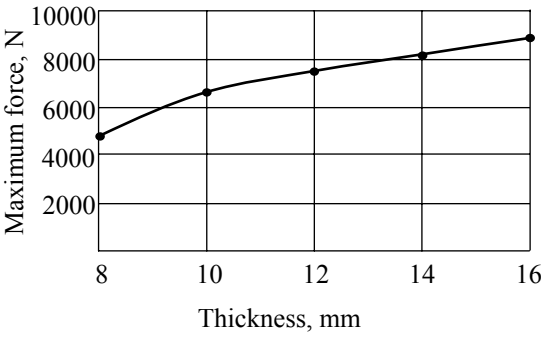

Fig. 6. *Variation of maximum stamping force with the height of the stamped part for thickness of 0.3 mm.*

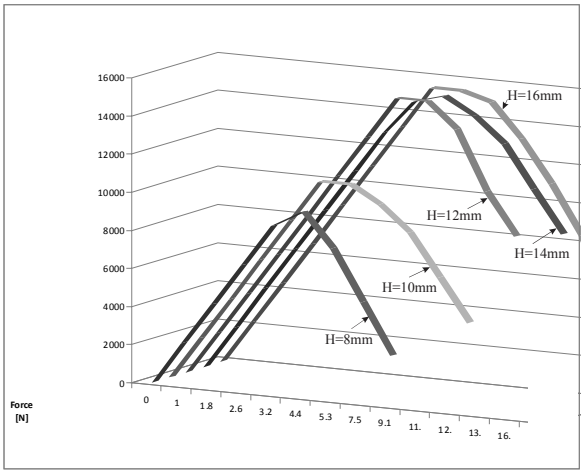

Fig. 7. *Stamping force for thickness of 0.5mm.*

The variation of the maximum stamping force in case of the thickness of 0.5 mm is rendered in Figure 8.

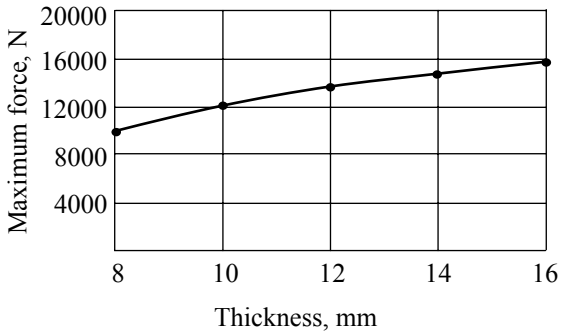

Fig. 8. *Variation of maximum stamping force with the height of the stamped part for thickness of 0.5 mm.*

The variation of the force during the deep drawing process for the thickness of the strip of 0.8 mm is rendered in Figure 9.

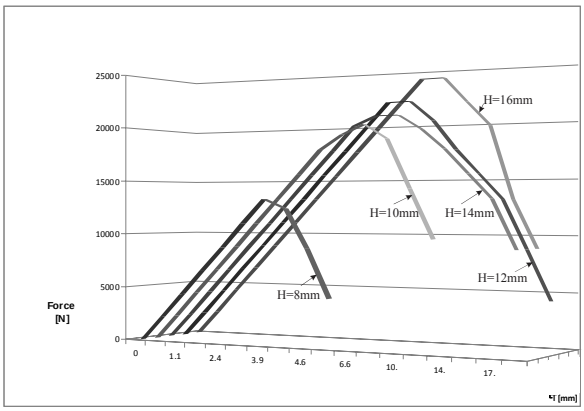

Fig. 9. *Stamping force for thickness of 0.8mm.*

The variation of the maximum deep drawing force in case of the thickness of 0.8 mm is rendered in Figure 10.

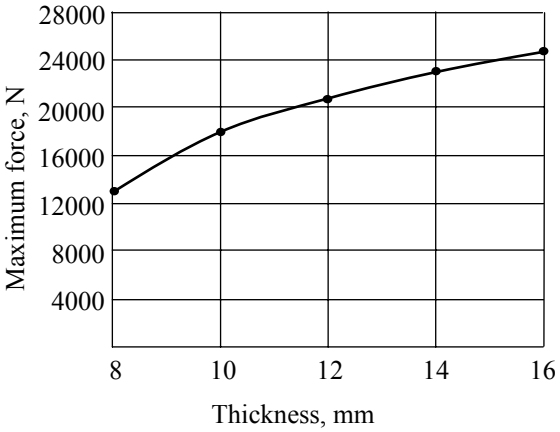

Fig. 10. *Variation of maximum stamping force with the height of the stamped part for thickness of 0.5 mm.*

In a 3D form, the variation of the maximum force in function of the thickness of the strip and the height of the stamped parts is rendered in Figure 11.

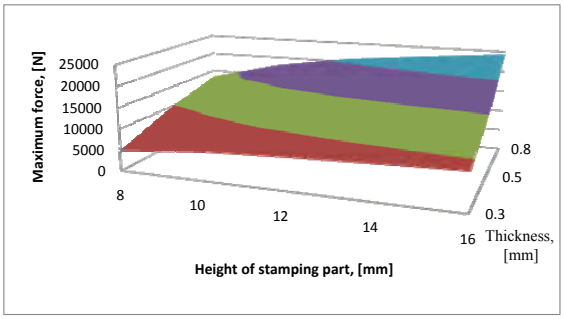

Fig. 11. *The variation of the maximum force with the thickness and the height of the parts.*

We can observe that the force during the deep drawing process increases attains a maximum value and decreases until the end of the deformation process.

The maximum value of the force corresponds to greater values of the removing of the superior stamping device when the stamped part height increases.

The thickness does not have a notable influence on the position of the maximum value of the stamping force.

The maximum value of the stamping force increases when the height of stamped parts and thickness of material increase.

3.2. Aspect of the microstructure at the stamping process

The great non-uniformity of the deep drawing process determines the variation of the microstructure of the deformed material, specially, in the corner zone. In Figure 12 we show the microstructure aspect in the frontal wall of the part. The microstructure corresponds to the base state of the material and consists of ferrite and carbide. The crystalline grains are, practically non-deformed.

Fig.12. *Micro-structure of material in the frontal wall of the stamped part (Nital 5).*

In Figure 13 we show the microstructure aspect in zone of the corner of stamped part. The deformation of the grains is evident.

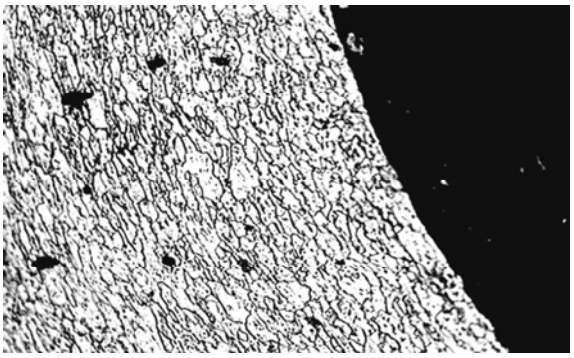

Fig.13. *Micro-structure of material in the corner zone of the stamped part (×200, Nital5).*

The strain intensity is great, relatively, and non-uniform. Because the strain intensity is greater in the points to the exterior of the part wall, the intensity of the crystalline grains deformation is greater in these points.

4. Conclusions

The deep drawing process of the rectangular part is very difficult because of the complex stress and strain states.

The quality of the process and product is defined by the quality of the material and the values of the technological factors.

For this reason the researches in the aim of the assurance of the quality are justified.

In the paper the variation of the force in the time of the stamping process and the variation of the maximum force with the thickness and the height of the part were established. The force variation in the time of the deep drawing process is a function with the maxim.

The maximum value of the force increases with the thickness and the height of the part.

The microstructure in the corner of the part is very affected.

The crystalline grains extend in the direction of the principal strain.

The extension of the grains is greater at the exterior of the part wall.

References

[1]. M. Ahmetoglu, T.R. Broek, G. Kinzel and T. Altan, *Control of Blank Holder Force to Eliminate Wrinkling and Fracture in Deep-Drawing Rectangular Parts*, CIRP Annals - Manufacturing Technology, Volume 44, Issue 1, 1995, Pages 247-250

[2]. François Ronde-Oustau, Bernard Baudelet, *Microstructure and strain path in deep-drawing*. Journal of Materials Processing Technology, Volume 50, Issues 1-4, March 1995, Pages 375-384

[3]. Joachim Danckert, *Experimental investigation of a square-cup deep-drawing process*. Journal of Material Processing Volume 50, Issues 1-4, March1995, Pages 375-384

[4]. Teodorescu, M. a.o. – *Elemente de proiectare a stantelor si matritelor*, EDP, Bucuresti, 1977.

[5]. Lazarescu, I., Stetiu G. – *Proiectarea stantelor si matritelor,* EDP, Bucuresti, 1973.

[6]. Roamnovski, V.P. - Stantarea si matritarea la rece, Ed. Tehn., Bucuresti, 1970.

[7]. ASM, Metals Handbook, vol.4, Forming, Ohio, SUA, 1969.

THE ANNALS OF "DUNAREA DE JOS" UNIVERSITY OF GALATI.
FASCICLE IX. METALLURGY AND MATERIALS SCIENCE
N^0. 2 – 2010, ISSN 1453 – 083X

CONSIDERATION REGARDING THE HEAT TREATMENT OF SHEETS AND STRIPS FROM ALUMINUM ALLOY 5052 TYPE

Alexandru STANCIOIU[1], Olga MITOSERIU[2], Marian BORDEI[2]
[1]SC ALRO Slatina
[2]"Dunărea de Jos" University of Galati
email: alexstancioiu@yahoo.com

ABSTRACT

The paper extends the laboratory investigations performed on samples taken from industrial production to the current technologies, the solutions proposed forming a fundamental change in the thermal treatment regimes by varying the temperature / time parameters. The aluminum alloys have outstanding physical and mechanical properties: specific gravity of small electrical conductivity and excellent heat resistance to corrosion and aggressive chemicals.

KEYWORDS: aluminum alloy, mechanical properties

1. Introduction

In the recent years, weight reduction has become a key issue for automotive manufacturers. For this reason, aluminum magnesium (Al-Mg) alloys (5XXX series) have great attention in automotive industry due to their excellent high strength to weight ratio, corrosion resistance, weldability and recycling potential.

Therefore, aluminum alloys could replace heavier materials in the automobiles to reduce the automobile weight. Requirements for fuel consumption, environmental laws, and global warming issues have significant influence on the choice of the materials 5XXX series alloys are mostly used for inner panel applications because of the stretcher lines problem on the product surfaces. These surface defects are limiting the usage of the Al-Mg alloys in the outer panel applications. Forming of these alloys at warm temperatures is quite attractive, since undesirable stretcher lines, which often appear on the surface of the sheets during the cold forming operations, will disappear at high temperatures. Al-Mg alloys show less ductility at room temperatures. In the literature, there are several investigations which have pointed out that the poor room temperature ductility can be improved by changing the forming temperature and the strain rate.

2. Characteristics of the analyzed alloy

The 5052 alloy is part of a group of deformable aluminum alloys and has magnesium as a main alloying element. The chemical composition of 5052 alloy is according to current norms (EN-485 / 2).

The alloy belongs to the group Al – Mg rolling alloys. The presence in the chemical composition of magnesium and chromium leads to a hardening, an increase in breaking strength up to values of 260 MPa and to an increase of yield to values of 125-130 MPa. From the analysis of thermodynamic equilibrium diagram of Al - Mg it results that the solubility of the magnesium in aluminum varies strongly with temperature.

Table.1. *Solubility variation of Mg in Al with temperature*

Temperature, [°C]	450	400	350	300	250	200	150	100	20
Solubility, [%]	17.5	13.5	9.9	6.5	4.4	3.1	2.3	1.9	0.8

Being a magnesium-based alloy, corrosion resistance and tensile strength are high because of α solid solution that best resists to the chemical agents action.

Al-Mg foundry alloys have a good fluidity than cutting machinability, high mechanical strength and corrosion. Instead, these alloys always have a tendency to porosity and microretasures formation which lead to the cracks formation, heat in the castings pieces.

In the case of rolled alloys, additions of Mn and Cr lead to hardening and an increased resistance to breakage. Titanium and vanadium, in small quantities, have the role decreasing and finishing the grains, fact that leads to the growth of mechanical characteristics. 5052 alloy has a specific gravity of 2.68 g/mm^2.

Table 2. *Mechanical characteristics required for the 5052 alloy for thickness between 0.5 to 1.5 mm*

State	R_m, MPa	$Rp_{0,2}$, MPa	A_{min}, %	Hardness HBW
H22/H32	210 - 260	min 130	12	61
H24/H34	230- 280	min 150	9	67
H26/H36	250-300	min 180	9	74

3. Experimental researches

Analyzing the current technology of roll of sheets and strips from 5052 alloy it was suggested the modification of the heat treatment technology for monitoring the influence of heat treatment on physical and mechanical characteristics, depending on the delivery status.

Table 3. *Chemical composition of the alloy analyzed, %*

Si	Fe	Cu	Mg	Mn	Cr	Ni	Zn	Ti	Other elements	Al
0.23	0.28	0.08	2.64	0.07	0.22	-	0.05	-	0.12	rest

We also wanted to find a technology for obtaining optimal physical and mechanical characteristics delivery for those states in a more restricted range.

Program for the tests:

- samples of 5052 alloy sheets were treated having 1 mm thickness at all combinations of temperatures: 150, 160, 160, 170, 180, 190, 200, 210, 220, 230 and respectively 240°C for maintenance times: 2, 4 and 6 hours.

-for each combination every three samples were taken;

-treated samples were tensile tested, determining the tensile test, and yield strength, respectively, elongation;

-treatment of samples was done in a calcination furnace can ignite with scheduling tests, with an accurate temperature control of ± 0.5°C.

Results from tensile testing are presented in Tables 4-6 (selective values).

Table 4. *Values of tensile test for some tested proves*

Code	Alloy type	Temperature	Maintaining time	Thickness	R_m pr.1	R_m pr.2	R_m pr.3
		[° C]	[h]	[mm[	[MPa]		
2- 1	5052	**150**	**2**	1	231	232	232
	5754			1.5	148	249	248
	5251			0.95	238	230	237
2- 2	5052	**150**	**4**	1	231	230	231
	5754			1.5	249	248	248
	5251			0.95	240	240	239
2- 3	5052	**150**	**6**	1	231	230	233
	5754			1.5	247	248	247
	5251			0.95	244	242	243

Table 5. *Values of yield strength test for some tested proves*

Code	Alloy type	Temperature	Maintaining time	Thickness	$R_{po.2}$ pr.1	$R_{po.2}$ pr.2	$R_{po.2}$ pr.3
u.m		[° C]	[h]	[mm[	[MPa]		
2- 1	5052	150	2	1	167	168	167
	5754			1.5	182	185	183
	5251			0.95	193	187	192
2- 2	5052	150	4	1	165	166	166
	5754			1.5	184	182	184
	5251			0.95	193	193	193
2- 3	5052	150	6	1	165	165	167
	5754			1.5	181	183	182
	5251			0.95	197	196	197

Table 6. *Values of elongation test for some tested proves*

Code	Alloy type	Temperature	Maintaining time	Thickness	A pr.1	A pr.2	A pr.3
u.m		[° C]	[h]	[mm[	[%]		
2- 1	**5052**	**150**	**2**	1	15	13	16
	5754			1.5	14.8	12.8	14.2
	5251			0.95	10	9	10
2- 2	**5052**	**150**	**4**	1	15	15	16
	5754			1.5	13.4	14.3	14.5
	5251			0.95	10	10	9
2- 3	**5052**	**150**	**6**	1	16	16	15
	5754			1.5	14.3	13.1	13.8
	5251			0.95	10	10	9

4. Results and discussion

Time-keeping influence is reduced in the range of values in which the experiment was done.

-Values for heat treatment performed at 190°C do not fall within the range required. However, the temperature of 190°C ensures a minimum value for tension and stress, but not a minimum value for the yield stress, respectively, the maximum for elongation. The latter are supplied at a temperature of 220°C for H22/H32-H24/H34 states.

R_m-values which can be obtained systematically are between 222 and 233 are MPa.

$R_{p0.2}$-values that can be systematically obtained are between 150 and 170 MPa.

The A%-values which are systematically obtained are between 13 to 21%.

5. Conclusions

After the research the heat treatment procedure has been optimized:

-it was established a maintenance period of 4 hours, to ensure optimal characteristics with respect to time;

-the temperature of heat treatment has to be correlated with the delivery status of the material as follows:

• for H22/H32 delivery states, T=150°C

• for H24/H34 delivery states, T=140°C (to achieve only the minimum value in case of tensile test);

• for H26/H36 delivery states none of the tested temperature, may have minimum values required by this state.

References

[1]. Dumitrescu E.- *Aluminiul metal al secolului XX*. Bucureşti, Editura Ştinţifică, 1967.
[2]. N. Geru – *Teoria structurală a proprietăţilor metalelor*- Editura Didactică şi Pedagogică –Bucureşti 1980
[3]. *Aluminium Standards and Data* –Aluminium Association- 2004
[4]. L.F. Moldolfo –*Aluminium Alloys Structure and Properties*- Butterworth 1976
[5]. Aluminium Asociation- SR-EN 485/2/2004
[6]. SECIM –*Laminoirs pour bandes d"aluminium,* 1989
[7]. IMNR- *Studiu de documentare privind capacităţile de producţie şi de prelucrare a metalelor neferoase*, 1994
[8]. Ioan Fara –*Aluminiul de la materia primă la produse finite*- Editura tehnică, Bucuresti,2000
[9]. Fielding- *Situaţia actuală şi perspectivele aliajelor de aluminiu utilizate in industria aerospaţială*, 1987
[10]. SR-EN 515/1995- *Aluminiu şi aliaje de aluminiu* –Produse deformabile-Simbolizarea starilor.

THE ANNALS OF "DUNAREA DE JOS" UNIVERSITY OF GALATI.
FASCICLE IX. METALLURGY AND MATERIALS SCIENCE
N^0. 2 – 2010, ISSN 1453 – 083X

THE SONIC WASTE WATER TREATMENT

Dumitru POPA, Aurel CIUREA, Marian BORDEI
"Dunărea de Jos" University of Galati
email: popadtru@yahoo.com

ABSTRACT

Sonic technology means the technology where the sonic devices are used and where the intensification of the heat and mass transfer is obtained owing to the pressure or flow capacity oscillations, introduced in the technological flux. This paper consists in the examination of the practical application results of the various technical systems with sonic injectors.

KEYWORDS: water treatment, sonic technology, ultrasound gas-dynamic generator

1. Introduction

A new method of intensifying the technological processes, generally, with low energy consumption, is based on the idea of using the pulsation energy which appears during non-stationary flows of the technological fluids [1]. Technological devices used for this aim can be named Sonics, after the great Romanian scientist George Constantinescu [3], because they do not have mechanical mobile pieces and run normally, in regime of self-oscillations, therefore, in sonic regime.

This paper consists in the examination of the practical application results of the various technical systems with sonic injectors [1].

The main element of a sonic injector represents the sonic generator according to which the sonic injectors are classified. The generator with pressure pulsation or flow capacity without mechanical mobile pieces which normally runs in self-oscillation regime will be called the sonic generator. Depending on the nature of the fluid used for the sonic generators running, the last ones can be hydrodynamic or gas-dynamic.

At the hydrodynamic sonic injectors the generation of the pulsations is produced by the liquid itself (or by the liquid combustible) which is sprayed. Owing to the self-oscillation phenomenon during instable turbionaire flows of the fluids, powerful pressure pulsations are produced.

The flow instability can appear because of the lack of balance between the supply network and generator, or because of the special geometry of the generator which produced the lack of balance between the capacity flow penetrated through the entrance channels and drained through its nozzle.

The gas-dynamic sonic injectors, or another name more famous – acoustic, for liquids combustible spraying (or liquids) use the energy of the high frequency shock waves which appear during non-stationary flows, in supersonic jets of gases, the well known phenomenon – in acoustic – as HARTMANN effect [2].

Sounds and ultrasounds gas-dynamic and hydrodynamic generators can be classified according to the way of producing the sonic field:

-Hartmann generators, which use the non-stationary processes from supersonic gas jets;

-Helmholtz generators (or acoustic "little whistle"), where the non-stationary processes from subsonic fluids jets are used;

-Generators with tourbillion, which use the instability phenomenon of the turbinate fluids fluxes.

Because the classical generator Hartmann, which represents a "mouthpiece-resonator" mechanical system, is not stable at low variations of supply gas pressure, Hartmann suggested in 1951 [2] the introduction of a central rod in the convergent mouthpiece, in order to fasten the resonator.

The "mouthpiece-rod-resonator" system (Figure 1, at the injectors: RD-1, AFR-2, -3, -4, -5, DRG-1) proved to be stable from an acoustic point of view and obtained large usage in various technological processes and mainly, as injectors for fine spraying of the combustibles and for liquids, in general. This universality takes place because of the phenomenon of the gas which flow "crisis" in mouthpiece, well known in the gases dynamics [2], to which after establishing the critical flowing regime, the flow capacity of gas passed through the generator mouthpiece remains unchanged at variations of state parameters of the medium, where the drain takes place.

In Table I, the technical characteristics, usage domains and several constructions (Figure 1) of the performant sonic injectors made by the authors [1, 2] are presented. The technological advantage of the gas-dynamic injectors represents the independence from the nature of the technological medium (liquids or gases) and the conditions in exterior medium (vacuum and overpressure) where they have to run [1].

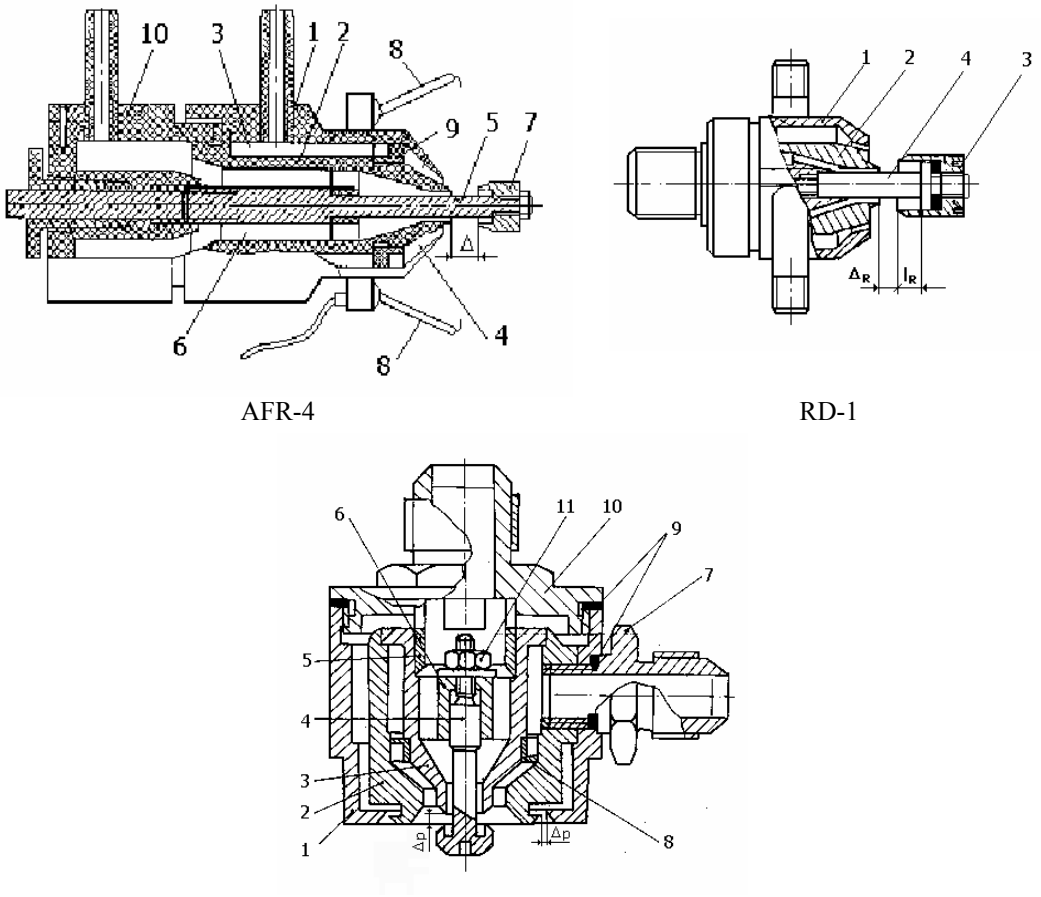

AFR-4 RD-1

DRG–1

Fig. 1. *Sonic injectors.*

Table 1. *The technical specification of the spraying sonic devices*

Type	**RD-1**	**AFR-4**	**DRG-1**
Capacity flow, $g \cdot s^{-1}$	150	20	100
Working air consumption, $g \cdot s^{-1}$	25	4	10
Working pressure, MPa	0.2-0.3	0.3	0.3
Liquid supply pressure, MPa	<0.3	<0.2	0.3
Working frequency, kHz	8.0	16	20
Sauter medium diameter (for water), μm	15-25	15-25	5-10
Angle of the dispersed jet	30-120	30-140	50-70
Dimensions, mm	40×60	30×100	50×70
Usage domains	Thermal engine, boiler, burning equipment	Thermo-isolating building materials, engineering zootechny	Metallurgy burning equipment, alimentary industry

2. Experimental hydro-pneumatic plant

In the research activity, the sonic treatment process requires certain technical requirements to ensure the directing and control of the technologic process, which are described in the experimental scheme of the technological water treatment (Fig. 2).

The plant allows the sonic generator supply to use, as working medium, the filtered air with filter 5 or the oxygen from the cylinder 4. The agency work (air or O_2) passes through generator 7, which is located inside the tank 10 and produces ultrasonic waves and bubbling, at the same time, thereby ensuring the sonic treatment of the technological fluid from the tank.

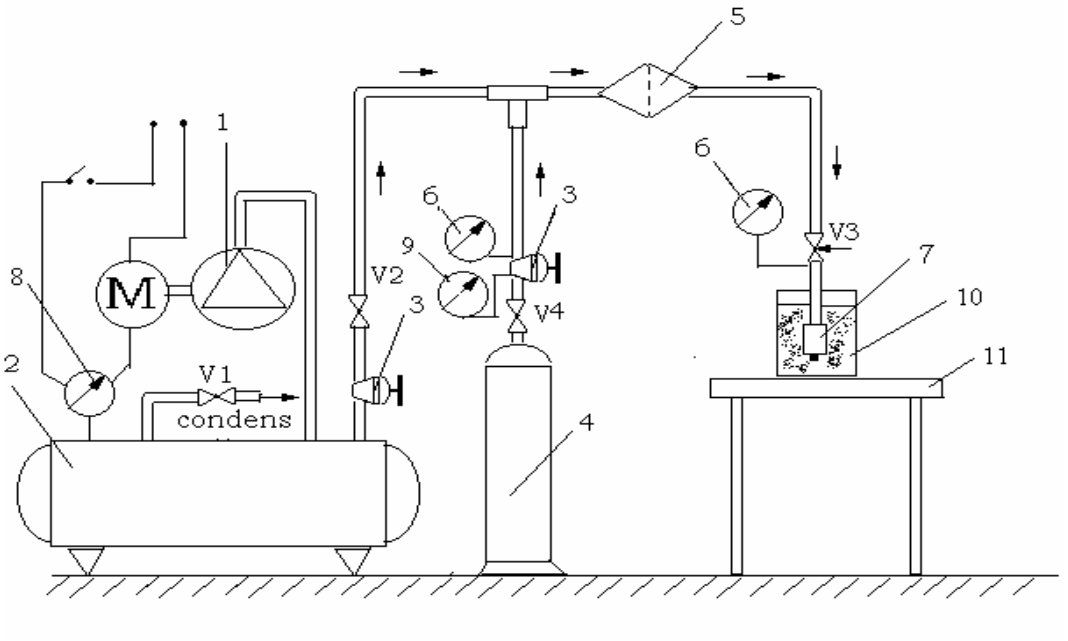

Fig. 2. *Experimental scheme for technological water treatment: 1. compressor, 2-tank battery, V_1-pressure control valve, M-electric motor, 3-pneumatic gearbox, V_2-way valve, 4-cylinder oxygen, 5-air filter 6-gauge, 7- ultrasounds gas-dynamic generator, 8-manometer, 9-gauge manometer, 10-tank work, H-depth work, V_3-control valves V_4-gas cylinder valve.*

3. Parametric study of the experimental gas-dynamic generator

Initial data required for calculation are the following:

ν - operating frequency, [kHz];

$\dot{m}_a$ - mass flow of working gas (air), [kg/s];

W_a - acoustic power, [W];

p = (0,1÷0,4) - working pressure gauge generator, [MPa],

The non-isobar parameter of the gas flow generator is determined as follows:

$$n = \frac{P_0}{P_{ex}} \cdot \pi(M_a) = \frac{p + P_{ex}}{P_{ex}} \cdot \pi(M_a), \qquad (1)$$

where: P_0 – total pressure nozzle;

P_{ex}– outside or atmospheric pressure (P_{ex}=0.1012 MPa);

p – value of the pressure gauge for compressed air supply;

$\pi(M_a)$ = 0.5263– gas-dynamic function π, from the gas–dynamic tables, corresponding to the Mach number M_a=1.0 in the nozzle exit section.

Depending on the parameter value of the jet n non-isobar jet, is determined the optimum dimensionless geometric parameters of the resonator (Fig.2), from which the maximum acoustic intensity power is obtained:

$$\overline{\Delta}_R = \frac{\Delta_R}{2\delta} = 0{,}74 \cdot n + 0{,}20 \qquad (2)$$

$$\bar{l}_R = 1.1 \cdot \overline{\Delta}_R \qquad (3)$$

$$\overline{D}_R = \frac{\delta_R}{\delta} = 0.34 \cdot n + 0.56 \qquad (4)$$

where:

δ is slot nozzle, $\delta = \frac{D_a - d_t}{2}$;

δ_R -is the slot resonator, $\delta_R = \frac{D_R - d_t}{2}$;

D_a, d_t – - nozzle diameter, respectively, the rod;

Δ_R, D_R, l_R - distance control, diameter and depth of the resonator (Fig. 3).

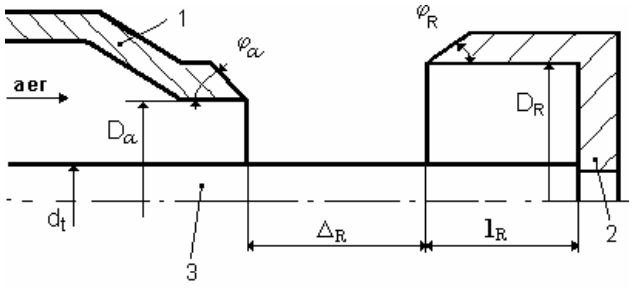

Fig. 3. *Design scheme for the dimensional calculation of the gas-dynamic generator with shaft: 1. nozzle 2. resonator, 3- rod; D_a – resonator diameter; dt–rod diameter, Δ_R – resonator control distance, D_R resonator diameter, l_R resonator depth.*

The optimal values of parameters $\overline{\Delta}_R$, $\overline{l}_R$, $\overline{D}_R$, the value of n and the frequency of the generator are used to determine the size of the slot nozzle, (ν =27 kHz):

$$\delta = 0{,}075 \frac{a \cdot n^{\frac{1}{3}}}{\nu \cdot \overline{l}_R^{\frac{1}{4}} \cdot \overline{\Delta}_R^{\frac{1}{6}} \cdot \overline{D}_R^{\frac{2}{3}}} \qquad (5)$$

where: a – sound speed in the nozzle exit section, $a = a_0 \cdot \left(\frac{2}{k+1}\right)^{\frac{1}{2}}$, m/s

a_0 - sound speed in air at rest at ambient temperature t.

Air mass flow is determined from the relationship:

$$\dot{m}_a = \frac{P_0 \cdot F_a}{\sqrt{T}} \left(\frac{k+1}{2}\right)^{\frac{k-1}{2(k-1)}} \left(\frac{k}{R}\right)^{\frac{1}{2}} \qquad (6)$$

where: F_a is section area of the generator nozzle exit,

$$F_a = \frac{\pi\left(D_a^2 - d_t^2\right)}{4} \qquad (7)$$

P_0 - total pressure,
T - supply gas temperature,
k - the adiabatic exponent, k = 1.41.

Using the parameter values D_a, d_t, D_R, l_R, Δ_R is determined the non-isobarity *n:*

$$n = \frac{\left(D_a - d_t\right)^3 \cdot \nu^3}{a^3 \cdot (0{,}15)^3} \cdot l_R^{\frac{3}{4}} \cdot D_R^2 \cdot \sqrt{\Delta_R} \qquad (8)$$

Acoustic power generator is obtained from the relationship:

$$W_a = \frac{\rho_0 \cdot a_0^3 \cdot n^{2\frac{1}{3}} \cdot F_a}{\overline{l}_R^{2\frac{1}{4}} \cdot \overline{D}_R^{2\frac{2}{3}} \cdot \overline{\Delta}_R^{\frac{1}{6}}} \cdot K_W, \text{ [W]} \qquad (9)$$

where: ρ_0 is the density of the compressed air supply, $\rho_0 = \frac{P_0}{a_0^2} \cdot k$.

Thus, by the method of calculation, the gas-dynamic sonic generator is designed and constructed with the following experimental dimensions:

D_a=4.0 mm, d_t=3.0 mm, D_R=4.0 mm, l_R =2.5 mm, Δ_R=1.42 mm. It results that the slot nozzle and the slot resonator have the same size: δ=δ_R=0.5 mm.

4. Construction of the gas-dynamic experimental sonic generator

The axial gas-dynamic sonic generator, used in the experimental wastewater treatment plant is illustrated in Figure 3:

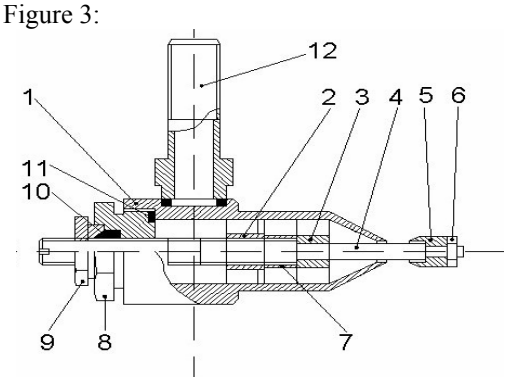

Fig. 3. *Axial gas-dynamic sonic generator: 1 - nozzle, 2,3 - cross support; 4 - rod, 5 - resonator, 6 - nut, 7 - bush, 8 - cover, 9 - nut, 10 - gasket; 11,13 - ring; 12 – socket.*

Compressed gas passes through nozzle 1 and resonator reaches 5. Supersonic gas jet from the nozzle, after interaction with the resonator cavity, loses its stability and emits high-frequency shock waves. The construction of the axial generator allows the adjustment of the dimensional parameters, which determine acoustics and gas-dynamics parameters change.

5. Conclusions

Recent research projects have underlined the potential of ultrasound as a chemical free treatment in water-related applications.

This article reviews the use of ultrasound technology, with a focus on wastewater, irrigation and aquaculture applications.

To reach this goal, the sonic systems use a 'blend' of very specific ultrasound frequencies of certain power which are emitted into the water by specific transducers.

To obtain the successful treatment of water, one should first know that no water body is the same -- every water body is unique and should be treated uniquely. Wastewater is any water that has undergone changes quality because of human intervention. Often, wastewater is being treated for re-use as drinking water or for other purposes. As high levels of nutrition are available in these waters, algae may grow rapidly as well as other micro-organisms such as bacteria. Algae can compete for nutrients against the bacteria in charge of sludge reduction and can also clog complete systems. The sonic technologies use the newest ultrasound techniques to remove the threat of algae from wastewater treatment plants and reclaimed water reservoirs.

Briefly, some of the results achieved in wastewater applications using the sonic technologies systems are:

• Reduction of biofilm formation;

• Reduction of TSS, turbidity, BOD, COD levels etc.;

• Reduction of free bacterial counts (E. coli, Enteroccoci, etc.);

•Ultrasound vibrations make it more efficient for bacteria present in the sludge to obtain nutrients, and speed up the utilizations of nutrients, accelerating the degradation of organic waste and the consumption of nitrates and phosphates.

References

[1]. Bălan G. - *Principles for elaboration of the technical system with sonic injectors,* Doctor Habilitation Thesis, U.T.M, Chisinau, 2001;

[2]. Bălan G. - *Aero-gas-dynamic*, Technical -INFO Ed., Chisinau, 2003;

[3]. Bălan G. - *Applied gas-dynamic. Calculus methods,* Technical - INFO Ed., Chisinau, 2000;

[4]. Constantinescu G. - *The theory of sonic technology*, Romanian Acad. Ed., ed. 2, vol. 2, 1985. **[1]. Avvaru B., Patil M.N., Gogate P.R., Pandit A.B.** - *Ultrasonic atomization: Effect of liquid phase properties*, Ultrasonics 44 (2006), pp. 146–158

[5]. Baukal C.E. - *Industrial burners handbook,* CRC Press LLC, USA, 2004.

[6]. Bălan G., Ciurea A., Bălan V., Bordei M. - *The Sonic Technologies*, Quatrieme edition du Colloque Francophone en Energie, Environnement, Economie et Thermodynamique *COFRET'08, 11 – 13 June 2008, Nantes - France*, pp. 20-29.

[7]. Gong J.S., Fu Wei-Biao - *The experimental study on the flow characteristics for a swirling gas–liquid spray atomizer*, Applied Thermal Engineering 27 (2007), pp. 2886–2892.

[8]. Kermes V., Belohradsky P., Oral J., Stehlk P. -*Testing of gas and liquid fuel burners for power and process industries*, Energy 33 (2008), pp. 1551–1561.

[9]. Lang R.J. - *Ultrasonic atomization of liquids*, Journal of the Acoustical Society of America, Vol. 34, 1962, pp. 6-8.

[10]. Rajan R., Pandit, A.B., *Correlations to predict droplet size in ultrasonic atomization*, Ultrasonic, Vol. 39, 2001, pp. 235–255.

[11]. *** SR EN ISO 3744:1997 - "*Acustică - Determinarea nivelurilor de putere acustică ale surselor de zgomot utilizând presiunea acustică - metoda tehnică aproximativă, în condiţii asemănătoare de câmp liber, deasupra unui plan reflectant*".

THE ANNALS OF "DUNAREA DE JOS" UNIVERSITY OF GALATI.
FASCICLE IX. METALLURGY AND MATERIALS SCIENCE
N^0. 2 – 2010, ISSN 1453 – 083X

MODELLING AND NUMERICAL SIMULATION OF THE ATMOSPHERIC DISPERSION OF POLLUTANTS FROM AN INTEGRATED IRON AND STEEL COMPLEX - PART II

Viorel MUNTEANU
"Dunărea de Jos" University of Galaţi
e-mail: viorel.munteanu@ugal.ro

ABSTRACT

The Iron and Steel Complex processes handle, store and undertake important amounts of raw materials (iron ores, coals, etc.) energy, fuels, waste waters, slags and other different types of wastes. These activities have an important environmental impact; therefore significant amounts of pollutants (gases, waste waters and wastes) are resulted.

In case of accidents involving emission of pollutants in the atmosphere, health authorities and local administrations often need to know what areas could be affected by dangerously high pollutant concentrations. The goal of the paper is to evaluate a ready-to-use and modelling system, including meteorological parameters and a dispersion model using FLUENT® 6.3, a flexible software and reliable to be used for such real-time evaluations, especially for trans-border regions.

KEYWORDS: pollutants dispersion, numerical modelling, chemical substances, air, water, soil

1. Numerical simulation and modelling using FLUENT® 6.3

1.1. Numerical modelling

The usual programs for numerical simulation of the pollutants factor dispersion in the atmosphere use relative simple dispersion mathematical models. This models use as entry data the meteorological parameters (wind speed and direction, air temperature, solar radiation level by the ground, etc.), but these are usually a priori imposed model, not calculated. The incapacity to simulate the flow phenomena themselves puts under question the utility of these programs in case of a hypothetical situation simulation and modelling (the results precision is strictly dependent on the accuracy of turbulence and speed fields, which can only be estimated in this case). FLUENT® uses the most advanced mathematical models for the chemical substances mixtures calculus, in any aggregation phase (gas, liquid - drops or solid –particles). But in the same time, FLUENT® allows the flow phenomena simulation and modelling with help from the most complex and complete mathematical model that describes fluids behaviour: the Navier – Stokes model.

This thing, although it significantly complicates the simulation process, brings to the user an enormous advantage: the possibility to numerically simulate situations that need a maximum detail and precision degree, vital situations (ecological accidents, natural catastrophes, etc.), pollutants dispersion in the air, water and even soil, etc. For the actual study there was chosen three different calculus situations. These are presented in Tab. 1. Their selection was made taking into account the annual meteorological conditions in the statistic Galaţi area (for the first two) and the risk degree (the third situation).

Tab. 1. *Calculus situation*

Situation	Wind direction	Wind speed	Probability/risk degree
1	N	7.5 m/s*	43.4% / minimum
2	S-E	Idem	9.02% / medium
3	V	Idem	- / big

* The value was chosen so it can be obtained the annual medium speed value of the wind at the normal measuring altitude (~10 m), v_{med} = 4.7 m/s

Fig.1. *Wind direction correspondent to each calculus situation.*

1.2. Determination of the limit conditions

As mentioned in chapter 4.1, the air flow near the soil surface is not uniform, the friction forces and the obstacles from the ground level determining the forming of so called the atmospheric layer limit.

For the numerical simulations to be very realistic and very correct, the limit conditions for the entry borders must be imposed so it can reproduce in the most truthful way this effect.

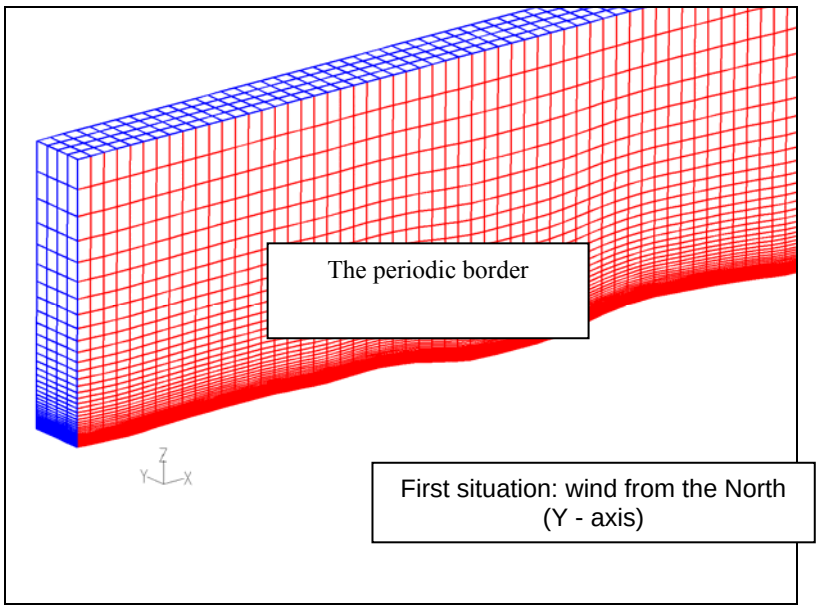

Fig. 2. *Calculus domain for determining the turbulence and speed profiles.*

To this purpose, there were made a series of supplementary simulations for each calculus situation. The FLUENT® program allows the user to obtain through calculus the dimensions that have to be provided in the limit conditions definition and imposing them through text files named „profiles". The quickest and the most elegant way to generate these files is the making of some simulations using the PERIODIC type at the limit conditions on the calculus domains with very much reduced dimensions in the flow direction (this type of what the limit condition permits the emulation of a length domain theoretically infinite).

In Fig. 2 is presented an implementation example, the case in which the wind blows from the North (the negative direction of the Y axis on the adopted coordinating system).

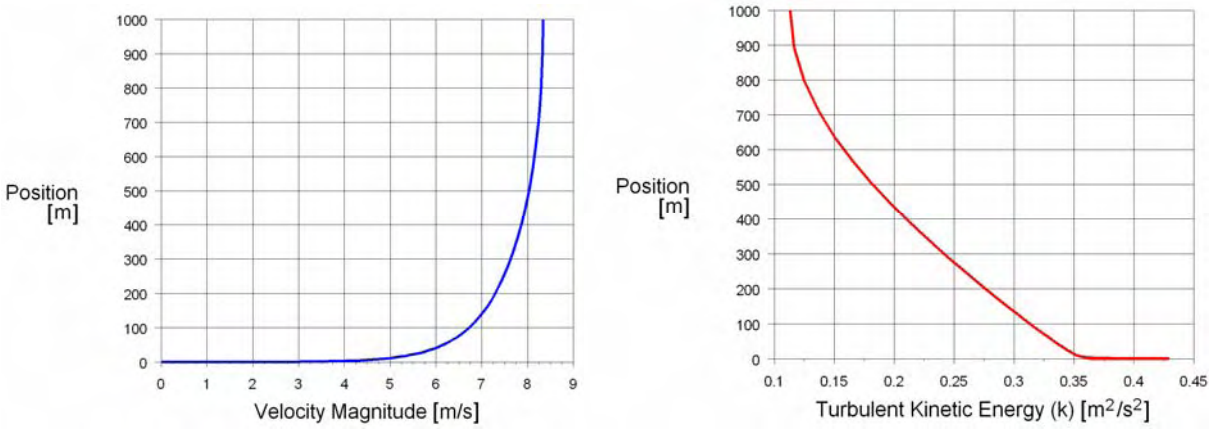

Fig. 3. *Wind speed value variation and atmospheric turbulence with the altitude.*

In Fig. 3 are represented the wind speed and atmospheric turbulences variations with the altitude, calculated for a medium speed of 7.5 m/s. It can be seen the very important effect that the friction with the ground has upon the speeds profiles, the wind speed value growing fast in the first 100 m.

Also it is interesting to point out the fact that the atmospheric turbulence, the most important factor of the pollutants dispersion, has the maximum value on the ground vicinity, but this value decreases pretty slowly with the height. The medium wind speed of 7.5 m/s corresponds to a speed of 4.7 m/s at a height of 10 m (pursuant to the meteorological standards, the wind speed is measured at 10 – 30 m height from the ground), which corresponds to the medium annual speed in the Galați region.

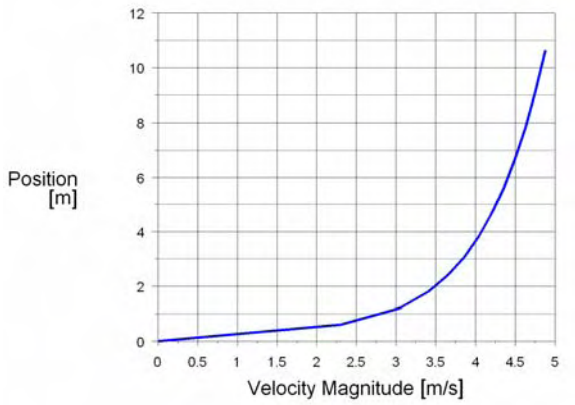

Fig. 4. *Wind speed variation on the ground immediate vicinity.*

The speed and turbulence profiles were extracted for all the study situations from numerical simulations made in the way previously described.

1.3. Physical models selection

The turbulence model selected for all the numerical simulations is SST k-omega. FLUENT® offers the user the possibility to choose no less than 14 turbulence models. Between these, the most adapted simulation model to the atmospheric limit layer flow from the offered precision and the calculus effort/performance proportion point of view is SST k-omega. There were made even some 2D numerical simulations so it can be determined the turbulence model influence on the obtained results. The comparison revealed that the models performances are very close, for this kind of flow, to those of more complex models, such as Reynolds Stress Model, performances obtained with a significantly less calculus effort.

Dispersion modelling was made with the chemical species transport model help available in FLUENT®. This model uses the Fick's law for the chemical species diffusion in laminar or turbulent regime

For species transport calculations, there are two ways to model the diffusion of chemical species. For most applications the Fick's law approximation is adequate, but for some applications (e.g., diffusion-dominated laminar flows such as chemical vapour deposition), the full multi-component diffusion model is recommended.

Mass diffusion coefficients are required whenever there are solved species transport equations in multi-component flows. Mass diffusion coefficients are used to compute the diffusion flux of a chemical species in a laminar flow using (by default) Fick's law:

$$J_i = -\rho D_{i,m} \nabla Y_i - D_{T,i} \frac{\nabla T}{T} \quad (1)$$

where $D_{i,m}$ is the mass diffusion coefficient for species I in the mixture and $D_{T,i}$ is the thermal (Soret) diffusion coefficient.

Equation (1) is strictly valid when the mixture composition is not changing, or when $D_{i,m}$ is independent of composition.

This is an acceptable approximation in dilute mixtures when $Y_i << 1$, for all i except the carrier gas. FLUENT® can also compute the transport of non-dilute mixtures in laminar flows by treating such mixtures as multi-component systems. Within FLUENT®, $D_{i,m}$ can be specified in a variety of ways , including by specifying D_{ij}, the binary mass diffusion coefficient of component i in the component j. D_{ij} is not used directly, however; instead, the diffusion coefficient in the mixture, $D_{i,m}$, is computed as:

$$D_{i,m} = \frac{1 - X_i}{\sum_{j, j \neq i} \left(X_j / D_{ij} \right)} \quad (2)$$

where X_i is the mole fraction of species i. There is the possibility to input $D_{i,m}$ or D_{ij} for each chemical species.

In turbulent flows, equation (1) is replaced with the following form:

$$J_i = -\left(\rho D_{i,m} + \frac{\mu_t}{Sc_t} \right) \nabla Y_i - D_{T,i} \frac{\nabla T}{T} \quad (3)$$

where: - J_i is the diffusive flux for the *"i"* species;
- Y_i is *"i"* species concentration;
- $D_{i,m}$ is the *"i"* species mass diffusion coefficient in the *"m"* mixture;
- μ_t is turbulent viscosity;
- $D_{T,i}$ is thermal diffusion coefficient of the *"i"* species;
- ρ is density;
- T is temperature;
- Sc_t is the turbulent Schmidt number for the turbulent flow:

$$Sc_t = \frac{\mu_t}{\rho D_t} \quad (4)$$

where D_t is the effective mass diffusion coefficient due to turbulence.

In turbulent flows the mass diffusion coefficient inputs consist of defining the molecular contribution to diffusion $D_{i,m}$ using the same methods available for the laminar case, with the added option to alter the default settings for the turbulent Schmidt number. This parameter relates the effective mass diffusion coefficient due to turbulence with the eddy viscosity μ_t. The turbulent diffusion coefficient normally overwhelms the laminar diffusion coefficient, so the default constant value for the laminar diffusion coefficient is usually acceptable.

2. Conclusions

This paper has reported on the development and evaluation of a new modelling system for air pollutants based on FLUENT® 6.3 software.

This software uses the most advanced mathematical models to calculate the chemical substances mixture situated in any state of aggregation (gaseous, liquid – droplets or solid - particles) and also permits the modelling and simulations of the flowing phenomena using a complete and complex mathematical model which describes the fluids behaviour namely the Navier-Stokes.

This fact, although it is making the simulation process significantly complicated, brings an enormous advantage to the user namely the possibility to simulate numerical situations that require a maximum degree of precision and detail, virtual situations (ecologic accidents, natural disasters, etc.), dispersion of pollutants in air, water and even soil.

FLUENT® 6.3 offers the user 4 different numerical solvers, every one of them being better fit to a particular class of numerical simulations.

In the analysed situations the PBCS solver ("Pressure - Based Coupled Solver") was used, due to the optimum precision and it is converging speed.

Qualitative simulations were realised, the fluxes values being considered identical for all pollutants and the same in all studied situations.

References

[1]. Nagel T., Flassak T., Bächlin W., Lohmeyer A., *Optimierung des Luftmessnetzes von Baden-Wurrrtemnerg*, Teil A Verfahren für Flächenhafte Immissionsdarstellung und Immissionsbezogene Klassifierung., UMEG, Karlruhe, 2002.

[2]. VDI-*Guidline 3945 Pt. 3: Environmental meteorology. Atmospheric dispersion models. Particle model,* Berlin, 1996.

[3]. Schädler G., Lohmeyer A., Bächlin W., Van Wees T., *Vergleich und Bewertung derzeit verfügbarer mikrokaliger Ausbreitungsmodelle. Forschungszentrum Karlsruhe*, Berichte Umweltforschung Baden-Württemberg, Karlsruhe, 1996.

[4]. Moussiopoulos N., *Recent advances in urban air pollution research*,The 8th Int. Conf. on Environmental Science and Technology in 2003, Greece.

[5]. Louka P., Moussiopoulos N., *Optimisation of CFD modeling methods methods for traffic pollution in streets within TRAPOS research network*, The 4th International Exhibition and Conference on Environmental Technology in 2003, Athens, Greece.

[6]. Bahmann W., Schmonsees N., Oestereicher R., *TA Luft 2002*, in: Neue Anforderungen an meteorologische Daten für Ausbreitungsrechnungen. Immissionsschutz, 8. Jahrgang, Heft Nr. 1, Berlin, Bielefeld, München, 2003.

[7]. Hout D., et al., *Guidance on Assessment under the EU Air Quality Directives*, in: European Environment Agency, draft, Copenhagen, 2000.

THE ANNALS OF "DUNAREA DE JOS" UNIVERSITY OF GALATI.
FASCICLE IX. METALLURGY AND MATERIALS SCIENCE
N^0. 2 – 2010, ISSN 1453 – 083X

A NEW VISION CONCERNING THE GENERATION AND ADMINISTRATION MUNICIPAL RESIDUES

Stefan DRAGOMIR, Georgeta DRAGOMIR, Marian BORDEI
"Dunărea de Jos" University of Galati
email: sdragomir@ugal.ro

ABSTRACT

In average urban, administration of municipal waste is realization in organized way by dint of own specialize services of his city halls of firms of salubrity. Proportion urban populations serve of services of bred at 76% in 2006, to approximately 90% in 2008.

In average rural, don't exist the organized services for administration of waste, the transport to the places of individually storage. This are serve in charge organized for administration of waste merely a little part from rural localities and in especial except needle rural localities found out contiguously urban centers. In the year 2008, approximately 12% from rural were service in charge of salubrity.

KEYWORDS: municipal residues, administration, depot, storage

1. Introduction

The amount of municipal waste produced varies from year to year, registering in the last six years a general tendency to increase, determined in particular by the growth of the population consumption (Table 1). From the amount of municipal waste, is biggest part is represented by organic and assimilated wastes, generated by individual households and also, by economic units, commercial offices, institutions, hospitals.

Table 1.

Types of residues	Generated residues	Capitalized residues	Eliminated residues
	[thousand tones]		
Housekeeper residues and assimilated - collected	5043.845	13.242	5030.603
Residues from municipal services (including mud from defecation city worn-out waters)	1573.715	76.784	1496.931
Residues from building and demolitions	247.286	2.253	245.033
Not collected residues (estimate in depending on the average index of generation)	1570.471	0	1570.471
Total municipal residues	8435.317	92.279	8343.038

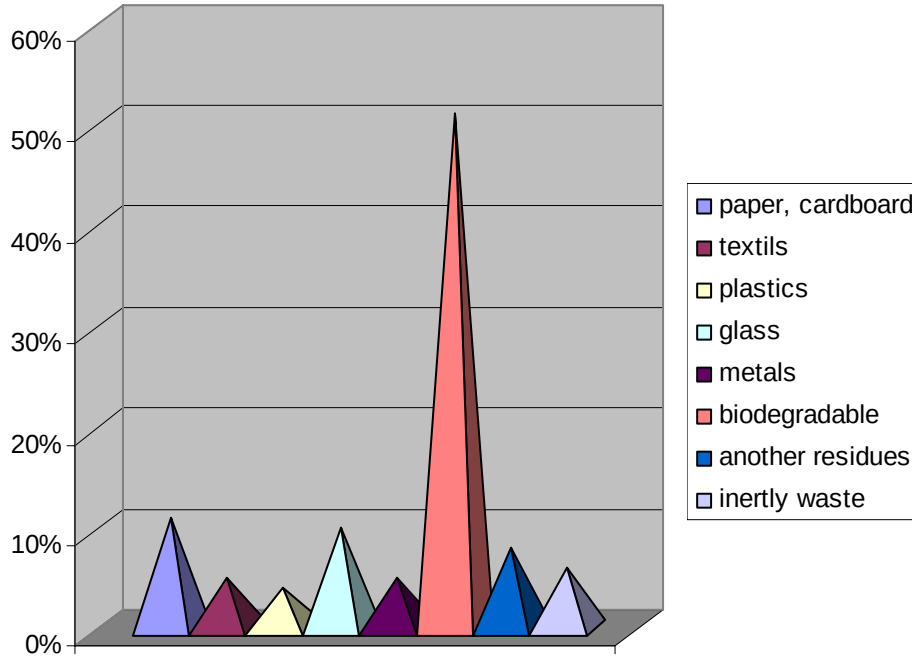

Fig.1. *Amounts in percent by type of waste.*

The residues composition varied in recent years, with the largest share of biodegradable waste. In 2008, the biodegradable waste (excluding paper and cardboard) represented approximately 51% of the total domestic collection. Municipal waste production preview was based on the predicted growth in population, the average time of life, the consumption increase; national waste management plan estimates an average increase of 0.8% of the municipal waste generated annually. There are also plans for other waste streams, for example, hazardous waste from scrapped vehicles, waste from electrical and electronic equipment, resulting from water treatment, from constructions and demolitions. The monitoring system includes: a performance evaluation and presentation of targets, the resulting indicators are presented in an annual public report "Regional Integrated Waste Management Plan (RIWMP) which includes: targets for improving waste collection in rural areas, the closure of old landfill and the redevelopment of the environment, the construction and operation of corresponding landfill, the reduction of the amount of biodegradable waste in landfill and waste recycling systems for packaging. The types of waste which are municipal waste are managed differently depending on their characteristics and the generated quantities.

2. Administration of organic waste

Approximately 40% of municipal waste is recyclable material component, 20% can be recovered. After a selected collection, through pilot projects, only 20% of recyclable materials can be reused.

The rest is excreted in storage, thus losing large quantities of secondary raw materials and energy resources.

In recent years, more and more private operators have begun the actions of collecting pets and cardboard. In some localities there are "points of collection and storage" and people are stimulated to recycle paper, cardboard, glass, plastics. In Romania, plants from: glass paper, cardboard and plastics industry production have begun to take the waste from the collection point for recycling.

3. The storage of municipal waste

The storage of municipal waste is the main method for municipal waste disposal. Municipal waste deposits in accordance with the Directive on the landfill of waste 1999/31.CE were renewed in early 2008. In Romania there are 283 municipal landfills in urban areas (which receive waste collected by sanitation companies in urban areas), which:

- 19 stores are in line or were predicted to be arranged in accordance with European regulations 31. 12. 2008;
- 238 deposits are not in accordance with European requirements, and that storage will cease operation until 2017;
- 13 storage landfills were closed in the period 2003-2004.

Necessary to ensure compliance costs by investing in municipal landfills were estimated at 1.775 million.

In addition to municipal waste landfills, in urban areas, in Romania there were 2686 storage facilities in rural areas up to 1 ha.

Some rural ecological landfills areas are organized starting with 16.07.2009; these landfills have waste collecting services at rural level, including transport systems.

3.1. Administration of municipally sludge

Nowadays, most of the sludge produced by municipal wastewater is treated by different methods being stored, only a small part of the annual amount is recovered and used in agriculture.

3.2. Administration of waste from building and demolitions

The amount of construction and demolition waste generated in Romania is relatively low, but their growth is expected, driven by the country's economic development.

Waste production is represented mainly by industrial and agricultural waste, including energy production.

Currently, there are very few companies that have lines of production for waste recovery and the services they provide are small, they also use a small number of types of waste, with reduced working capacity.

During 2003, waste produced by mining and industry, were 370 million tones, the main part (90%) being waste resulting from mining activities (mining) - 331 millions tons, and 30.5 million tones are from industry and agriculture.

The economic activities which have produced the largest quantities of waste in 2003, excepting the mining industry, were the chemical, petrochemical, rubber and plastics (27%), metallurgy and metal construction (17%) , energy industries (13%), food, beverages, tobacco (10%), other economic activities (33%).

The industrial branches which generate high quantities of waste are the energy industry, petrochemical industry, metallurgy, food industry. From the amount of waste generated, approximately 30% is recovered, the other part is removed by incineration or disposal.

4. Residues from medical activities

From the total quantity of waste produced in hospitals, 75-90% are non-hazardous being assimilated with organic waste, and only 10-25% represents hazardous waste.

Hazardous medical waste can be eliminated through incineration crematoria or heat treatment installation.

The final disposal of hazardous waste from healthcare activities in 2003 was as follows: 76% through its crematorium, 13% used other firms, 7.5% of hazardous waste were burned in open air.

The hazardous waste from medical activities represents approximately 30% of the total 190000 tons /year.

5. Conclusions

Since 2006 the amount of generated municipal waste has exceeded 1 million tons and in 2008 1,165,000 tons. The biggest part of municipal waste is represented by the food waste (57%), collected from households, this amount is constant over the last eight years, but is expected to increase due to expansion of coverage of health services.

The household waste collected, is equivalent to the industrial, commerce and institutions waste, being about 16%, or about 190,000 tons / year.

Other categories of waste collected have a lower percentage, ie:

-1.3-2.6% of separately municipal waste collected;

- 1.5-2.3% waste from parks and gardens;

-1.6 -2.1% market waste;

- 3.5 - 4.3% waste from the streets.

Selective and systematic collection of recyclable materials (paper / cardboard, glass, plastic, metals, etc.), has already begun and will continually develop through several projects.

Nowadays, the quantities of waste selectively collected represent those for authorized firms of recyclable waste collection. They come from industry and commerce, as shown previously, in more detailed a statistical analysis.

Uncollected waste is about 15% of total municipal waste generated, the calculation was made using an index of generation of 0.9 kg/year x population in urban areas and 0.4 kg/year x population in rural areas.

In most of resulted cases submitted not in accordance with European and national service so that those areas have become "contaminated areas".

Currently a study is done is to inventory "of contaminated sites, and clarify their legal position. After this inventory is an assessment of risk made more of the inventory for the specific situation of the present resolution and taking appropriate measures for their rehabilitation or closure.

References

[1]. Leopa, A. - *Reciclarea deşeurilor* - Editura Mongabit, Galaţi, 2005;
[2]. Prodea, V. - *Povestea celor 3R*, Editura Albatros, Bucureşti 1985;
[3]. Rojanschi, V. - *Protecţia şi ingineria mediului*, Editura Economică, Bucureşti, 1992;
[4]. *** Directiva nr 2006/12/CE privind deşeurile,
[5]. *** Directiva nr. 91/689/EEC privind deşeurile periculoase;
[6]. *** Ordonanţa de Urgenţă nr. 78/2000 privind regimul deşeurilor *(Monitorul Oficial Nr. 283 din 22. 6.2000*), Legea nr. 426/2001 pentru aprobarea Ordonanţei de Urgenţă nr.78/2000 privind regimul deşeurilor, completată şi modificată *(Monitorul Oficial Partea I Nr.411 din 25. 07. 2001);*
[7]. *** Ordonanţa de Guvern nr. 61/2006 pentru modificarea şi completarea Ordonanţei de Urgenţă nr. 78/2000 privind regimul deşeurilor *(Monitorul Oficial Nr. 790 din 19. 08. 2006);*
[8]. *** Directiva nr. 99/31/EC privind depozitarea deşeurilor, Hotararea Guvernului nr. 349/2005 privind depozitarea deşeurilor *(Monitorul Oficial nr. 394 din 05.2005);*
[9]. *** Directiva nr. 2000/76/EC privind încinerarea deşeului;
[10]. *** Hotararea Guvernului nr. 128/2002 privind incinerarea deşeurilor *(Monitorul Oficial, Partea I nr.160 din 6.03.2002);*
[11]. *** Directiva nr. 94/62/EC privind ambalajele şi deşeurile din ambalaje cu modificarile ulterioare.

MANUSCRISELE, CĂRŢILE ŞI REVISTELE PENTRU SCHIMB, PRECUM ŞI ORICE CORESPONDENŢE SE VOR TRIMITE PE ADRESA:

MANUSCRIPTS, REVIEWS AND BOOKS FOR EXCHANGE COOPERATION, AS WELL AS ANY CORRESPONDANCE WILL BE MAILED TO:

LES MANUSCRIPTS, LES REVUES ET LES LIVRES POUR L'ECHANGE, TOUT AUSSI QUE LA CORRESPONDANCE SERONT ENVOYES A L'ADRESSE:

MANUSCKRIPTEN, ZIETSCHRITFTEN UND BUCHER FUR AUSTAUCH SOWIE DIE KORRESPONDENZ SID AN FOLGENDE ANSCHRIFT ZU SEDEN:

UNIVERSITATEA "DUNĂREA DE JOS" DIN GALAŢI
REDACŢIA ANALELOR
Str. Domnească nr. 47 – 800036 Galaţi,
ROMÂNIA
email: mbordei@ugal.ro

After the latest evaluation of the journals achieved by National Center for the Science and Scientometry Politics (**CENAPOSS**), as recognition of its quality and impact at national level, the journal is included in B category, 215 code (http://www.cncsis.ro/2006_evaluare_rev.php).

The journal is indexed in Cambridge Scientific Abstract (http://www.csa.com/ids70/serials_source_list.php?db=materials-set-c).

The papers published in this journal can be visualized on the "Dunarea de Jos" University of Galati site, the Faculty of Metallurgy, Material Science and Environment, page: www.fmsm.ugal.ro.

AFFILIATED WITH:

- *ROMANIAN SOCIETY FOR METALLURGY*
- *ROMANIAN SOCIETY FOR CHEMISTRY*
- *ROMANIAN SOCIETY FOR BIOMATERIALS*
- *ROMANIAN TECHNICAL FOUNDRY SOCIETY*
- *THE MATERIALS INFORMATION SOCIETY (ASM INTERNATIONAL)*

Annual subscription (4 issues per year)

Edited under the care of
Faculty of
METALLURGY, MATERIALS SCIENCE AND ENVIRONMENT
and Research Center
QUALITY OF MATERIALS AND ENVIRONMENT

Edited date: 30.06.2010
Issues number: 200
Printed by
Galati University Press
accredited CNCSIS
47 Domneasca Street, 800036 Galati,
Romania